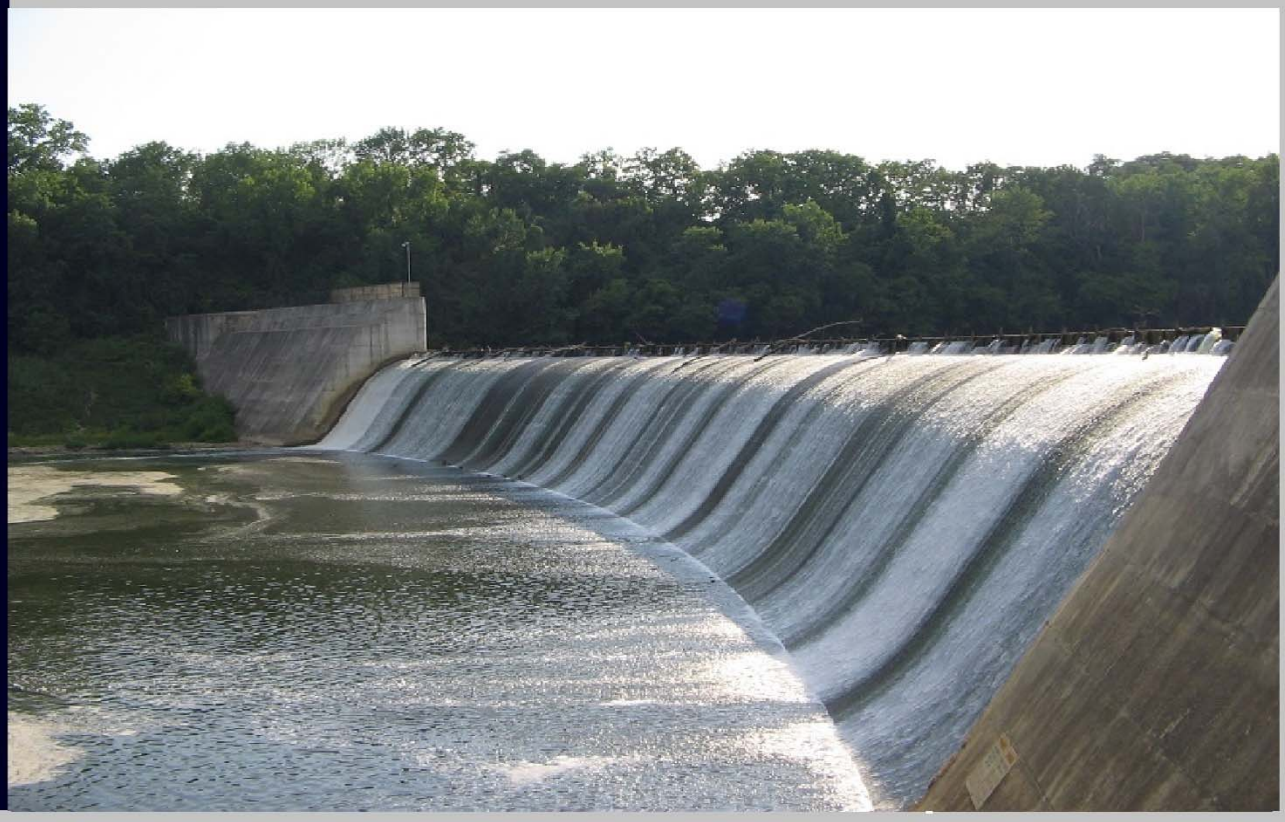
Shahid Chamran University of Ahvaz

Journal of Hydraulic Structures

Scientific Professional Journal

Autumn 2017
Volume 3, No 2



انجمن هیدرولیک ایران
Iranian Hydraulic Association

نشریه علمی پژوهشی

ISC
Islamic World Science Citation Center

In the name of GOD

Journal of Hydraulic Structures
Department of Civil Engineering
Shahid Chamran University of Ahvaz

JORNAL OF
HYDRAULIC STRUCTURES
SHAHID CHAMRAN UNIVERSITY OF AHVAZ

Manager: *Prof. Hamid R. Ghafouri*
Editor-in-chief: *Dr. Ali Haghighi*
Editorial coordinator: *Dr. Seyed Mohammad Ashrafi*
Department of Civil Engineering, Engineering Faculty, Shahid Chamran University of Ahvaz, Ahvaz, Iran.

Members
Prof. Hossein M. V.Samani
Civil Engineering Department, Shahid Chamran University of Ahvaz, Ahvaz, Iran
Prof. Hamid R. Ghafouri
Civil Engineering Department, Shahid Chamran University of Ahvaz, Ahvaz, Iran
Dr. Ali Haghighi
Civil Engineering Department, Shahid Chamran University of Ahvaz, Ahvaz, Iran
Prof. Mahmood S. Bajestan
Hydraulic Structures Department, Shahid Chamran University of Ahvaz, Ahvaz, Iran
Prof. Saeed R. S. Yazdi
Civil Engineering Department, K.N.Toosi University of Technology, Tehran, Iran
Dr. Mohammad S. Pakbaz
Civil Engineering Department, Shahid Chamran University of Ahvaz, Ahvaz, Iran
Dr. Arash Adib
Civil Engeering Department, Shahid Chamran University of Ahvaz, Ahvaz, Iran
Dr. Mojtaba Labibzadeh
Civil Engineering Department, Shahid Chamran University of Ahvaz, Ahvaz, Iran
Prof. Helena M. Ramos
Instituto Superior Técnico (IST), University of Lisbon
Dr. S. Mohammad Ashrafi
Civil Engineering Department, Shahid Chamran University of Ahvaz, Ahvaz, Iran
Dr. S. Abbas Haghshenas
Institute of Geophysics, University of Tehran | UT, Tehran, Iran
Dr. Mohammad Zounemat-Kermani
Department of Water Engineering, Shahid Bahonar University of Kerman, Kerman, Iran
Dr. Taher Rajaee
Civil Engineering Department, University of Qom, Qom, Iran
Dr. Mohammad Vaghefi
Civil Engineering Department, Faculty of Engineering, Persian Gulf University, Bushehr, Iran
Dr. A. A. Telvari
Soil Conservation and Watershed Management Research Institute; Department of Civil Engineering, Islamic Azad University, Ahvaz branch, Ahvaz, Iran

Shahid Chamran Univeristy of Ahvaz

انجمن هیدرولیک ایران

CONTENTS

VOL 3, NO II, Autumn 2017

II ***Aims and Scope***

01 Investigating the vulnerability downstream area of Taleghan dam due to dam failure
H. Goharnejad; M. Azizkhani; M. Zakeri Niri; S. Moazami

10 An experimental study on hydraulic behavior of free-surface radial flow in coarse-grained porous media
A. Rajabi; E. Hatamkhani; J. Sadeghian

22 Three-dimensional numerical modeling of score hole in rectangular side weir with finite volume method
S. Ghotbi; A. Abdollahi; M. Azhdari Moghadam

32 Experimental Study of the Effect of Base-level fall at the Beginning of the Bend on Reduction of Scour around a Rectangular Bridge Pier Located in the 180 Degree Sharp Bend
M. vaghefi; M. moghanloo; D. Dehghan; A. keshavarz

47 Developing optimal operating reservoir rule-curves in drought periods
S. Alahdin; H.R. Ghafouri

62 Finding the Causes and Evaluating Their Impacts on Urmia Lake Crisis Using a Comprehensive Water Resources Simulation Model
A. B. Dariane; L. Eamen

Aims and Scope

Hydraulic Structure Journal is an interdisciplinary journal which publishes high-quality peer-reviewed articles addressing the latest developments and applied methods **in construction, maintenance, management, and operation policy of Hydraulic Structures.**
The Journal aims at providing an efficient route to fast-track publication, **within 10-12 weeks after manuscript submission**. Manuscripts will be considered for publication in the following categories: **research articles**, **technical notes**, **case reports** and **discussions**.

The general areas covered by the Journal include:

- Technical and methodological advances in application, design/selection, production, modification of construction materials
- Advances in numerical and analytical methods
- Hydro informatics and soft computing
- Hydraulic aspects of hydraulic structures
- Applied surface and subsurface hydrology and hydrometeorology
- Forecasting approaches in water resources engineering
- Economic and social aspects of hydraulic structures
- Uncertainty analysis and risk management in hydraulics and water resources engineering
- Application of Nanotechnology in Hydraulic Structures
- Geotechnics of Hydraulic Structures
- Damage detection techniques

The following might be considered as hydraulic structures:

- Dams and associated structures
- River and Watershed Structures
- Offshore and Onshore Structures
- Irrigation and Drainage Channel Networks
- Bridges
- Water Storage and Conveyance Structures
- Pipelines and Pump Stations
- Sewerage Systems
- Water and Wastewater Treatment Plants
- Historical Water Structures

General Information

Title: Journal of Hydraulic Structures
Subject: Hydraulics and water resources engineering
Coverage area: International
Journal Type: Scientific and technical
License Holder: Shahid Chamran University
Editor-in-Chief: Dr. Ali Haghighi
Manager: Prof. Hamid R. Ghafouri
Editorial coordinator: Dr. Seyed Mohammad Ashrafi

Language Editors:
Majid SadollahKhani
Soroosh Kamali
Address: Engineering Faculty, Shahid Chamran University of Ahvaz
Phone #: +986113330010-20 (5610 & 5603)
Fax #: +986113337010
Language: English
Email: jhs@scu.ac.ir
Website: jhs.scu.ac.ir

Journal of Hydraulic Structures
***J. Hydraul. Struct.*, 2017; 3(2):1-9**
DOI: 10.22055/jhs.2017.13435



OPEN ACCESS

Investigating the vulnerability downstream area of Taleghan dam due to dam failure

Hamid Goharnejad[1]
Mahyar Azizkhani[2]
Mahmoud Zakeri Niri[3]
Saber Moazami[4]

Abstract

Due to the immense damage caused by dam failure, especially dams constructed near large cities, it is necessary to consider the breaking phenomena as well as studying and designing different parts of the dam. For this purpose, the hydrograph of the outflow due to dam failure must be identified according to size of the fracture and then flood routing, and flood zone must be determined based on the downstream topography and morphology. The integration of hydraulic models and geographic information system is used to achieve this objective. In this research the effect of breaking Taleghan storage dam due to the slip of a pile of reservoir abutment and the creation of current wave toward the dam body as well as the vulnerability analysis due to the breaking of the dam on downstream lands was studied. At first, Taleghan dam failure for five different scenarios was modeled using the FLOW-3D numerical software and then the geometric data of the river was extracted using the ArcGIS software and modeling the flood due to dam failure was conducted in Hec-GeoRas model. Then, the risk analysis was performed for each break scenario of Taleghan dam. The results indicated that the maximum amount of inundation would occur in Razmian city at an approximate distance of 45 kilometers from Taleghan dam site.

Keywords: Dam breaking, Inundation, Vulnerability, Risk analysis, Taleghan dam.

Received: 17 September 2017; Accepted: 07 November 2017

[1] Department of Civil Engineering, Environmental Sciences Research Center, Islamshahr Branch, Islamic Azad university, Islamshahr, Iran, H.Goharnejad@iiau.ac.ir (**Corresponding author**)
[2] Department of Civil Engineering, Environmental Sciences Research Center, Islamshahr Branch, Islamic Azad university, Islamshahr, Iran, m.azizkhani78@gmail.com.
[3] Department of Civil Engineering, Environmental Sciences Research Center, Islamshahr Branch, Islamic Azad university, Islamshahr, Iran, m.zakeri.w90@gmail.com
[4] Department of Civil Engineering, Environmental Sciences Research Center, Islamshahr Branch, Islamic Azad university, Islamshahr, Iran, saber.moazami@gmail.com

CC BY

1. Introduction

Dams are always considered as a potential threat for their downstream areas because of creation of large water reservoirs. Dam designers attempt to lower vulnerability potentials by applying safety factors; however, natural and non-natural factors like floods, piping phenomenon, foundation weakness and exploding can cause a dam to break [1]. The problem of dam failure and effects of surges on downstream areas attracted many scholars and experts' attention, after several important dams like Teton were broken [2]. To reduce the effects of a large reservoir dam failure, it is important to know the changes of hydraulic parameters due to break in dam, such as depth, speed, flow, and the time when the wave forehead reaches the downstream area and finally to determine the border and designing the flood zone in order to reduce the financial losses and casualties. In this regard, in the last few decades, different researchers have done numerous theoretical and practical studies in order to determine the mechanism of dam failure and the trends of hydraulic parameters as a function of time and space [3]. One of the most important methods for erosion control in rivers in these situations is ston masonery and riprap. A general dimensionless equation for the prediction of maximum particle size of stable riprap into the tributary channel at river confluences has been developed by Ghanbari Adivi et al. [4]. Their results showed that the stability number of riprap into the tributary channel increases with increasing the ratio of tailwater depth to particle size.

Fliervoet et al. [5], Lim [6] and Chiew [7] found that during flooding, the emergence of various forms such as Ripple and Dune and live bed is natural. These processes, despite the intersectional structures, can cause inconstancy in these structures. Andam [8] investigated the changes in speed and number of landing by using HECGeo-RAS model in a research entitled as the comparison of river regime inside and outside of forest area, and compared the influence of vegetation on the physical behavior of the flow. He concluded that using the HECGeo-RAS model can offer researchers suitable numbers to study the diet and other hydraulic characteristics of river flow. Sholtes [10] used HEC-RAS software to route flood dynamics in rural and urban areas of Northern California and concluded that the decrease in slope and increase in roughness of floodplain and river have more influence on flood attenuation. Nagy et al., [11] investigated the sand grinding attrition and meanders evolution in an answer to Tisza River engineering in Hungary and found that due to severe attrition in the area and human intervention (performing engineering projects), this river has reached a balance by shortcuts in its route. However, the purpose of this article is to investigate and determine the flood plain area. Then the amount of vulnerability risk over all path of the river for five different scenarios of dam break and for wave arrival times of 30 and 120 minutes were identified.

2. Methodology

The conducted research is presented in details in this section.

2.1. Study area

Taleghan dam at 135 km of north west of Tehran with longitude of 50˚, 37' to 51˚, 10' and latitude of 36˚, 5' to 36˚, 25' is built on Taleghan river in Roshanabdar rural area. Figure 1 shows the study area, including dam, river, and the topography of area.

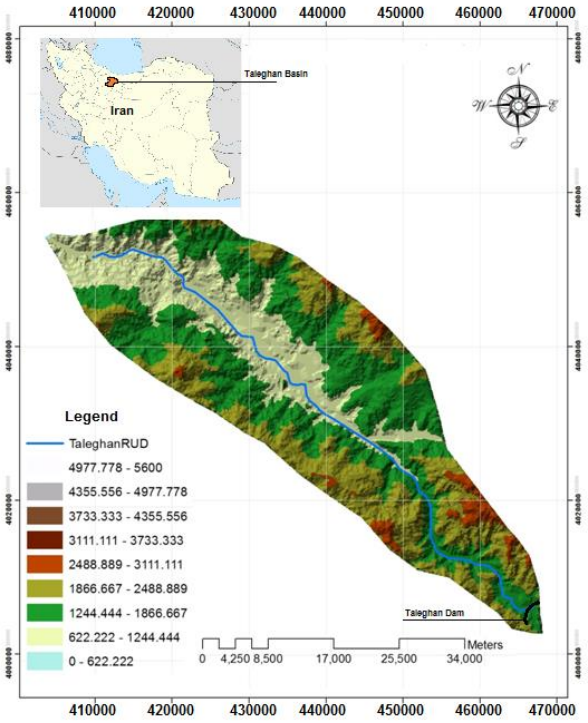


Figure 1. Map of Taleghan river in Taleghan dam downstream

2.2 Physical characteristics of Taleghan river in Taleghan dam downstream

In order to perform the model, it is necessary to determine the river characteristics such as the left and right bank, riverbed, and roughness coefficient of each section. Therefore, after several field studies and inspections, the required data were determined and entered the model. Then using the Arc-GIS, the cross sections were provided and entered the model. Considering the high length of the study area, the distance of cross sections in straight parts of the river was chosen about 4000 meters and 1500 meters in sudden intersections and arches. Among the factors affecting the manning coefficient are the grading substrate material, the rippling degree of river, the relative effect of obstacles, the density of vegetation and morphology form of the river. Therefore, in order to determine and estimate the manning coefficient in a part of river, it should be divided to three main parts including the mainstream and flood plains of right and left banks. Because of the important role of roughness coefficient, the model were calibrated using this parameter.

2.3 Determining boundary conditions

In order to predict the characteristics of the flow in the study period, real boundary conditions are needed. Boundary condition is in fact representative of the output and input status of the downstream and upstream flows. It is obvious that expecting the exact characteristics of flow includes offering correct data in boundaries. In the current research, the introduced boundary condition for hydraulic model to simulate the hydraulic flow of Taleghan river in downstream of Taleghan dam, used the normal depth condition in upstream and also normal depth boundary condition in downstream. The HEC-RAS model can calculate the normal depth using Manning's equation and the slope of river. After simulation, the hydraulic model identifies the slope and

suitable level of water in upstream.

2.4 Discharge inflow

Five scenarios are defined to investigate embankment dam failure resulting from overtopping. Inflow volume to the reservoir is different in each scenario. Based on the reviews, minimum flood volume that overtops and damages the dam body is about 5 MCM. In addition, maximum flood volume that fully destroys the dam body is about 25 MCM. In the range of 5 to 25 MCM, flood volumes of 7.5, 9 and 13 MCM have been considered. The charecteristics of scenarios have been presented in Table 1. ([12])

Table1. Flow modeling conditions for five states of overtopping in Taleghan dam

Scenario	Water Height in Reservoir (m)	Storage (MCM)	Flood Volume (m3)	Flood Discharge (cms)
1	82	420	5.0	54,269
2	82	420	7.5	59,390
3	82	420	9.0	78,913
4	82	420	13.0	89,129
5	82	420	25.0	97,054

2.5 The risk taking theory due to dam failure

The researchers consider the three parameters of escape time, velocity, and depth of flooding as the appropriate criteria of dam failure risk. Considering the importance of the escape time in reducing life loss of downstream areas, the 30 to 120 minutes after the beginning of dam failure are selected as the risk criteria of these areas over time [13].

The flow velocity and depth of flooding is considered simultaneously in assessing the consequences of dam failure. In this regard, the flooding area along the river and flood plains and risk index HR are assigned to the grid cells according to the following definition [14].

$$HR=D(V+0.5) \quad (1)$$

Table 2. Flood risk levels based on risk amount and risk description [14](Vrouwenvelder et al., 2003.)

HR	Flood risk level	Sign	Risk description
<0.75	Low	R1	Warning: flooded area with shallow running water with deep water remain
0.75 – 1.25	Average	R2	Dangerous for some people (For example children): flooded area with deep or fast flowing running water
1.25 – 2.5	High	R3	Dangerous for most people: flooded area with deep and fast flowing water
>2.5	Very high	R4	Dangerous for everyone: flooded area with deep and fast flowing water

Where, in the above equation D is the depth of flood flow in meters and V is the flow

velocity in meters per second. In general, risk areas are classified into four levels of low, medium, high and very high-risk areas that flood risk levels based on the amount of risk and the descriptions of each level are provided in table 2.

3. Results

Using the HEC-RAS model and geographic information system GIS, modeling the flow of Taleghan river in the downstream of Taleghan dam and caused by the dam break was investigated. Using the topographic data of Taleghan river basin in the downstream of the dam, TIN layer and raster maps of the mentioned area were obtained. Then, using the Hec-GeoRas in the GIS environment, various layers of the river route, banks and river cross sections were prepared. It should be noted that the above data are among the requirements of flow modeling due to dam failure in the HEC-RAS model. After preparing the geometric model of the river, the necessary information was inserted into the HEC-RAS model and flow modeling was carried out after editing the information and peocessing the data.

Modeling the flow for discharges of 54269, 59390, 78913, 89129 and 97054 cubic meters per seconds was conducted. Considering the importance of model calibration after the model simulation, the results for the maximum discharge (scenario 5) and minimum discharge (scenario 1) were calibrated in accordance with the roughness coefficient values. So that the minimum, medium and maximum roughness coefficient values for the right and left side of the river were considered to be respectively as 0.035, 0.040, and 0.045. The minimum, medium, and maximum roughness coefficient values for the riverbed were respectively considered as 0.030, 0.035, and 0.040.

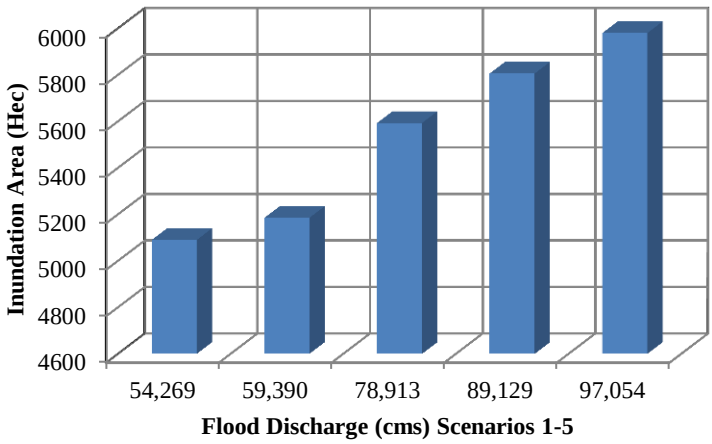


Figure 2. The inundation area due to flooding scenarios 1 to 5 along Taleghan River because of dam breaking

The results indicated that in all studied sections, the amount of water level difference for maximum and minimum roughness coefficients was less than 5%. Therefore, the roughness coefficient values with sufficient accuracy was considered as equal to the average roughness coefficient, that is over the two sides of the river as equal to 0.040 and the river bed as 0.035.

After modeling the flow in HEC-RAS, the data of the flow was exported into the Arc-GIS

and the inundation area for each scenario is provided in Figure 2.

Then, the values of HR index for the escape times of 30 and 120 minutes after the dam break was calculated and provided in figures 3 and 4. For the escape time of 120 minutes and 30 minutes, the sections with high flood risk level (HR> 2.5) are respectively provided in tables 3 and 4.

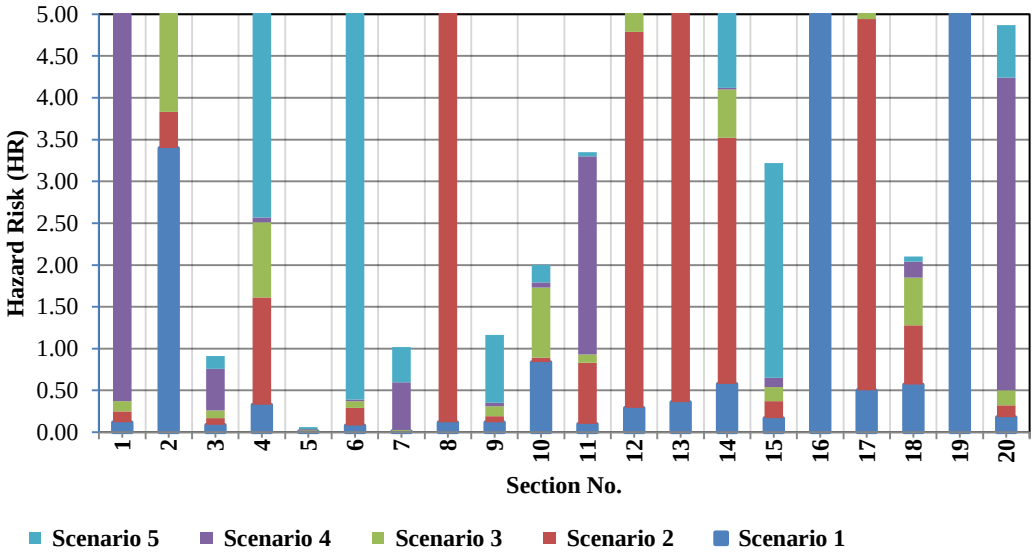


Figure 3. Risk index values for the escape time of 120 minutes in all sections of the river and different dam failure scenarios

Table 3. Sections with very high-risk levels for the escape time of 120 minutes and different dam failure scenarios

Dam failure scenario	Sections with very high risk levels (HR>2.5)																			
	1	2	3	4	5	6	7	8	9	10	11	12	13	14	15	16	17	18	19	20
1		×														×			×	
2		×						×				×	×	×		×	×		×	
3		×		×				×				×	×	×		×	×		×	
4	×	×		×				×			×	×	×	×		×	×		×	×
5	×	×		×		×		×			×	×	×	×	×	×	×		×	×

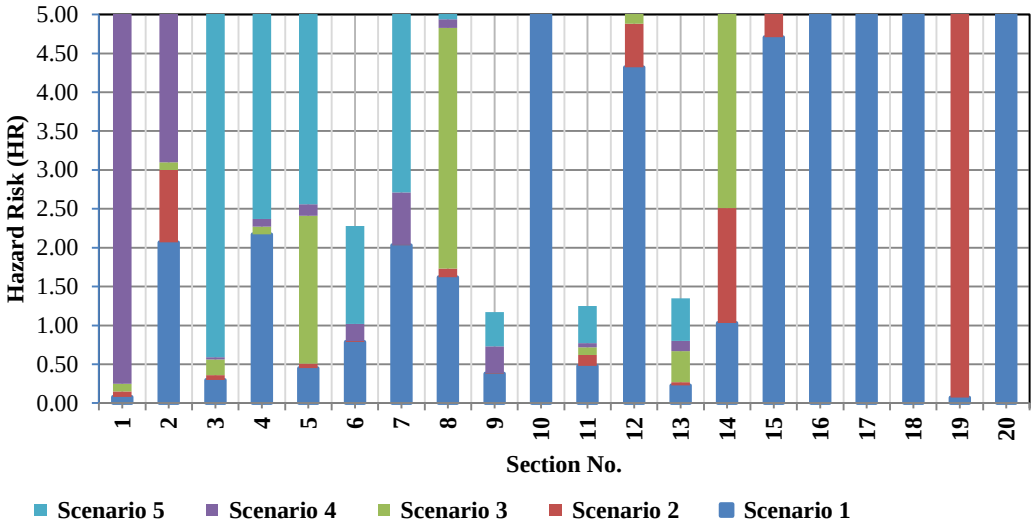


Figure 4. Risk index values for the escape time of 30 minutes in all sections of the river and different dam failure scenarios

Table 4. Sections with very high-risk levels for the escape time of 30 minutes and different dam failure scenarios

Dam failure scenario	Sections with very high risk levels (HR>2.5)																			
	1	2	3	4	5	6	7	8	9	10	11	12	13	14	15	16	17	18	19	20
1										×		×			×	×	×	×		×
2		×								×		×		×	×	×	×	×	×	×
3		×						×		×		×		×	×	×	×	×	×	×
4	×	×			×		×	×		×		×		×	×	×	×	×	×	×
5	×	×	×	×	×		×	×		×		×		×	×	×	×	×	×	×

4. Conclusion

Flood plains and areas adjacent to rivers are suitable regions to carry out economic and social activities due to specific conditions. The effect of break and the risk of flooding due to Taleghan dam failure in the downstream area of the dam were investigated in the present study.

Flood zoning due to Taleghan dam failure with discharges of 54269, 59390, 78913, 89129, 97054 cubic meters per second on Taleghan river and the downstream of the dam were investigated. For modeling the study river, HEC-GeoRAS hydraulic model was applied. In the downstream of Taleghan dam, a total of 80 km of the river from the dam site located in the Alborz mountain was modeled. After zoning the areas with a high risk, the vulnerabilities were

identified. Through calculating the risk index (HR) in any sections of Taleghan river after dam failure, the risk of the flood caused by dam failure in the downstream area was quantified. Therefore, we can easily classify high-risk areas. Observed zoning maps indicate that a great flooding can occur in Razmian city at an approximate distance of 45 kilometers from Taleghan dam site and due to dam failure and also indicate the necessity of adopting special measures to deal with this risk.

References

1. Miller S.N. Kepner W.G. and Mehaffey M.H.2002 .Integration Landscape Assessment and Hydrologic Modeling for Land Cover Change Analysis. Journal of the American Water Resources Association. 38(4):919-929.

4. Ghanbari Adivi, E., Shafai Bajestan, M., Kermannezhad, J., " Riprap sizing for scour protection at river confluence", Journal of Hydraulic Structures J. Hydraul. Struct., 2016; 2(1): 1-11,DOI: 10.22055/jhs.2016.12646

3. Goharnejad, H., Noury, M., Noorzad, A., Shamsaie, A., Gohanejad, A., "The Effect of Clay Blanket Thickness to Prevent Seepage in Dam Reservoir", International Journal of Environmental Sciences, 2010, 4 (6), 556-565.

5. Jan M. Fliervoet, Riyan J.G. van den Born & Sander V. Meijerink (2017) A stakeholder's evaluation of collaborative processes for maintaining multi-functional floodplains: a Dutch case study, International Journal of River Basin Management, 15:2, 175-186, DOI:10.1080/15715124.2017.1295384

2. Litrico, X. Fromion, V. Baume, J.P. Arranja, C. Rijo, M. 2005. Experimental Validation Of A Methodology To Control Irrigation Canals Based On Saint-Venant Equations. Control Engineering Practice 13 (1425–1437).

7. Chiew, Y. M. 1999. Time scale for local scour at bridge piers. Journal of Hydraulic Engineering, ASCE ,125(1) :59-65.

6. Lim, S. Y., 2001. Parametric study of riprap failure around bridge piers. Journal of Hydraulic Research ,39(1):61-72.

8. Andam, K. S. 2003. Comparing physical habitat conditions in forested and non-forested streams. Thesis of Partial Fulfillment of the Requirements for the Degree of Master of Science Specializing in Civil and Environmental Engineering, University of Vermont, 136 pp.

10. Sholtes, J. 2009. Hydraulic analysis of stream restoration on flood wave propagation. A thesis submitted to the faculty of the University of North Carolina at Chapel Hill.

11. Nagy, A. C., Toth, T., Vajk, O. & Sztano, O., 2010 , Erosional scours and meander development in response to river engineering: middle Tisza region, Proceedings of the Geologists' Association, Vol. 121 (4): 238–247.

12. Goharnejad, H. ; Moalem, M. ; Niri, M. ; Abadi, L. (2016), 'Taleghan Dam Break Numerical Modeling', World Academy of Science, Engineering and Technology, International Science Index, Geotechnical and Geological Engineering, 10(9), 170.

13. Dncergok, T., (2007), The Role of Dam Safety in Dam-Break Induced Flood Management ,International Congress River Basin Management, Antalya, Turkey, 22-24 March.

14. Vrouwenvelder A., Van der Veen, A., Stuyt, L.C.P.M and Reinders, J.E.A., (2003), Methodology for Flood Damage Evaluation", Delft Cluster Seminar: The Role of Flood Impact Assessment in Flood Defense Policies, IHE, Delft, The Netherlands.

Journal of Hydraulic Structures
***J. Hydraul. Struct.*, 2017; 3(2):10-21**
DOI: 10.22055/jhs.2018.24185.1059



OPEN ACCESS

An experimental study on hydraulic behavior of free-surface radial flow in coarse-grained porous media

Ali M. Rajabi[1]
Elham Hatamkhani[2]
Jalal Sadeghian[3]

Abstract

In this paper, we have been used an experimental model to analyze the nonlinear free surface radial flows and to introduce an equation compliant with these flows. This is a semi cylindrical model including a type of coarse grained aggregate which leads the radial flow into the center of a well. Thereafter, the hydraulic gradient was measured on different points of the experimental model by three distinguished methods of difference of successive radii, keeping constant the minimum and maximum radii. An equation, describing the behavior of free surface radial flow, was then proposed by measured data (as regression data) from the laboratory and analysis of the results. Verification of the proposed equation by test data shows that the equation is valid on the established limits of the data.

Keywords: Hydraulic gradient, Hydraulic behavior, Forchheimer, Porous media, Radial flow.

Received: 15 September 2017; Accepted 27 November 2017.

1. Introduction

The equations of fluids in porous media are very useful in engineering, especially, the rockfill dams, diversion dams, gabions, breakwaters, and ground water reserves (Bazargan and Zamanisabzi 2011). Flows in porous media are generally categorized into Darcy (linear) and non-Darcy (non-linear) ones. Several studies have been conducted in the field of flow in the porous media by researchers such as Ward)1964); Ahmed and Sunada (1969); Hansen et al.)1995), Li et al.)1998); Bazargan and Shoaei)2010) Bazargan and Zamznisabzi(2011); Wright(1958); Mc Corquodale)1970); Nasser(1970); Thiruvengadam and Kumar(1997); Reddy)2006); Reddy and Mohan)2006); Sadeghian et al.)2013). The Darcy equation, which is valid only in a limited interval of Reynolds numbers, provides a hydraulic description of Darcy

[1] Engineering Geology Department, School of Geology, College of Science, University of Tehran, Tehran, Iran, amrajabi@ut.ac.ir; amrajabi@ymail.com (**Corresponding author**)
[2] Department of Civil Engineering, University of Qom, Qom, Iran, elhamhatamkhani@yahoo.com
[3] Department of Civil Engineering, Bu-Ali Sina University, Hamedan. Iran, j.sadeghian@basu.ac.ir

CC BY

flows (Mc Whorter and Sunada 1977). Turning a linear flow into a transitive and turbulent flow makes the Reynolds number violate its critical value, making the Darcy law null afterwards. Non-Darcy flow dominates these physical conditions (Das and Sobhan 2012; Hansen et al 1995; Bazargan and Bayat 2002; Wright, 1958). The analysis of the flow in porous media over the years, has been studied both analytically and empirically. Physicists, engineers, hydrologists have investigated the behavior of flow in porous media in the range of a variety of material in the laboratory and have also tried to formulate responses to the systems (Ahmed and Sunada 1969; Bazargan and Zamanisabzi 2011). Nonlinear flows in coarse-grained porous media may be classified into two categories. In the first category, i.e. parallel flow, the flow lines are relatively parallel and there is no curvature in the plan of flow lines. This type of flow is found in both pressurized (flows do not make contacts with the free surface) and free-surface (flows make contacts with the free surface) modes. The flows in the confined aquifers and earth dams are included in this category (Mc Corquodale 1970; Thiruvengadam and Kumar1997; Wright 1958). Venkataraman and Roma Mohan Rao (2000) and Reddy (2006) proposed the equations (1) and (2), respectively, as the governing equations of parallel flows.

$$I = a_c V + b_c V^2 \quad (1)$$

$$I = a_c V + b_c V \quad (2)$$

where I is the hydraulic gradient, V *is* the average velocity and a_c and b_c are constant values. In the second group of non-Darcy flow, the flow lines are contracted along the way and are known as radial (convergent) flows. These flows are, also, found under compressed or free-surface conditions. Flow through gravel filters used in water treatment plants is an example of pressurized converging flows (Sadeghian et al. 2013; Reddy 2006; Venkataraman and Roma Mohan Rao 2000). There can be seen a compression in the flow lines in radial, as opposed to parallel, flows. In the free surface radial flows, the compression of flow lines along the way, inflates the flow (Sadeghian, 2013). Sadeghian et al, 2013 provided the Equation (3) as their proposed model for description of radial flows:

$$i_{cf} = a_{cf} V_{ave} + b_{cf} V^2{}_{ave} \quad (3)$$

Where i_{cf} is the hydraulic gradient, V_{ave} is the average velocity, and a_{cf} and b_{cf} are constant coefficients. Ferdos and Dargahi 2016a addressed this issue through comprehensive numerical modelling. The novelty of the proposed approach lies in a combination of large-scale experiments and three-dimensional numerical simulations, leading to a fully calibrated and validated model that is applicable to flows through cobble-sized materials at high Reynolds numbers. Ferdos and Dargahi 2016b exerted a Lagrangian particle tracking model to estimate the lengths of the flow channels that developed in the porous media. Gamma distributions fitted to the normalized channel lengths, and the scale and shape parameters of the gamma distribution found to be Reynolds number dependent. Their proposed normalized length parameter can be used to evaluate permeability, energy dissipation, induced forces, and diffusion. They also found that shear forces exerted on the coarse particles depend on the inertial forces of the flow and can be estimated using the proposed equation for the developed turbulent flows in porous media. Sedghi-Asl et al. (2014) studied a fully developed turbulent regime considering as a specific case of non-Darcy flow, and developed an analytical approach to determine normal depth, water surface profile and seepage discharge of the flow through coarse porous medium in steady condition. Then the results of an experimental model compared with the analytical solution developed in their research. The results showed a good agreement between analytical and experimental data. The hydraulic behaviors of the parallel and radial flows are totally different.

Conspicuous among the differences, the flow's cross section in the parallel and radial flows are constant and variable, respectively. This is not a difference to be taken into account in the equations related to radial flows and the hydraulic behavior of the flow is still studied by modified linear relations inferred from Darcy equation. Due to the real world applications of radial flows, especially for pumping in oil and water wells in the course grained unconfined alluvial beds and also the necessity of modifying the computational methods provided as linear relations of adjusted from Darcy equation (Sadeghian et al. 2013) to be used in the investigation of nonlinear flows, it is necessary to develop equations that model the radial flows appropriately. In this paper, in order to describe the free surface radial flows in the coarse grained porous media, an experimental equation is provided by physical laboratory modeling that is used in especial cases of porous media.

2 Materials and methods

The cylindrical form was used in the present study due primarily to the adaptability and compliance of the cylinder coordinates with the physical conditions of radial flows problems. Semi cylindrical model allows the convergent (radial) flow towards the center of a well. The semi cylindrical physical model is of 6 and 3 meters in diameter and height, respectively. In 1 meter of the bottom is included a tank for required water supply during the experiments. The 2 meters above accommodates the porous media (aggregates) with a volume of about 28 m^3. Fig. 1 illustrates a schematic of the laboratory model. The aggregates used in the physical model are course-grained. The specifications of model have been provided in Table 1.



Figure 1. Schematic of the physical model used in the study

Table 1. Specification of the aggregates used in the physical model

Grains diameter (mm)	150-20
Grains shape	Rounded
Porosity (%)	43
Uniformity coefficient	2.13
Coefficient of curvature	1.016
Special weight (t/m^3)	1.68

According to Fig. 2, five metal meshes divide the semi cylinder to six equal sections. On every reticular section, 42 piezometers were installed in the apparatus to measure the piezometeric pressure of the flows.

A total of 210 piezometers show the pressure changes in the model. For a precise piezometeric pressure reading, a number of scaled dials were used with millimeter precision. Since the experiment was performed on various levels of the water surface, the model was filled up to the intended level for every experiment and the numbers on four meters (mechanical and digital) were read, showing the flow volume that crossed through the pumps (V_1). By looking at the water surface profile on the glass view of the physical model, piezometeric pressure was read on the piezometers panel. After a few minutes, the pumps and stopwatches were turned off simultaneously and the number on the four counters were noted again (V_2). The tank was filled up to a determined depth. The considered depths were 52, 70, 85, 95,110, 120, 140, 150, 160 cm. After every experiment, the data were noted for different depths and levels. Table 2 and 3 show a sample of the data for the depth of 85 cm.

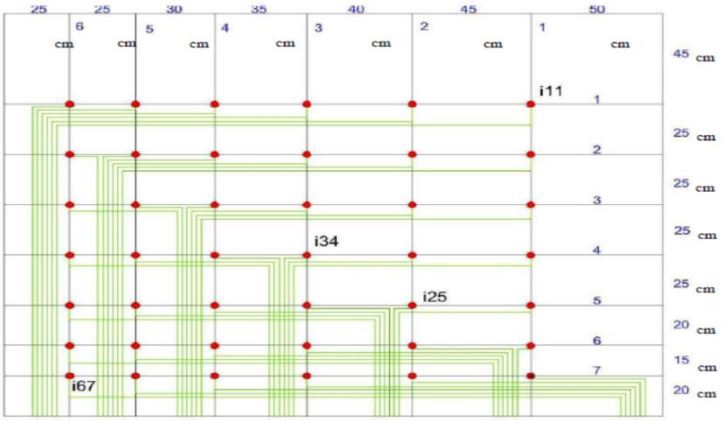


Figure 2. Position of piezometers on every section of the physical model

Table 2. Hydraulic specifications of the flow, measured for the depth of 85 cm

Radial (cm)	Section Number	Water Level (cm)	Flow Rate (cm/s)	Mean Flow Velocity (cm/s)
275	External Border	70.2	0.83	-
225	1	85.6	0.84	0.76
180	2	85.3	1.06	0.95
140	3	84.9	1.36	1.21
105	4	84.5	1.83	1.60
75	5	83.9	2.58	3.90
50	6	83.1	3.90	3.24
25	Internal Border	81.3	7.98	5.94

Table 3. Values of piezometeric pressure in different levels (z) for the depth of 85 cm

R*	z			
225	85.1	85.1	85.2	85.2
180	84.6	84.8	84.8	84.8
140	84.4	84.4	84.5	84.4
105	84	84.1	84.1	84.1
75	83.4	83.5	83.7	83.6
50	82.8	82.8	83	83

*R: Radial (cm); z: Water level (cm)

In the physical models of parallel flows, the cross section is constant. So, the hydraulic gradient is calculated for successive points, while the cross section in the radial flows is variable. Base on this, in this study, the hydraulic gradient was calculated by the three following methods; difference of successive radii (R_1-R_2), (Method I); keeping constant the minimum radius (R_1-R_{min}), (Method II), and keeping constant the maximum radius (R_1-R_{max}), (Method III). The hydraulic gradient sample values (i_{obs}) in the depth of 85 cm and level of 20 cm are shown in Tables 4, 5 to 6 for the three methods.

Table 4. i_{obs} values measured by the *Method I* in the depth of 85 cm and level of 20 cm

i_{obs} *	Δl	ΔH	H	R	r(cm)	v(m/s)
0.011	45	0.5	85.1	202.5	225	0.009
0.005	40	0.2	84.6	160	180	0.012
0.011	35	0.4	84.4	122.5	140	0.016
0.02	30	0.6	84	90	105	0.022
0.024	25	0.6	83.4	62.5	75	0.032

* The observed hydraulic gradient (i_{obs}) is obtained by the ratio of the difference between two successive points ($\Delta H = H_1 - H_2$) and the radial distance between them($\Delta l = R_1 - R_2$). Average radius was used in the calculations($R = (r_1 + r_{2)}/2$), H_1:The first point piezometeric pressure, H_2:The second point piezometeric pressure, R_1: The first average radius, R_2: The second average radius, H: Piezometeric pressure, R:radial, v: Velocity

Table 5. i_{obs} values measured by the *Method II* in the depth of 85 cm and level of 20 cm

i_{obs} *	Δl	ΔH	H	R	r(cm)	v(m/s)
0.013	175	2.3	85.1	137.5	225	0.023
0.013	130	1.8	84.6	115	180	0.024
0.017	90	1.6	84.4	95	140	0.026
0.021	55	1.2	84	77.5	105	0.028
0.024	25	0.6	83.4	62.5	75	0.032

* The observed hydraulic gradient (i_{obs}) is obtained by the ratio between the piezometeric pressure difference of a point and the minimum-radius point ($\Delta H = H - H_{min}$) and the radial distance between them ($\Delta l = R - R_{min}$) Average radius was used in the calculations($R = (r_1 + r_2)/2$); H_{min}:The minimum-radius point piezometeric pressure, R:Average radius, R_{min}: The minimum-radius point, H: Piezometeric pressure , r:Radial,v: Velocity

Table 6. i_{obs} values measured by the *Method III* in the depth of 85 cm and level of 20 cm

i_{obs} *	Δl	ΔH	H	R	r(cm)	v(m/s)
0.011	45	0.5	84.6	202.5	180	0.009
0.008	85	0.7	84.4	182.5	140	0.011
0.009	120	1.1	84	165	105	0.013
0.011	150	1.7	83.4	150	75	0.017
0.013	175	2.3	82.8	137.5	50	0.023

* The observed hydraulic gradient (i_{obs}) is obtained by the ratio between the piezometeric pressure difference of a point and the minimum-radius point ($\Delta H = H_{max} - H$) and the radial distance between them ($\Delta l = R_{max} - R$)Average radius was used in the calculations($R = (r_1 + r_2)/2$), H_{max}: The maximum-radius point piezometeric pressure, R: Average radius, R_{max}: The maximum-radius point, H: Piezometeric pressure , R:radial, v:Velocity

3 Results and discussion

Using the hydraulic gradient and the average velocity obtained by the experimental data, *a*

and *b* coefficients were calculated in the binomial Forchheimer equations for different levels and depths. Table 7 shows a sample of *a* and *b* values for the levels of 20 and 35 cm and the depth of 52 cm. The results show that in contradiction to the basic Forchheimer equation, the nonlinear coefficient of *b* (the slope of the hydraulic gradient-velocity curve (i-v), which is a positive) obtains negative values (Table 7 and Fig. 3).

Table 7. The calculated value of Forchheimer *a* and *b* constant coefficients for the levels of 20 and 35 cm and the depth of 52 cm

z	*a*	*B*
20	1.311	-7.310
35	1.409	-7.779

z: Water level (cm); a & b: The coefficients of Forchheimer equation

As seen previously, the hydraulic behaviors of parallel and radial flows are totally different. One of the differences is the constant and variable cross sections in parallel and radial flows. This declares the type of changes between hydraulic gradient and velocity of the flow along the way and the i-v curve form. On this basis, in the parallel flow, the flow's cross section is constant along the way. So, the variations of hydraulic gradient are more pronounced than the velocity variations. However, in radial flow, the cross section of the flow is not constant along the way. So, the velocity variations are more than the pear hydraulic gradient variations. The i-v curve for the parallel flows (Forchheimer equation) is shown in the Fig. 3 which tends toward the orthogonal axis of the hydraulic gradient (i) and shows the higher variations of hydraulic gradient relative to the velocity in the parallel flows(v). However, in radial flows, the velocity variations are more significant than the hydraulic gradient variations and it is expected that the i-v curve tends towards the horizontal velocity axis (Fig. 3).

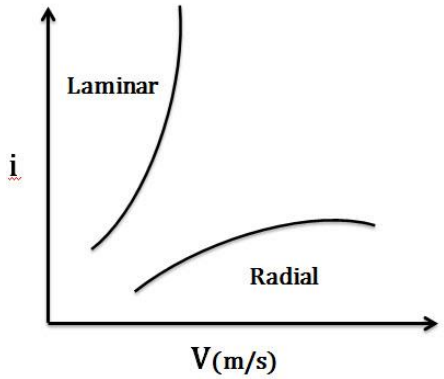


Figure 3. The schematic velocity – hydraulic gradient (i-v) curve of the parallel and radial flow

According to the Forchheimer equation, *a* and *b* parameters in the hydraulic gradient – average velocity curve (i-v) are the y-intercept and slope of the curve, respectively. Due to the positive *b*, the functional form of the equation shows an upward concavity and a positive slope for the curve. This is true in the curves related to the parallel flows (Fig. 3). Studying the radial flows has made clear the contradiction that in this kind of flow, the nonlinear *b* parameter has a negative value (Table 6). So, i-v curve shows a downward concavity, hence a negative slope. This is in contradiction to the Forchheimer principle. Therefore, this equation doesn't allow the investigation of radial flows similar to the parallel ones. Thus, in this paper, we developed an alternative equation using an experimental model. The cross section of the flow is variable from point to point in the radial flows, as against the parallel flows. So, in order to obtain an equation for the analysis of the free-surface radial flows, unlike Forchheimer binomial, the radial

independent variable (R) is also required in addition to the independent variable of velocity (v) and the dependent variable of hydraulic gradient (i). To provide the intended equation, some of the data related to the experimental readings for the depths of 52, 70, 85 and 95 cm and the levels of 20, 35, 55 and 80 cm were taken as regression data, and those related to the depths of 110, 120, 140, 150 and 160 cm and the levels of 20, 35, 55, 80, 105, 130 and 155 cm were taken as test or verification data. Therefore, the equations of (4), (5) and (6) were obtained for the methods I, II, III, respectively, in order to predict the hydraulic gradient i_{pre} by regression data (measured in various conditions in the laboratory, Tables 4, 5 and 6), including the hydraulic gradient(i), radius(R) and velocity (v) variables and using the common statistical software. The predicted hydraulic gradient, i_{pre}, was calculated as a sample using these equations for the depth of 85 and level of 20 cm, the values are provided in the Tables 8.

$$i_{pre} = {}^{v}/_{-a + bR} \tag{4}$$

$$i_{pre} = aR^{-b/v} \tag{5}$$

$$i_{pre} = V \,/\, (a - bR^2) \tag{6}$$

where i_{pre} is the predicted hydraulic gradient, R is the average radius, V is the average velocity, and a and b are the constant coefficients.

Table 8. The values of i_{pre} predicted by the *Method I*, II, III in the depth of 85 and level of 20 cm

	i_{pre}	i_{obs}	R	r	v
Method I	0.006	0.011	202.5	225	0.009
	0.008	0.005	160	180	0.012
	0.012	0.011	122.5	140	0.016
	0.017	0.02	90	105	0.022
	0.028	0.024	62.5	75	0.032
Method II	0.013	0.013	137.5	225	0.023
	0.014	0.013	115	180	0.024
	0.017	0.017	95	140	0.026
	0.020	0.021	77.5	105	0.028
	0.024	0.024	62.5	75	0.032
Method III	0.010	0.011	202.5	180	0.009
	0.009	0.008	182.5	140	0.011
	0.009	0.009	165	105	0.013
	0.010	0.011	150	75	0.017
	0.013	0.013	137.5	50	0.023

i_{pre}:Predicted hydraulic gradient, i_{obs}:Observed hydraulic gradient, R:Mean radius(cm), r: Radial(cm); v: Velocity(m/sec)

In this study, using the three parameters of the variations percentage of equations' empirical coefficients, the Nash coefficient (E) and the root mean square error (RMSE), the effectiveness of the three Methods have been analyzed. The variations percentage of a and b coefficients used in the calculation of gradient (relations 4, 5 and 6) is shown in the Table 9 in terms of the three methods I, II and III. According to these values, using the equations (4), (5), related to the Methods I and II (difference of successive radii, and keeping constant the minimum radius) is not appropriate due to high variations of the experimental coefficients. Considering the Table 9, the variations of a and b coefficients in the Method III are 0.128% and 0.301%, respectively. Considering these values, the equation (6) is more appropriate than others in the calculation of

hydraulic gradient by keeping the maximum radius constant.

Table 9. Variation percentage of a and b coefficients in the three methods

Variation percentage	*a*	*b*
Method I	0.671	0.236
Method II	0.294	0.173
Method III	0.128	0.301

In this study, Nash coefficient (E) and Root Mean Square (RMS) are used to measure the hydrological prediction ability as the equations (7) & (8).

$$E = 1 - \frac{\sum_{i=1}^{n}(N_{i(0)} - N_{i(p)})^2}{\sum_{i=1}^{n}(N_{i(0)} - N_m)^2} \quad (7)$$

$$RMSE = \sqrt{\frac{\sum_{i=1}^{n}(N_{i(0)} - N_{i(p)})^2}{n}} \quad (8)$$

In these equations, $N_{i(0)}$, $N_{i(p)}$ and N_m are the observed, predicted and mean values, respectively, and n is the number of the data. The closer the E and RMSE to 1 and 0, respectively, the more suitable the behavior of the model or equation. Table 10 shows the values of E and RMSE to evaluate the three methods related to different depths and levels. According to the Table 10, the values of E and RMSE related to the Method III are closer to 1 and 0, respectively.

Table 10. The values of E and RMSE in the three Methods (*I, I* and *III*)

Depth	z	RMSE			E		
		(I)	*(II)*	*(III)*	*(I)*	*(II)*	*(III)*
52	20	0.0118	0.0007	0.0007	0.4762	0.7143	0.9989
52	35	0.0123	0.0013	0.0007	0.5760	0.4140	0.9993
70	20	0.0082	0.0009	0.0005	0.3759	0.5138	0.9989
70	35	0.0093	0.0007	0.001	0.5759	0.2139	0.9971
70	55	0.0071	0.0004	0.0219	0.3762	0.3144	0.9452
85	20	0.0949	0.0008	0.00061	0.4763	0.7145	0.9991
85	35	0.0057	0.0005	0.0005	0.7760	0.6141	0.95125
85	55	0.0041	0.0007	0.00028	0.8758	0.7137	0.9300
85	80	0.0053	0.0004	0.00057	0.3762	0.7144	0.9776
95	20	0.0044	0.0002	0.0003	0.8761	0.5142	0.8943
95	35	0.8354	0.0003	0.0005	0.9762	0.3143	0.9416
95	55	0.8372	0.0002	0.0005	0.5760	0.6141	0.9971
95	80	0.0043	0.0003	0.000629	0.0763	0.7145	0.9743

D: Depth (cm); z: Water level (cm); RMSE: Root Mean Square; E: Nash Coefficient

For example, the data in Table 6 for the Method III (Equation 6) is provided in Fig. 4 as a relationship between i_{pre} and i_{obs} values and the average velocity. The values of RMSE and E obtained by Table 10 are, respectively, 0.0006 and 0.9991, showing the closeness of i_{pre} values to i_{obs} values using the equation (6). Then this equation would be an appropriate equation for the description of free-surface radial flow behavior.

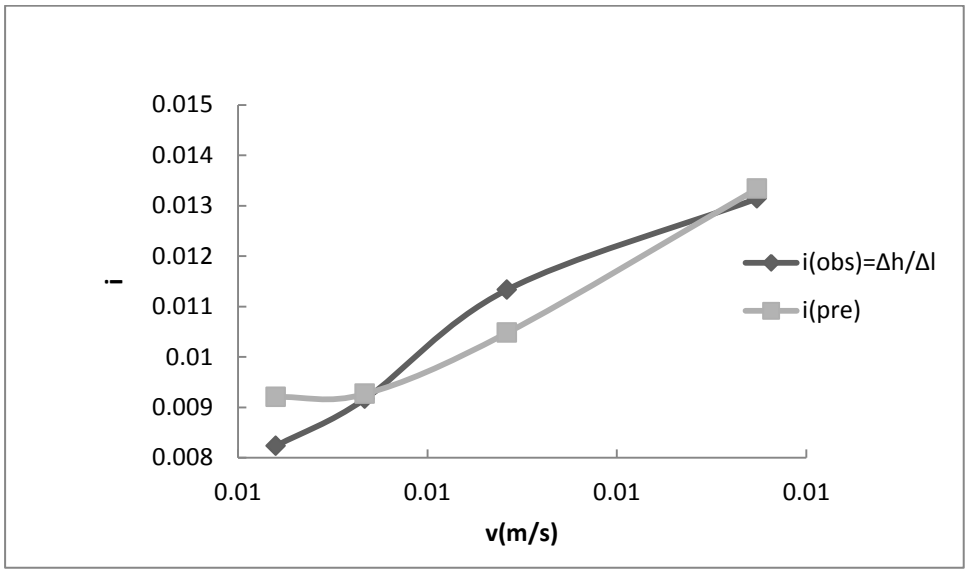


Figure 4. i-v curve for the depth of 85 cm and levels of 20 cm

In order to assess the consistency of the values obtained by the experimental results (observed values) with the values predicted by the equation (6), verification was performed by test data. For verification of the equation (6), the values of *a* and *b* coefficients should be determined for studied aggregates. Table 11 shows *a* and *b* coefficients and their average for the test data.

Table 11. *a* and *b* coefficients used in calculation of the gradient based on the equation (6) for the aggregates tested in this study

	*a**	*b*	*z*	D
	2.542	4.05×10^{-5}	20	85
	2.521	3.58×10^{-5}	55	85
	2.458	3.53×10^{-5}	80	85
	2.394	2.84×10^{-5}	20	95
	2.409	2.96×10^{-5}	35	95
	2.724	4.07×10^{-5}	55	95
	2.748	3.82×10^{-5}	80	95
Average	2.542	3.546×10^{-5}	-	-

* a & b: the coefficients of Forchheimer equation; z: water level(cm); D: depth (cm)

By averaging the experimental coefficients of *a* and *b* and their substitution in the equation (6), a basic equation is obtained for the verification of the proposed equation for tested aggregates as follows:

$$i = V \,/\, (2.542 - 3.546 \times 10^{-5} R^2) \quad (7)$$

In this equation, *i* is the hydraulic gradient, *R* is the average radius, and *V* is the average velocity.

Using the hydraulic gradient values obtained by the Method III and the average radius (R), the velocity of the flow (v_{pre}) was acquired according to the equation (7). Fig. 5 shows the relationship between the hydraulic gradient and the observed and predicted velocities and shows the acceptable consistency of the graphs. According to the Fig. 5, there is a small difference between the values of v_{obs} (average velocity between every point and the most distant point from the center of the well) and v_{pre} (obtained by the equation 7). So, the equation (6) is an appropriate

functional form for the analysis of the hydraulic behavior of the free surface radial flows.

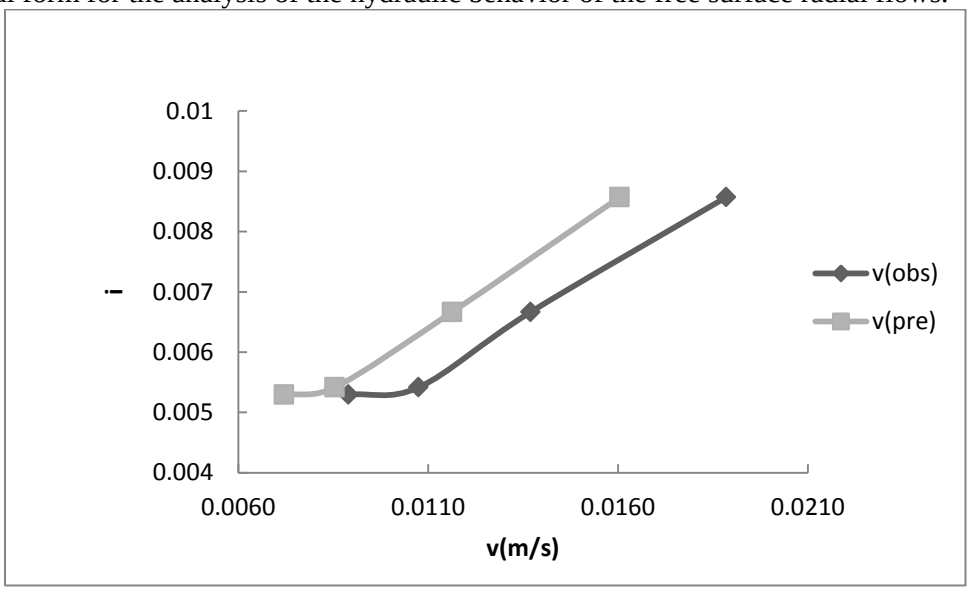


Figure 5. i-v curve for the depth of 110 cm and the levels of 20 cm

4 Conclusions

Equations of fluids in porous media are very useful in designing the rockfill dams, diversion dams, gabions, breakwaters, and ground water reserves. The behaviors of the parallel and radial flows are totally different. Of importance among the differences is the constant and variable cross section of the flow in parallel and radial flows, respectively. This determines the type of variations between the flow velocity and hydraulic gradient along the way, and also variations in the profile of velocity-hydraulic gradient (i-v) curve. A new equation has to be developed which is applicable for the course grained porous media due to the negative coefficient of the nonlinear binomial Forchheimer equation in practical applications of the radial flows on the one hand, and the invalidity of the mentioned equation for the description of the free surface radial flows in the course grained porous media, on the other. Accordingly, in the present paper, a radial flow to the center of a well was modeled by developing a semi cylindrical physical model. Thereafter, different flow parameters were measured, including flow rate, hydraulic gradient, velocity, radial distance from the center of the model and various levels. Then, choosing a series of data as regression data, different equations were obtained for the prediction of hydraulic gradient by the three methods of difference of successive radii, keeping constant the minimum radius and keeping constant the maximum radius. The comparison of the attained the equations and verification of results obtained by them was shown that the functional form of the equation $i = V / (a - bR^2)$ is appropriate for the analysis of the hydraulic behavior of free surface radial flows. This study was performed on a bed with a predetermined grain size and flow rate and in the laboratory conditions. This phenomena is slightly different in nature than what has been observed in the study. This study can be carried out in a porous medium with different granulation, different flow rates and hydraulic gradients and compared to the results of this study. Also, changing the dimensions of the physical model and therefore the boundary conditions, can yield different results.

5. References

1. Ahmed, N., Sunada, D.K.: Nonlinear flow in porous media. J. Hydra. Divi. ASCE. **95**(6), 847-1857 (1969)
2. Bazargan, J., Zamanisabzi, H.: Application of New Dimensionless Number for Analysis of Laminar, Transitional and Turbulent Flow through Rock-fill Materials. Canadian Journal on Environmental, Construction and Civil Engineering. **2**(7), 2011
3. Bazargan, J., Byatt, H.: A new method to supply water from the sea through rockfill intakes. Proceeding of 5th international conference on coasts, ports and marine structures (ICOPMAS), October 14-17, Ramsar, Iran, PP.276-279 (2002)
4. Bazargan, J., Shoaie, M.: Non-Darcy flow analysis of rockfill materials using gradually varied flow theory. Journal of Civil Engineering and Surveying, **44**(2), 131-139 (2010)
5. Ferdos, F., Dargahi, B.: A study of turbulent flow in large-scale porous media at high Reynolds numbers. Part I: numerical validation, Journal of Hydraulic Research. **54** (6), 663-677 (2016 a)
6. Ferdos, F., Dargahi, B.: A study of turbulent flow in large-scale porous media at high Reynolds numbers. Part II: flow physics, Journal of Hydraulic Research, **54** (6), 678-691 (2016 b)
7. Hansen, Garga, V.K., Townsend, D.R.: Selection and application of a one-dimensional non-darcy flow equation for two dimensional flow through rockfill embankment. Can. Geotech. J. **33**, 223-232 (1995)
8. Sadeghian, J., Khayat Kholghi, M., Horfar, A., Bazargan, J.: Comparison of Binomial and Power Equations in Radial Non-Darcy Flows in Coarse Porous Media. JWSR Journal. **5** (1) 65- 75 (2013)
9. Li, B., Garga, V.K., Davies, M.H.: Relationship for non-Darcy flow in rockfill. J. Hydraul. Eng., ASCE. **124**(2), 206-212 (1998)
10. Mc Whorter, D.B., Sunada, D.K.: Groundwater Hydrology and hydraulics. Water Resources Publication, Fort Collins, Colorado, USA, PP. 65-73 (1977)
11. Mc Corquodale J.A.: Finite Element Analysis of Non-Darcy Flow. Ph D Thesis, University of Windsor, Windsor, Canada (1970).
12. Sedghi-Asl, M., Rahimi, H., Farhoudi, J., Hoorfar A., Hartmann, S.: One-Dimensional Fully Developed Turbulent Flow through Coarse Porous Medium. Journal of Hydrologic Engineering. **19**(7), 2014.
13. Nasser, M.S.S.: Radial Non-Darcy flow through porous media. Master of Applies science thesis, University of Windsor, Windsor, Canada (1970)
14. Reddy, N.B.: Convergence factors effect on non- uniform flow through porous media. IE(I) Journal.CV. **86**, (2006)
15. Reddy, N.B., Roma Mohan Rao, P.: Effect of convergence on nonlinear flow in porous media.Hydr. Engrs ASCE. April 420-427 (2006)
16. Sadegian. J.: Nonlinear analysis of radial flow in coarse alluvial beds, Ph.D Thesis, College of Agriculture, University of Tehran, Iran (2013)
17. Das, B.M, Sobhan, K.: Principles of Geotechnical Engineering, Eighth Edition, SI , Publisher, Global Engineering: Christopher M. Shortt; Printed in the USA (2012)
18. Thiruvengadam, M., Pradip Kumar G.N.: Validity of forchheimer equation in radial flow through Coarse granular media. Journal of engineering mechanics, **123**(7), (1997)
19. Venkataraman, P., Roma Mohan Rao, P.: Validation of Forchheimer law for flow through porous Media with converging boundaries. J. of Hydr. Engrs. ASCE. Jan. 63-71 (2000)

20. Ward, J.C.: Turbulent flow in porous media. J. Hydra. Div. ASCE. **95** (6), 1-11 (1964)
21. Wright D.E.: Seepage Patterns Arising from Laminar, Transitional and Turbulent Flow through Granular Media. Ph.D Thesis, University of London, UK 1958.

Journal of Hydraulic Structures
***J. Hydraul. Struct.*, 2017; 3(2): 22-31**
DOI: 10.22055/jhs.2018.24654.1062



OPEN ACCESS

Three-dimensional numerical modeling of score hole in rectangular side weir with finite volume method

Samira Ghotbi[1]
Azam Abdollahi[2]
Mehdi Azhdari Moghadam[3]

Abstract

Local scouring in the downstream of hydraulic structures is one of the important issues in river and hydraulic engineering, which involves a lot of costs every year, so the prediction of the rate of scour is important in hydraulic design. Side weirs are the most important of hydraulic structures that are used in passing flow. This study investigates the scouring due to falling jet from side weir in downstream in side channel numerically. The simulation was done with finite volume method. The comparison of numerical and experimental results of flow fields shows agreement. Results show that from upstream to downstream of side weir located in side channel, scoring is increased and the dimensions of the scour hole in the downstream of the rectangular side weirs increase along it. In fact, at the downstream of the lower edge of side weirs in side channel, scouring has the greatest dimensions; in particular the depth.

Keywords: Scour, Side weir, Three-dimensional Modeling, Finite volume method.

Received: 08 October 2017; Accepted: 06 November 2017

1. Introduction

Side weirs are common hydraulic structures that are used to transfer water from the main canal to the side channel, these structures are used to control flood and divert temporary flow. So far, many studies have been conducted on the discharge coefficient ([1], to [4]) and changes in the geometry of these side weirs ([5], to [7]) in a fixed bed. G. Michellazo, in an experimental study investigated the effect of the moving bed in the main channel on the flow properties of rectangular side weir. Finally, the results showed that the side weir in the moving bed for deviating the flow is much more effective than in the fixed bed [8]. Scouring is a natural

[1] Faculty of Civil Engineering, University of Sistan and Baluchestan, Zahedan, Iran, sami_ghotbi@yahoo.com (**Corresponding author**)
[2] Faculty of Civil Engineering, University of Sistan and Baluchestan, Zahedan, Iran, abdollahiazam@yahoo.com
[3] Faculty of Civil Engineering, University of Sistan and Baluchestan, Zahedan, Iran, mazhdary@eng.usb.ac.ir

phenomenon due to water flow on erosion bed's rivers and canals. Also local scouring is part of the morphological changes of the waterways, which is mainly due to various structures made by human [9]. Up to now, a lot of study has carried out on the local scoring in the downstream of the conserved bed. Farhoudi & Smith, examined the scour profiles in the downstream of hydraulic jump and presented the scour hole according to dimensionless profiles [10]. Balachandar et al., investigated the effect of a tail water depth on scour hole development on a loose bed of cohesion less sand material then provided diagrams for the development of the scour hole at different times [11]. The outflow of hydraulic structures is often as a jet that may causes significant changes in the topography of the river and surrounding these structures. It is caused substantial damages and environmental effects. The jet with high speed creates a great shear stress which often has a critical shear stress to start moving particles. Passing time, bed scour increases scour depth also reduces shear stress that causes a reduction the rate of scour [12]. With time, this leads to equilibrium a scour depth [13]. Equilibrating in the scour depth is an approximation phenomenon [11]. Jo Jong-Song, in a 2D numerical model investigate the local scour alteration in open channels of a tideland dike and concluded as the width of open channel between tideland dikes decreased, due to increased flow velocity, the scoured depth intensely increased [14]. M. Burkow, M. Griebel, investigate a 3D numerical simulation of fluid flow and sediment transport at rectangular obstacle. Results show the typical vortex system for the sediment transport and its interplay with shear stress and transport rates [15]. Török et al., offered a combined application of two bedload transport formulas that extends the application usage. Consequently more suitable simulation results [16].

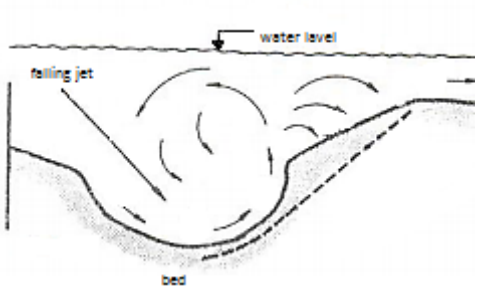


Figure1. Flow pattern of falling jet in score hole

Sediment transmission and Problems concerning its caused existence challenge in hydraulic structures. This subject is studied by engineers and river morphologists. In recent years, hydraulic and sediment science have progressed vastly. For the first time Shields examined the threshold of sediment motion. He presented a diagram that is surveyed the stability of soil channel and rivers. There are several insight for estimating the dimension of scour hole in the downstream of hydraulic structures. Several analytical, experimental, and laboratory relationship has been proposed to determine the depth, width and length of scour hole ([17], [18]). One of the Relationships for estimating the depth of the scour hole in the downstream of Falling jet is Veronese [19]:

$$d_s = 1.9 q^{0.54} H_1^{0.225} \quad (1)$$

That q is flow rate and H_1 is the height of the cascade. The above relation is very simple and just using these two parameters, the depth of the scour hole can be calculated and the effect of

sediment properties is not considered. Another relationship to calculate the depth of scouring is given that In addition to the the above parameters, also the physical properties of the sediment, are considered [20].

$$d_s = 3.27 \frac{q^{0.6} H_1^{0.05} d_w^{0.15}}{g^{0.3} d^{0.1}} \quad (2)$$

g, dw and d, are Gravity acceleration, the depth of tail water depth, and the particle diameter index respectively which, according to their suggestion, is the same as the average particle diameter d50. According to the previews studies, Investigation of scouring in downstream of side wires is unprecedented. Thus in this research a numerical model of scouring due to falling jet from rectangular lateral side weir has been investigated. Although the prediction of scour depth and the estimation of the final shape of the bed by laboratory models seems reasonable, but from the point of view of cost and time, it is not affordable. Using a series of assumptions, the governing equations of the flow and sediment can be simplified. In this research, a three dimensional numerical model is used.

2. Mathematical modeling

In this research, mathematical simulation of flow over the rectangular side weir and sediment transport in the bed of side channel in downstream the side weir has been developed. For this purpose, finite volume (VOF) method has been used for numerical solution of equations. Rectangular cube cells grid has been used for the domain mesh generation. Selection of this grid is because of easy to generation, the proper order and less memory need.

3. Governing equations:

Sediment scouring models are sensitive to the turbulence model because the turbulence model directly affects the viscosity. Using viscosity, the shear stress is calculated locally. Also, for calculating the transport rate and erosion of the load, the local shear stress is used. The RNG turbulence model is mainly recommended for scouring modeling in this software [21] that used in this study. In the present study, following assumptions are used:

(a) An incompressible fluid (water) flows.
(b) The pressure distributed hydrostatically.
(c) Flow is shallow enough thus Vertical accelerations be neglected.
(d) The effects of wind and wave are ignored.

The governing equations for fluid flow in this study are the continuity and momentum equations that are presented below.

Mass continuity equation:

$$V_F \frac{\partial \rho}{\partial t} + \frac{\partial}{\partial x}(\rho u A_x) + R\frac{\partial}{\partial y}(\rho v A_y) + \frac{\partial}{\partial z}(\rho w A_z) + \xi \frac{\rho u A_x}{x} = R_{DIF} + R_{SOR} \quad (3)$$

Where VF is the volume fraction of the flow, ρ is the fluid density, R is the coefficient of the cylindrical or Cartesian coordinates in the equation, R_{DIF} is Disturbance phrase, and R_{SOR} is the mass source. u , v and w represent the velocity along x, y and z. A_x ، A_y and A_z Equal to the fractions of the surface for flow along x, y and z. The first term on the right hand side of the

above equation is related to the disturbances and defined as:

$$R_{DIF} = \frac{\partial}{\partial x}(\rho A_x \frac{\partial \rho}{\partial x}) + R\frac{\partial}{\partial y}(\rho A_y \frac{\partial \rho}{\partial y}) + \frac{\partial}{\partial z}(\rho A_z \frac{\partial \rho}{\partial z}) + \zeta \frac{\rho A_x}{x} \quad (4)$$

And the second term on the right hand side of equation represents the change in density.

$$\frac{V_F}{\rho c^2}\frac{\partial P}{\partial t} + \frac{\partial u A_x}{\partial x} + R\frac{\partial v A_y}{\partial y} + \frac{\partial w A_z}{\partial z} + \xi \frac{u A_x}{x} = \frac{R_{SOR}}{\rho} \quad (5)$$

That P is the pressure and c is the velocity of the wave. The momentum equation in three directions in three dimensions are:

$$\frac{\partial u}{\partial t} + \frac{1}{V_F}\left\{uA_x\frac{\partial u}{\partial x} + vA_y\frac{\partial u}{\partial y} + wA_z\frac{\partial u}{\partial z}\right\} - \xi\frac{A_y v^2}{xV_F} = -\frac{1}{\rho}\frac{\partial P}{\partial x} + G_x + f_x - b_x - \frac{R_{SOR}}{\rho V_F}(u - u_w - \delta u_s) \quad (6)$$

$$\frac{\partial v}{\partial t} + \frac{1}{V_F}\left\{uA_x\frac{\partial v}{\partial x} + vA_y\frac{\partial v}{\partial y} + wA_z\frac{\partial v}{\partial z}\right\} + \xi\frac{A_y v u}{xV_F} = -\frac{1}{\rho}\frac{\partial P}{\partial y} + G_y + f_y - b_y - \frac{R_{SOR}}{\rho V_F}(v - v_w - \delta v_s) \quad (7)$$

$$\frac{\partial w}{\partial t} + \frac{1}{V_F}\left\{uA_x\frac{\partial w}{\partial x} + vA_y\frac{\partial w}{\partial y} + wA_z\frac{\partial w}{\partial z}\right\} = -\frac{1}{\rho}\frac{\partial P}{\partial z} + G_z + f_z - b_z - \frac{R_{SOR}}{\rho V_F}(w - w_w - \delta w_s) \quad (8)$$

f_x ،f_y and f_z parameters are the viscosity accelerations and G_x ،G_y and G_z are Volumetric accelerations and b_x ،b_y and b_z are Flow drops in permeable environments.

4. Computational domain:

In order to validate the numerical model in this study, the experimental results of rectangular side weir were studied by Bagheri and Haydarpour [22], is used. The specifications of the hydraulic structure are as follows. The main channel was designed with a length of 3 meters and a width of 0.4 meters and a height of 35/0. The rectangular side weirs location is 1.8 meters from the beginning of the channel. The side weirs specifications is presented in the table below. The side channel is along the main channel with a same width to main channel. Bottom of the side channel has been covered with aggregate materials. Sediment height at the bottom of the side channel is 10 cm. The diameter of sediment aggregates in this study is equal to 0.005 mm and their density is 2650 kg / m3.

Table1. Specifications of side weir [22]

inflow (m3/s)	Length (cm)	Height (cm)
0.042	30	15.4

Sediment characteristic parameters in the side channel are presented in table 2. The soil is cohesion less.

Table2. Specifications of sediment

Bed loading Suspension coeff.	Critical shields	Bed loading coeff.	Angle (degree)
0.018	0.05	8	32

The coefficient of bed loading and bed loading in this numerical model are defined as the sediment components. The first step in calculating the critical Shields number is to compute the

dimensionless parameter R_i^*.

$$R_i^* = d_{s,i}\frac{\sqrt{0.1(\rho_{s,i}-\rho_f)\rho_f \|g\| d_{s,i}}}{\mu_f} \quad (9)$$

Using the above equation, the critical Shields number is calculated from the following equation.

$$\theta_{cr,i} = \frac{0.1}{(R_i^*)^{\frac{2}{3}}} + 0.054[1-\exp(\frac{-R_i^{*0.52}}{10})] \quad (10)$$

5. Boundary Conditions:

The boundary conditions for the walls in main and lateral channel are Wall no slip condition. The symmetry boundary condition, for the water surface boundary, fixed velocity with the specified head for the input channel and the continuative boundary condition for downstream boundary is used. It is assumed that inlet flow is a fully developed flow. This assumption was reasonable.

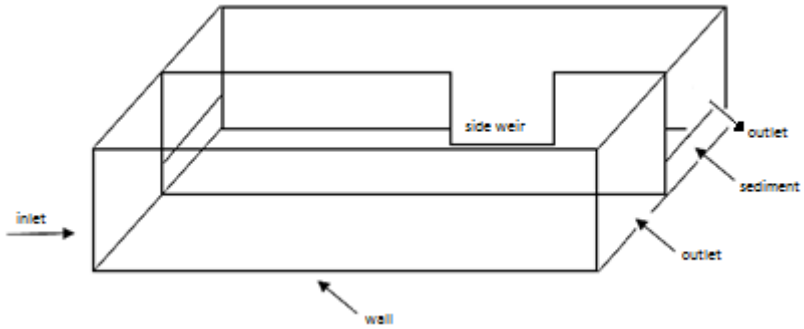


Figure2. scheme for computational domain and boundary conditions

6. Model Validation:

Given that only at the bottom of the side weirs, i.e. in the sub-channel of sediment and there is no deposition in the main channel, the flow conditions are precisely the same as the flow field in the range of side weirs of laboratory without sediment models. And for validation, the results of similar laboratory models can be used. To this purposes, Bagheri et al.'s [21] laboratory model has been used. Therefore, it is used to confirm accuracy of flow velocity profile on the side weir. As can be seen, the results are reasonable.

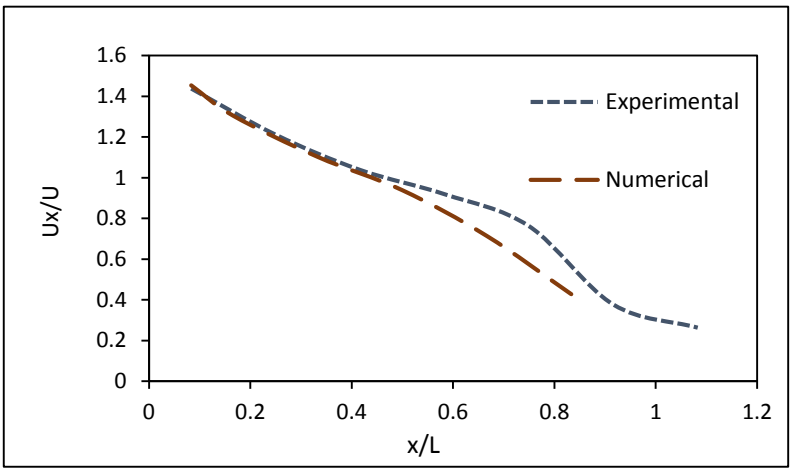


Figure4. Comparison of the normalized velocity-length profiles obtained from the mathematical and Bagheri et al.'s laboratory [22] model

7. Results and Discussion:

Figure 5-7 shows the scour depth at the three upstream, downstream, and center points in the channel cross-section. As you can see, the scouring rate in the downstream is increased by moving from the top of the weirs to the end of it. This indicate increased eddy velocities during the side weirs. The maximum scour at the lateral side of the side weir is 5.76 cm. The times are relative and represent to the balance for scouring equilibrium.

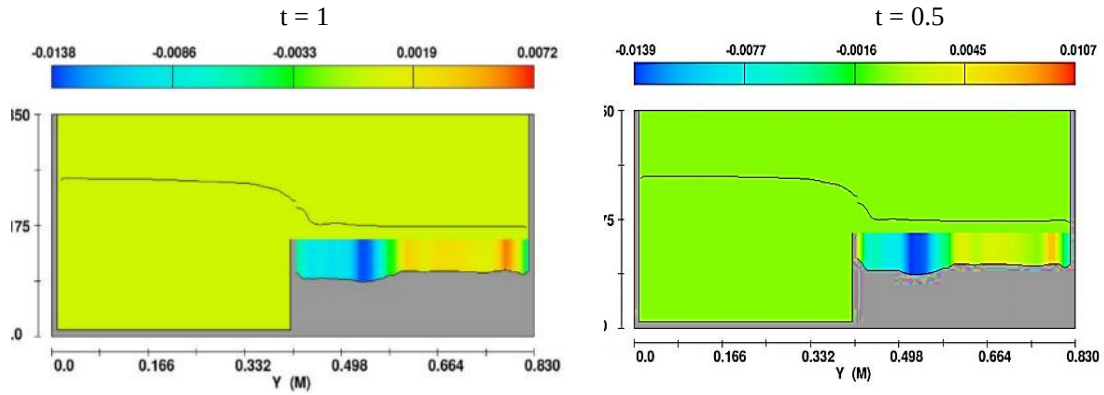


Figure 5. Cross section of the channel at the upstream of side weir(x = 1.8 m)

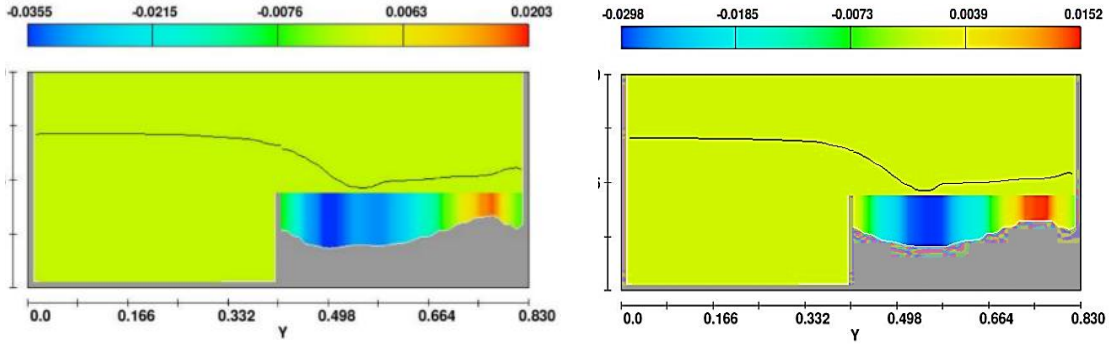


Figure 6.- Cross section of the channel at the center of side weir (x = 1.95 m)

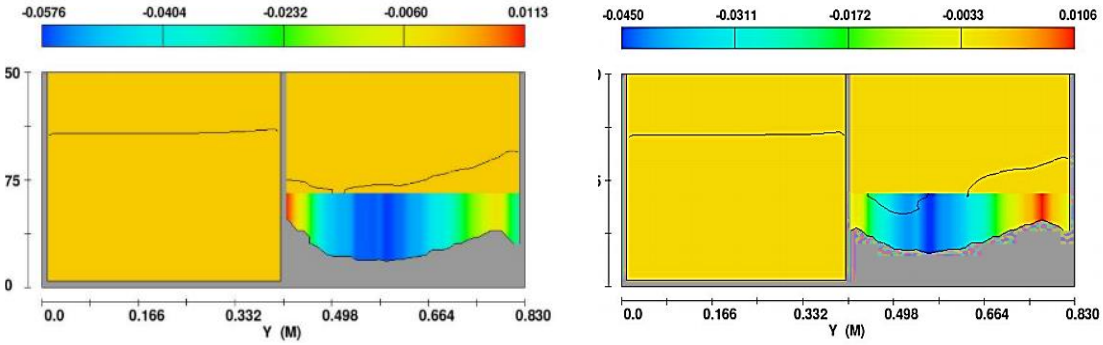


Figure 7. Channel cross section in downstream of side weir (x = 2.1 m)

Figure 8, which is related to scouring in the downstream of side weirs, Compared the maximum depth of the scour hole in the three upstream, downstream, and center points of side weirs. As it can be seen, at all three points in the downstream of the side weirs, the greatest amount of scouring occurs in the initial times, and then the slope of the changes and the scouring is reduced to equilibrium.

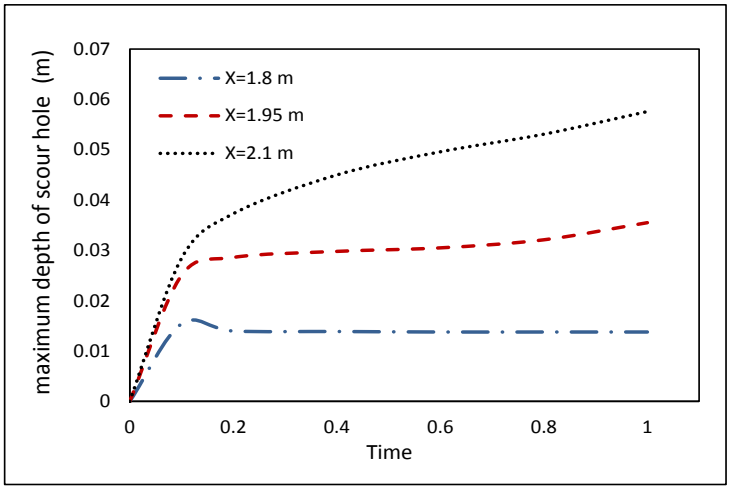


Figure 8. Comparison of maximum depth of the scour hole in upstream, downstream, and center points of the side weirs

As can be seen, Figure 9 shows the variation of scour along the sub channel during the simulation. What emerges from this is that as time progresses, scour is increased and the dimensions of the scour hole (length, width and depth) are increasing. There are also other points around the hole that have scoured and have eroded in very small parts, due to the creating flow of falling jet from the weir. Also, points with brown and red colors around the hole represent the sedimentary hills caused by the sediment deposition in the downstream of weir. In fact, at these points, the height of the bed is increasing. The negative sign in this figure indicates a decrease in depth and scour, and a positive sign indicates an increase in the depth and formation of sedimentary hills. Figure 10 shows the scouring pattern in the sub-channel. As can be seen, the depth of the scour hole in the downstream of weir is higher at the lower edge than the other points.

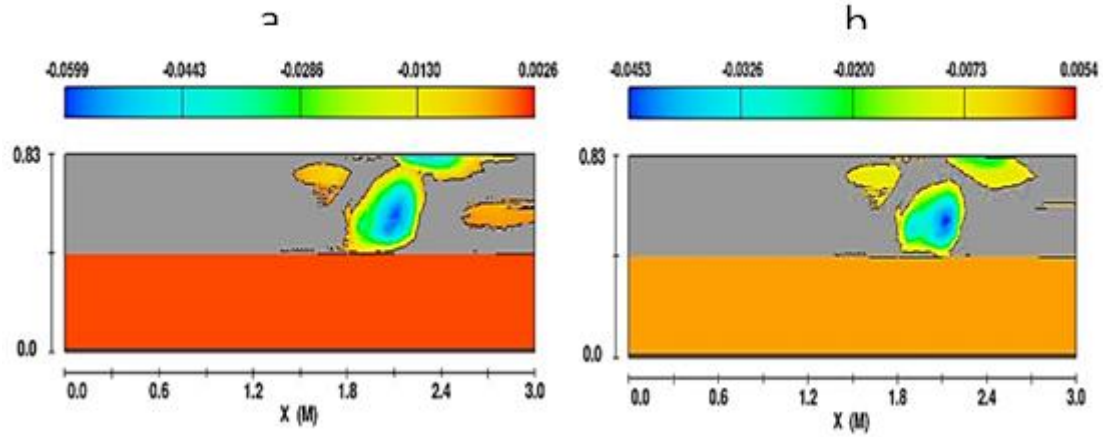


Figure 9. plan for scoring in lateral channel

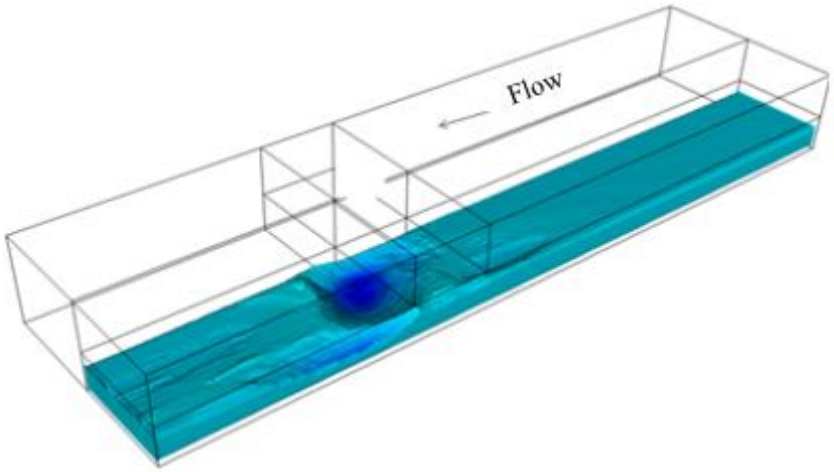


Figure 10. score hole in downstream of side weir

As shown in Fig. 11, from the upstream to the downstream of the weir, due to the increase in velocity, the kinetic energy is increased and has the highest value at the lower edge of the weir. Also, over time, this amount has increased. In general, in areas where scouring occurs, the amount of kinetic energy is higher than other areas. This figure is in agreement with previous figures to scouring changes.

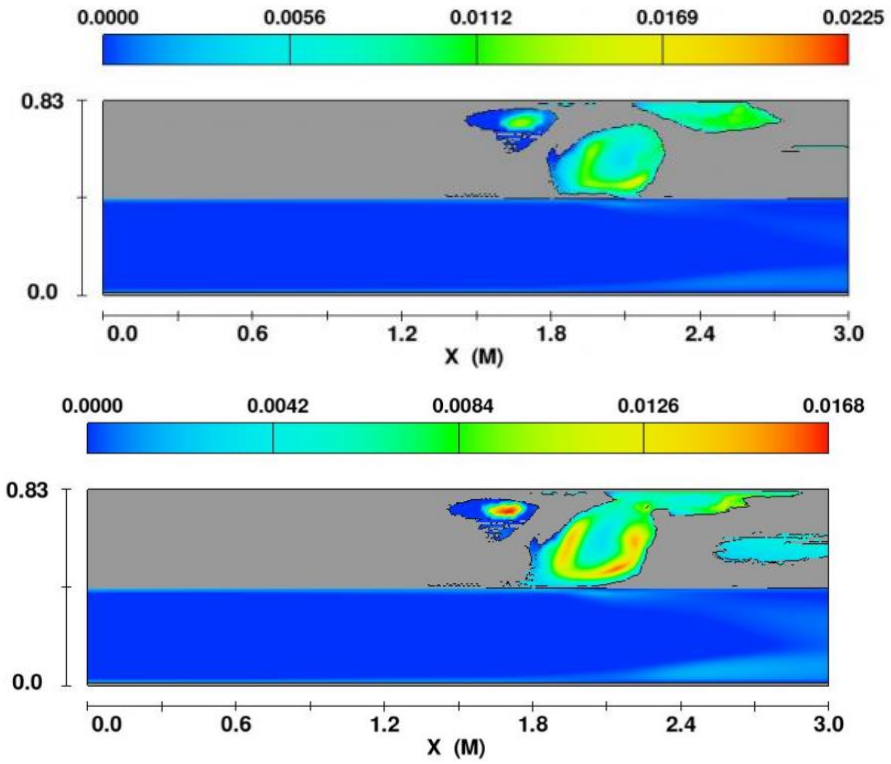


Figure11. Turbulent kinetic energy in downstream of side weir in side channel

8. Conclusions

The issue of sediment, its transmission and the problems due to its existence in hydraulic structures is a serious subject studied by river engineers and morphologists. Side weirs are the hydraulic structures used to transfer water from the main channel to the sub channel in order to flood control and temporary flow transmission. At the downstream of these side weirs, due to falling jet, erosion and scouring occur that results destruction in downstream and impose much cost. Therefore, the investigation of the dimensions of the scour at the downstream of these structures is very important and can be used in hydraulic design related to downstream protection. The present study numerically investigated this issue with finite volume method and RNG turbulence method. The results of simulations to scouring equilibrium indicate that the dimensions of the scour hole in the downstream of the rectangular side weirs increase along it. In fact, at the downstream of the lower edge of side weirs, scouring has the greatest dimensions and in particular the depth. Also, sedimentary hills around the hole indicate the accuracy of this result. This is due to the increase in the flow velocity over the weir from the upstream to downstream, which increases the kinetic energy and, as a result, the shear stresses that arise at the downstream are more than the critical shear stress of the sediment particles and consequently erosion and scouring occur.

9. References

1. Swamee PK, Pathak SK, Ali MS, (1994). Side-weir analysis using elementary discharge coefficient. Irrigation and drainage engineering, pp: 120(4):742-55.
2. Singh R, Manivannan D, Satyanarayana T, (1994). Discharge coefficient of rectangular side weirs. Irrigation and Drainage Engineering, pp: 120(4):814-9.
3. Borghei SM, Jalili MR, Ghodsian MA, (1999). Discharge coefficient for sharp-crested side weir in subcritical flow. Hydraulic Engineering, pp: 125(10):1051-6.
4. Ghodsian M, (2003). Supercritical flow over a rectangular side weir. Canadian Journal of Civil Engineering, pp: 30(3):596-600.
5. Cheong HF, (1991). Discharge coefficient of lateral diversion from trapezoidal channel. Irrigation and Drainage Engineering, pp: 117(4):461-75.
6. Emiroglu ME, Kaya N, Agaccioglu H, (2009). Discharge capacity of labyrinth side weir located on a straight channel. Irrigation and drainage engineering, pp: 136(1):37-46.
7. Kaya N, Emiroglu ME, Agaccioglu H, (2011). Discharge coefficient of a semi-elliptical side weir in subcritical flow. Flow Measurement and Instrumentation, pp: 22(1):25-32.
8. Michelazzo G, Minatti L, Paris E, Solari L, (2016). Side Weir Flow on a Movable Bed. Hydraulic Engineering, pp: 142(6):04016007.
9. Hoffmans G. J. C. M, Pilarczyk K. W, (1995). Local scour downstream of hydraulic structures. Hydra. Eng, pp: 121(4): 326-340.
10. Farhoudi J, Smith K. V. H, (1985). Local scour profiles downstream of hydraulic jump. Hydra. Res, pp: 23(4): 343-358.
11. Balachandar R, Kells J. A, Thiessen R. J, (2000). The effect of tailwater depth on the dynamics of local scour. Can. J. Civ. Eng, pp: 27, 138-150.
12. Kells J. A, Balachandar R, Hagel K. P, (2001). Effect of grain size on local channel scour below a sluice gate. Can. J. Civ. Eng, pp: 28, 440-451.
13. Kurniawan, A., Altinakar, M. S. Graf, W. H. (2001). Flow pattern of an eroding jet. Proceedings of XXIX IAHR Congress, Beijing, China.
14. Jo J. S, (2017). Numerical Simulation of Scour Depth in Open Channels of Tideland Dike. American Journal of Naval Architecture and Marine Engineering, pp: 9(4):91-98.
15. Burkow M, Griebel M, (2015). A full three dimensional numerical simulation of the sediment transport and the scouring at a rectangular obstacle. Preprint submitted to Elsevier.
16. Török G. T, Baranya S, Rüther N, (2017). 3D CFD Modeling of Local Scouring, Bed Armoring and Sediment Deposition. Water, pp: 9(1):56.
17. Martins RB, (1975). Scouring of Rocky River beds by free jet spillways. Int. Water Power Dam Constr, pp: 27(4):152-3.
18. Rajaratnam N, Mazurek K, (2003). Erosion of sand by circular impinging water jets with small tailwater. Hydraulic Engineering, ASCE, pp: 129(3):225-229
19. Veronese A., Erosion of a bed downstream from an outlet, Colorado A & M College, Fort Collins, United States, 1937.
20. Mason PJ, Arumugam K, (1985). Free jet scour below dams and flip buckets. Hydraulic Engineering, pp: 111(2):220-35.
21. Brethour J, Burnham J, (2010). Modeling sediment erosion and deposition with the FLOW-3D sedimentation & scour model. Flow Science Technical Note, FSI-10-TN85, pp: 1-22.
22. Bagheri S, Heidarpour M, (2011). Characteristics of flow over rectangular sharp-crested side weirs. Irrigation and Drainage Engineering, pp: 138(6):541-7.

Journal of Hydraulic Structures
***J. Hydraul. Struct.*, 2017; 3(2):32-46**
DOI: 10.22055/jhs.2018.24900.1065



OPEN ACCESS

Experimental Study of the Effect of Base-level fall at the Beginning of the Bend on Reduction of Scour around a Rectangular Bridge Pier Located in the 180 Degree Sharp Bend

Mohammad Vaghefi[1]
Mohammad Moghanloo[2]
Danesh Dehghan[2]
Arsalan Keshavarz[2]

Abstract

Base-level fall in river beds occurs due to varying natural or unnatural causes. Base-level fall causes the change in the behavior of flow at the location of drop in base-level. In such situations, most of scour occur at the foot of the slope, and slope wall retreats in the upstream direction. This phenomenon widens the wall of the river bank, thus leading to its destruction. The amount of bed topography variations and scour around a rectangular bridge pier with an oblong nose located in the 90 degree angle of a 180 degree sharp bend was studied in this work by generating base-level fall at the beginning of the 180 degree sharp bend, and it was compared with a case without a base-level fall. The results indicated that in the case of base-level fall at the upstream side of the bridge pier, increase in flow depth, as well as reduction in velocity at the area around the pier, is observed, and the maximum depth of scour hole and the volume of scour hole around the pier respectively reduce by 73 and 97% in comparison with those in the case where no base-level fall occurs.

Keywords: 180 degree sharp bend, base-level fall, scour, bridge pier, topography.

Received: 18 October 2017; Accepted: 25 November 2017

1. Introduction

As in all the other natural phenomena, rivers tend to preserve their sustainability system. Hence, any geometric or hydraulic change in rivers entails a dynamic response from the river in order to restore equilibrium. Such a response is at times too widespread and uncontrollable. Base-level drop and bed erosion in rivers result in an abrupt change in bed slope and generation of knickpoints, all leading to base-level fall. In geomorphology, knickpoints are a part of rivers

[1] Civil Engineering Department, Persian Gulf University, Bushehr, Iran. vaghefi@pgu.ac.ir (**Corresponding author**)
[2] Civil Engineering Department, Persian Gulf University, Bushehr, Iran.

CC BY

or channels, causing discontinuities on the slope and bed level of channels, and they occur vertically or inclined on channel bed.

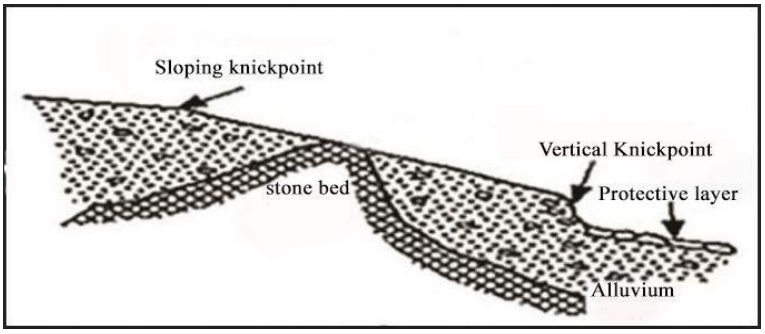


Figure 1. Inclined and vertical knickpoints (Julien, 2002)

Knickpoints make river beds unstable. River system confronts bed degradation and erosion at the upstream, and sedimentation at the downstream sides of the knickpoint. This process means expansion and migration of the knickpoint, damage to surrounding structures and lands, and bed topography variations. Several studies have been conducted on bed level variations before, a summary of which is presented in the following:

Brush and Wolman (1960) carried out an experimental study of the behavior of a drop in a bed constituted of non-cohesive material. The generated knickpoints in these experiments retreated from base-level fall. Consequently, the slope at the upstream side of the drop sharpened, while the downstream slope reduced. Transported sediments settled in the form of dunes at the downstream side of base-level fall. Holland and Pickup (1976) studied the knickpoint transport at the layered and cohesive sedimentary bed by creating a base-level fall in a laboratory flume. The results indicated that placing a thin sand layer through cohesive layers reduces the retreat velocity of the knickpoint in upstream direction. Begin et al (1980) examined knickpoint transport in upstream direction by making a base-level fall in a 15-meter-long laboratory flume with a 1% slope. The results revealed that under constant discharge, the velocity of knickpoint transport upstream is reduced in time. May et al. (1989) experimentally analyzed knickpoint erosion under the influence of hydrodynamics and geology factors. Results showed that knickpoint erosion depends on factors including knickpoint geometry, water velocity, and the pressure developed at the downstream side of the knickpoint, so that the occurrence of base-level fall as well as water velocity and pressure drop can help control bed erosion at the downstream side of the knickpoint to a great extent. Garcia and Parker (1993) conducted an experimental study of water jump resulting from a turbid flow by creating base-level fall in a channel. The results indicated that varying the level in a turbid flow (converting a supercritical flow into a subcritical flow due to water jump) leads to a great decrease in bed shear stress at the downstream side of the water jump. Migeon et al. (2011) studied the effect of changing the slope on turbid flows existing in nature by using field data. Their results demonstrated that the hydraulic jump caused by slope reduction leads to a drop in velocity of the turbid flow and in bed shear stress; thus the sediments of turbid flow in this zone suddenly settle. Turmel and Locat (2012) created a base-level fall in a laboratory flume in order to examine factors influencing the knickpoint displacement towards upstream under turbid flow conditions. The results suggested that upstream movement of knickpoint in a turbid flow occurs as a result of two erosive factors of turbid flow and the process of sedimentary material slippage at the upstream side of the base-level fall area. Cantelli and Muto (2014) conducted an experimental study on the effect of an abrupt drop at the base-level of the river on formation of knickpoints

migrating upstream. The drop caused numerous staircase knickpoints on the bed of the channel, all of which retreated in upstream direction, and a hydraulic jump occurred on every stair. The results indicated that an abrupt change in base-level led to conversion of the supercritical flow into a subcritical flow at the downstream side of the slope, thus reducing bed shear stress of the flow at the downstream side of the slope. Grimaud et al (2016) experimentally examined the profile of river and knickpoint, and concluded that for a constant rate of base-level fall, knickpoints of similar forms occur. Retreat velocity, the front slope angle, and the hole depth at the downstream side of the knickpoint highly depend upon the structure of bed material. Also, time intervals between knickpoint formations depend on bed thickness and rate of base-level drop. Meandering rivers are the most common type of rivers in plan. However, a comprehensive study is yet required to be conducted on base-level variations in a bend.

The current study experimentally addresses a method of preventing destruction of downstream structures, and retreating erosion. In this method, the amount of local scour around a rectangular bridge pier with an oblong nose located in the 90 degree position is examined by dropping base level at the beginning of a 180 degree sharp bend and creating a base-level fall. Bed topography variations, material displacement at the beginning of the bend and the sideway banks, and the difference in the maximum scour, dimensions, and the volume of scour hole were studied.

2. Materials and Methods

Experiments were carried out in a bended channel with a 180 degree bend. Figure (2) depicts the channel. This rectangular channel is 1 meter wide and 70 cm high at the section. The straight upstream- and downstream-directed paths are respectively 6.5, and 5 meters long. The central curvature radius of the bend is 2 meters. With a ratio of R/B=2, according to classification proposed by Leschziner & Rodi (1979), this channel falls into the category of sharp bends, where R denotes the central radius of the bend, and B the channel width. Considering the research efforts by Chiew & Melville (1987), the standard deviation of sediment particles must be less than 1.3 in order to preserve the effect of non-uniformity of particles on scour. Also, according to experiments conducted by Raudkivi & Ettema (1983) aiming at prevention of ripple formation upstream, the average diameter of the particles must not be smaller than 0.7 mm. Hence, particles with an average diameter of 1.5 mm and standard deviation of 1.14 were employed in this laboratory. All the experiments were conducted under inception motion conditions with a ratio of flow velocity to critical velocity (U/U_c) equal to 0.97.According to Oliveto & Hager (2002), in order to prevent roughness effects, the water depth must exceed 20 mm; therefore, a discharge capacity of 70 liters per second and a depth of 18 cm were selected for conducting the experiments.

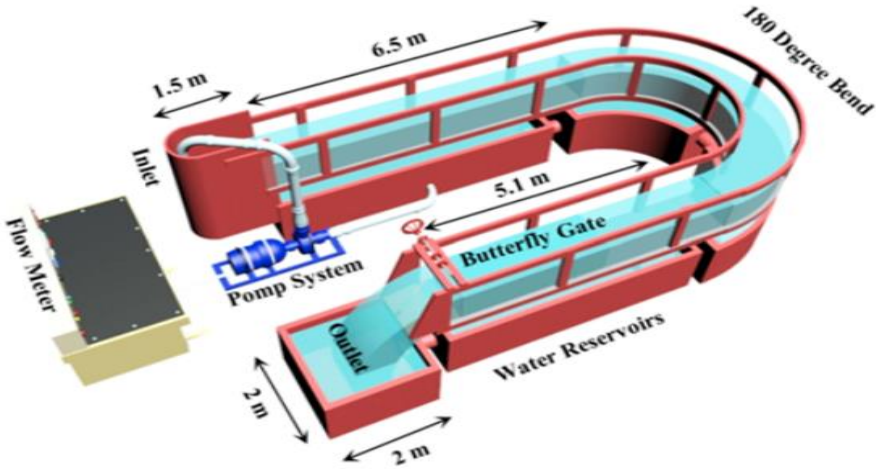


Figure 2. Laboratory flume employed by Vaghefi et al (2016)

As suggested by Chiew & Melville (1987), pier diameter must not exceed 10% of channel width, so that the effect of walls on local scour around the pier will fade. Additionally, as recommended by Melvill & Sutherland (1988), the length of the rectangular pier must be at least 3 times its width. Therefore, a 20 cm long, and 5 cm wide pier (L/b=4) was used for the experiments, where L denotes length and b is the pier width. The pier is made of PVC, and cut by CNC. Prior to the experiments, the whole bed was cleared by a metal plate connected to a cart moving on the rail, so that the upstream straight channel was covered by 30 cm of material, and the bed from the beginning of the bend to the end of the downstream straight path was covered by 20 cm of material. Then, the pump was turned on, and water was slowly let into the channel. As water level rose, when the sediments were evidently wet, and in a period of about 40 minutes, the motor rotation was gradually increased up to 70 liters per second. Also, at the end of the experiment, when the pump was turned off, and after 2 hours of full drainage, bed topography was collected by using ± 1 mm laser meter. Figure (3) illustrates base-level drop at the beginning of the bend. Such a drop encompasses the beginning of the bend to the end of the downstream straight path. Base-level drop was achieved with a 20 degree angle (slope of 36%) in proportion to horizon, and a 30-meter-long sloped.



Figure 3. Base-level fall from the beginning of the bend to the end of the downstream straight path

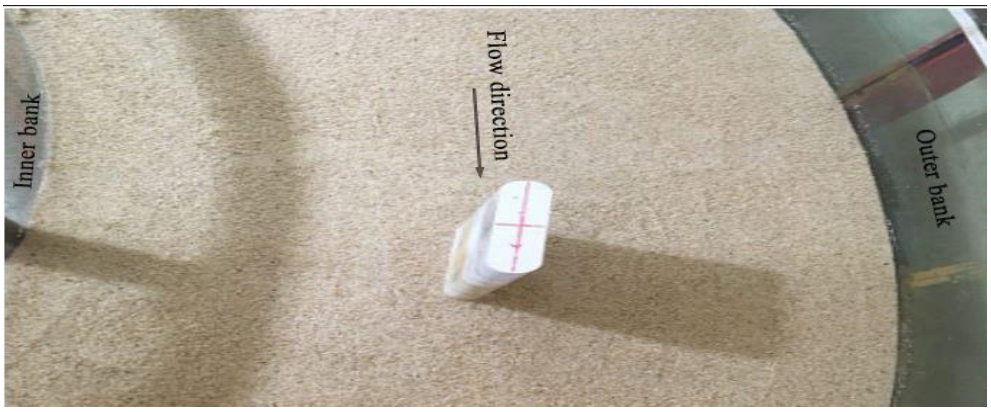


Figure 4. A view of the rectangular pier with an oblong nose, located in the 90 degree position in the 180 degree sharp bend

In the first stage, a 34-hour-long equilibrium time test was carried out on the oblong-nosed rectangular pier located in the 90 degree bend without changing the base level in order to determine the relative equilibrium time for conducting the experiments. In the equilibrium time test, increase in the maximum scour depth (d_s) was continuously measured in time. Measurement lasted until 4 hours of consecutive intervals did not reveal any perceptible change in the maximum scour depth. As is observed in Figure (5), approximately 95% of the maximum scour occurred in the first 15 hours of the experiment, which is in agreement with the results of Melville & Chiew (1999). Therefore, 15 hours was selected as the relative equilibrium time for conducting each experiment.

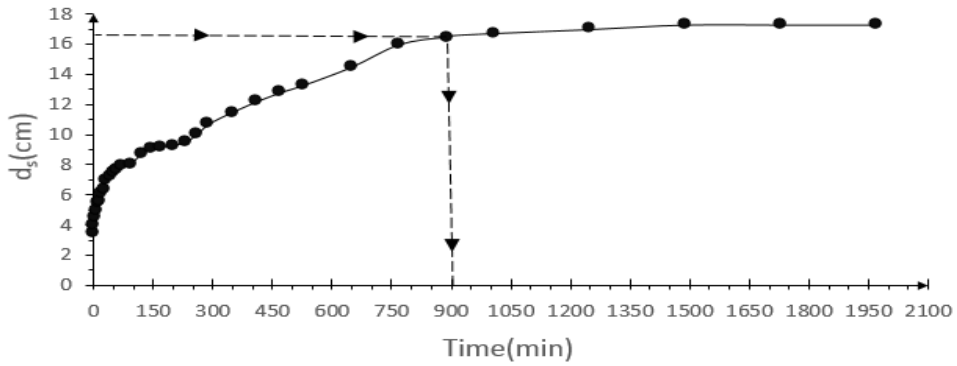


Figure 5. Variations of the maximum scour depth in time in the test on equilibrium time

Three tests were run in order to conduct the experiments and study the effect of base-level fall on reduction of scour around the rectangular bridge pier, and bed topography variations. First, a test was conducted in order to investigate bed topography variations in the bed without creating base-level fall, and with a bend empty of pier along the flow. This aimed to help identify the behavior of the bend when there are no base-level changes or existing hydraulic structures, under the influence of hydraulic conditions. The second test was run in order to examine bed topography variations in the bend by placing the rectangular bridge pier with an oblong nose in the 90 degree position of the bend without creating base-level fall.

This experiment aimed at studying the effect of placing the pier in this position on bed topography variations and amount of scour in comparison with the experiment on the bend

without a pier. The third test was conducted with the aim of examining the effect of drop on bed topography of the bend and scour around the rectangular bridge pier. The results are addressed in the following section.

3. Results and Discussion

After determination of the relative equilibrium time, the experiment was conducted in an empty bend without a pier in order to provide a better understanding of flow behavior and bed topography variations in the bend. Bed topography after equilibrium time is presented in Figure (6). As is evident in the figure, bed topography in the bend is accompanied by sedimentation at the inner bank as well as erosion at the outer bank, due to formation of helical flows.

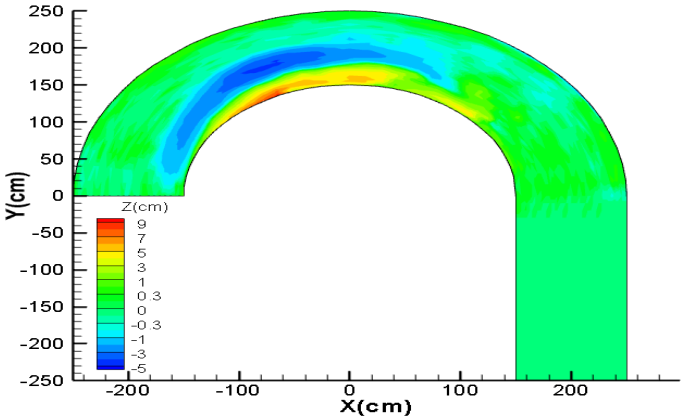
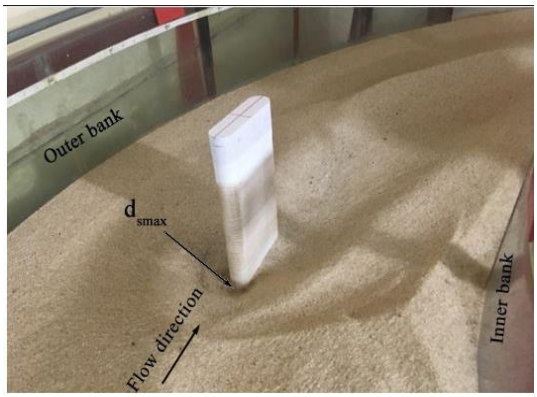
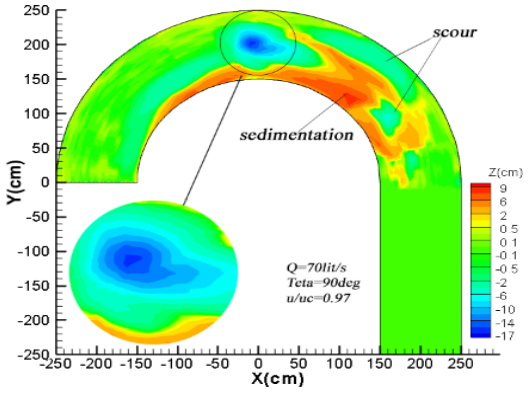


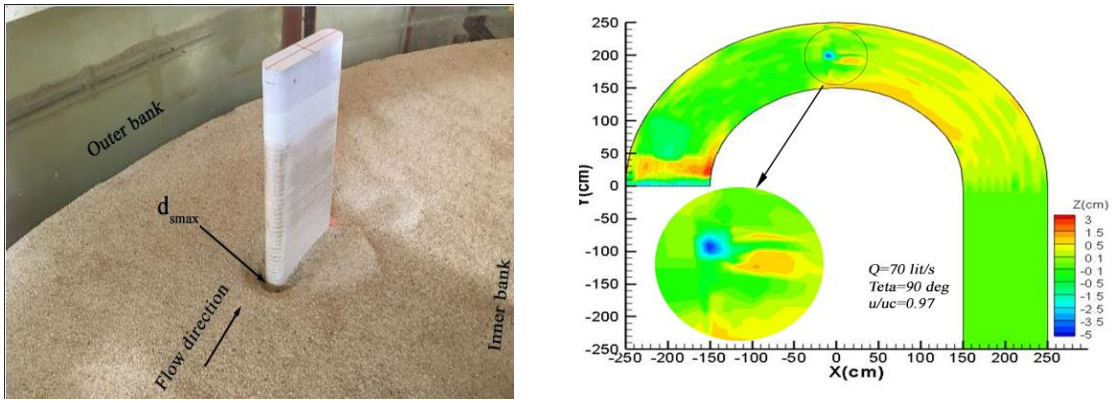
Figure 6. Bed topography variations in the case of empty bend (without a pier)

As noted in Figure (6), sedimentation in the vicinity of the inner wall began at the 35 degree and lasted until the 145 degree angle. The maximum sedimentation has occurred for 8.7 cm (equivalent to 0.087 times the channel width) in the 65 degree position. Further, the scour began at the 35 degree angle and lasted until the 95 degree angle, as is observed in the figure. The maximum scour also occurred for 4.2 cm (equivalent to 0.042 times the channel width) at the 65 degree angle. Results refer to the maximum degree of helical flow strengths at the 60 to 70 degree interval of the bend. Then, a better understanding of the effect of base-level fall in the presence of the pier on bed topography of the bend is achieved by conducting the following experiments and comparing their topographies with the experiment on the bend without a pier.

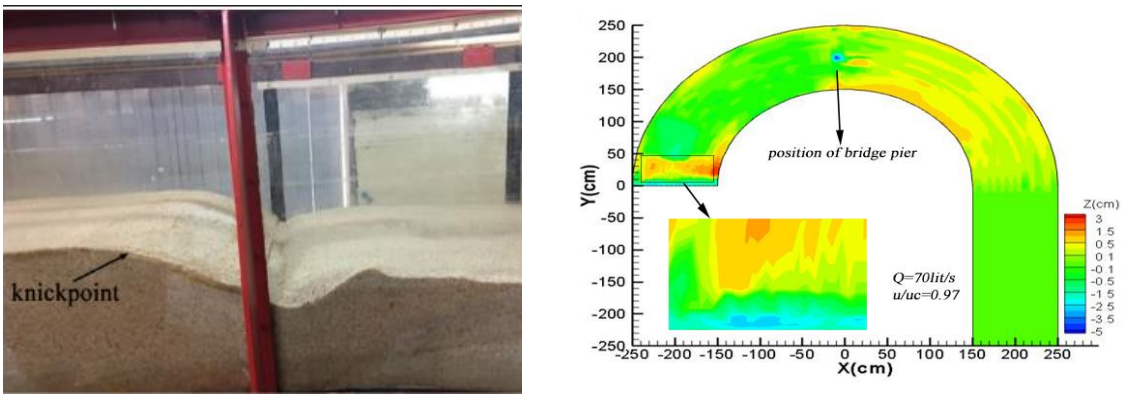




(a)



(b)



(c)

Figure 7. bed topography variations of the experiment on the oblong-nosed rectangular pier in the 90 degree position of the bend a) without base-level drop, b) with base-level drop, and c) for the hole created at the beginning of the bend due to water crossing the inclined surface

As is seen in Figures 7-a, and 7-b, the maximum scour at the pier nose (the 87 degree angle) occurred in both experiments. This maximum scour depth in the case of no base-level fall was equal to 3.3 times the pier width, and it was equal to 0.9 times the pier width in the case of base-level fall. Comparison reveals a 73% reduction in the maximum scour depth due to base-level drop. This could be due to the fact that, according to continuity equation, with base-level drop and raise in water depth, the velocity of water reduces upon entering the bend, thus reducing the strength of horseshoe vortices generated as a result of the collision of water with the pier and helical flows. This has led to a significant reduction in the maximum depth and width of scour hole, and decrease in sediments advancing towards the downstream side of the pier in the case of base-level drop. It should be noted that at the onset of the experiment at the beginning of the bend, a hole with the maximum depth of 0.6 times the pier width is created due to water crossing an inclined surface with formation of falling submerged flows (Figure 7-c).

Figure (8) shows scour holes created around the pier in the experiments with and without base-level drop, as well as the hole created at the beginning of the bend as a result of the falling submerged flow crossing the inclined surface. Surfer software was employed for the sake of

more precise calculations in measuring the volume of the hole, and drawing the figures. As presented in Figures 8-a and 8-b, the volume of the hole created around the pier in the case of no base-level drop and in the case of base-level drop, is respectively around 28750 and 750 cm^3, equal to 230 and 6 times the third power of the pier width. Also, according to Figure 8-c, due to falling submerged flow crossing the knick point and the inclined surface, a wide hole of $3500cm^3$, equal to 28 times the third power of the pier width, is formed at the beginning of the bend.

Figure (9) presents an instance of cross sections along the bend. Figure 9-a presents sedimentation in the vicinity of the inner bank in the case of empty bend (without a pier), and the case without base-level fall. This sedimentation may be due to the effect of the onset of the bend and change in flow conditions under the influence of the sharp bend. Also, in the case of base-level fall, because the base-level fall created at the beginning of the bend extended all through the channel width, the width of the created hole in this area occupied 100% of the channel width, forming a wide hole. Figure 9-b depicts a transverse profile of the channel at a distance equal to 17 times the pier depth in the upstream direction (the 65 degree position). As is observed, in the cases of the bend without a pier, and no base-level fall, sedimentation in the vicinity of the inner bank is respectively 1.65 and 1.15 times the pier depth, the fact which is due to the effect of the secondary flows, their interaction with longitudinal flows, and formation of helical flows in the bend. The maximum scour in this section occurs in the case of the bend without a pier. This scour is 0.84 times the pier width, and occurs at a distance of 0.4 times the channel width from the inner bank. Also, the bed in this section undergoes little change in the case of base-level fall. Figure 9-c, the cross section is at a distance of 3 times the pier width towards the upstream side of the pier. This section undergoes the maximum sedimentation in the case of empty bend. Such sedimentation occurs at a distance of 0.05 times the channel width from the inner bank, at a height of 0.38 times the pier width. The maximum scour in this section occurs in the case of no base-level fall at a distance of 0.52 times the channel width from the inner bank at a depth of 2.68 times the pier width. This scour is a result of proximity to the pier, and presence of horseshoe vortices. This section also undergoes little change in the case of base-level fall. As provided in Figure 9-d, the scour hole, created at the pier nose, has occupied 60% of channel width in the case of no base-level fall. However, after creating a base-level fall, the created hole has occupied only 8% of channel width. Then it can be stated that base-level fall has led to 87% decrease in the width of scour hole. The maximum scour depth in the cases with and without a base-level drop is respectively 16.6 and 4.5 cm, equal to 3.32 and 0.9 times the pier width, i.e. a 73% reduction in the maximum scour depth due to base-level drop. The maximum sedimentation of this section occurs for the empty bend, equal to the pier width at a distance of 0.05 times the channel width from the inner bank.

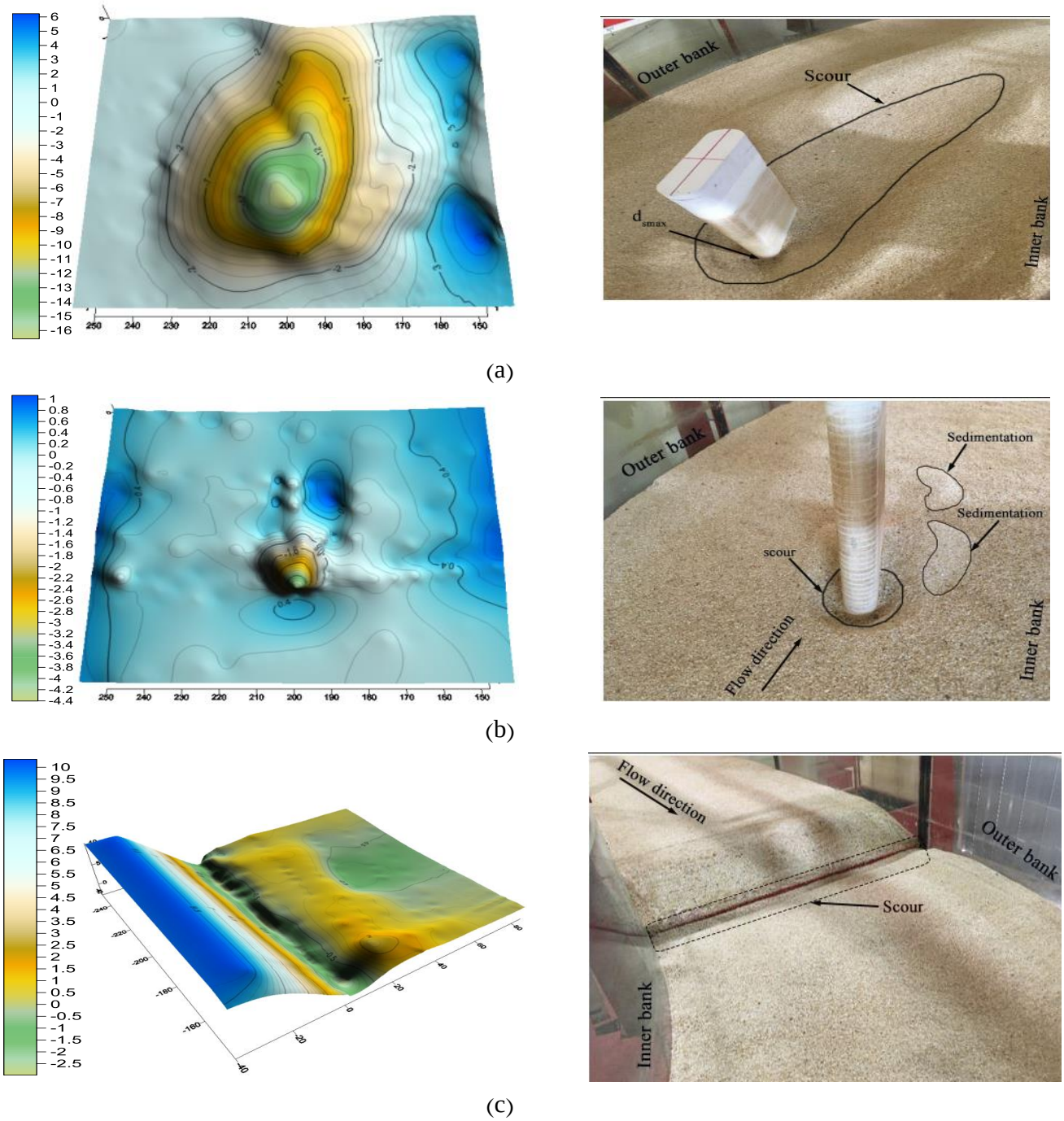


Figure 8. Scour holes created a) around the bridge pier in the case of no base-level drop, b) around the bridge pier in the case of base-level drop, and c) at the beginning of the bend in the case of base-level drop

As is evident in Figure 9-e, sediments transported from the pier nose by horseshoe vortices pile up at a distance of 3 times the pier width at the downstream side with a height of 0.16 times

the pier width in the case of base-level drop. However, in the case of no base-level drop, in the same situation, the scour hole lasts at a depth equal to 2.22 times the pier width. The maximum sedimentation at this section in the case of an empty bend has occurred 1.06 times the pier depth at a distance of 0.05 times the channel width from the inner bank. At a distance of 17 times the pier width downstream, at the 115 degree section, as in Figure 9-f, in the case of no base-level drop, sedimentation piles are formed at intervals equal to 0.1 and 0.6 times the channel width from the inner bank with a height of 1.28 and 0.86 times the pier width. Also, presence of secondary flows leads to creation of the secondary scour hole as deep as 0.66 times the pier width at a distance of 0.22 times the channel width from the outer bank. Under the empty bend conditions, the sediment pile is formed with a height of 0.6 times the pier width at a distance of 0.025 times the channel width from the inner bank, and the scour hole occurs as deep as 0.28 times the pier width at a distance of 0.3 times the channel width from the inner bank.

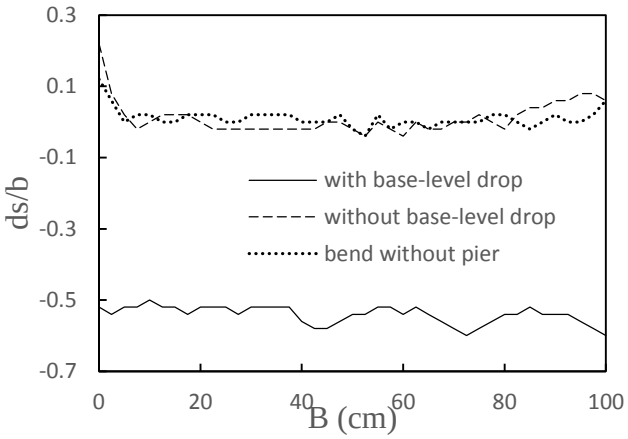
Table (1) presents the size of the scour hole nondimensionalized with the third power of the pier diameter, and the width of scour hole nondimensionalized with the channel width. According to this table, due to the base-level drop, the size and maximum width of the scour hole have reduced by respectively 97 and 87% in comparison to the case of no base-level drop.

Table 1. The volume of the scour hole nondimensionalized with the third power of the pier diameter, and the width of the scour hole nondimensionalized with the channel width

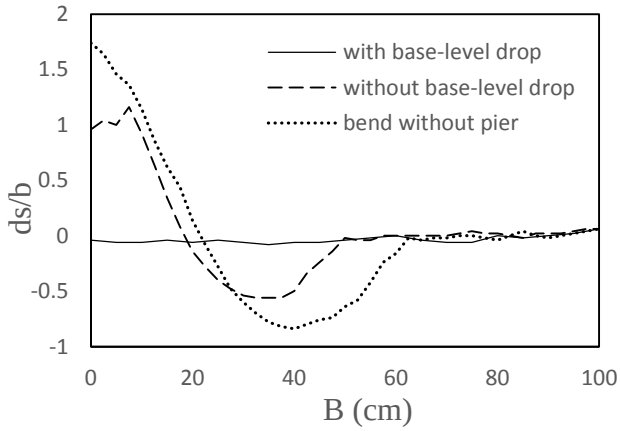
Scour hole position	Around the pier in the experiment with no base-level drop	Around the pier in the experiment with the base-level drop	Percentage of reduction
Ratio of hole volume to the third power of pier diameter	230	6	97
Ratio of hole width to channel width	0.6	0.08	87
Ratio of the maximum scour depth to pier width	3.32	0.9	73

Figure (10) illustrates an instance of bed longitudinal profiles at different distances from the inner bank. As can be seen in Figure 10-a, in the case of base-level drop, the sediments are carried from the base of the slope and piled up to the 30 degree section of the bend. Whereas, in the cases of no base-level drop and empty bend, sedimentation occurs from the 30 to 165 degree sections of the bend, in the vicinity of the inner bank. Its maximum height respectively occurs at distances of 1.5 times the pier width in the 135 degree angle, and 1.46 times the pier width in the 65 degree angle of the bend. As in Figure 10-b, in the case of base-level drop, the scour hole with a depth of 0.4 times the pier width is created at the beginning of the bend due to falling submerged flows crossing the knickpoint. In cases of no base-level drop and empty bend, the scour occurs from the 30 to 70 degree sections. In the case of an empty bend, the sediments carried with the maximum height of 0.48 times the pier width pile up in the 100 degree section. Whereas, in the case of no base-level drop, the presence of the pier results in occurrence of scour with a depth of 0.86 times the pier width in the 85 degree section. Sediments carried through this scour have piled up to the 140 degree section of the bend with the maximum height of 1.6 times the pier width. According to Figure 10-c, it is evident that bed properties up to the 75 degree section of the bend are the same under both conditions of with and without base-level drop in the longitudinal profile of the center of the channel. In the case of no base-level drop, the scour hole

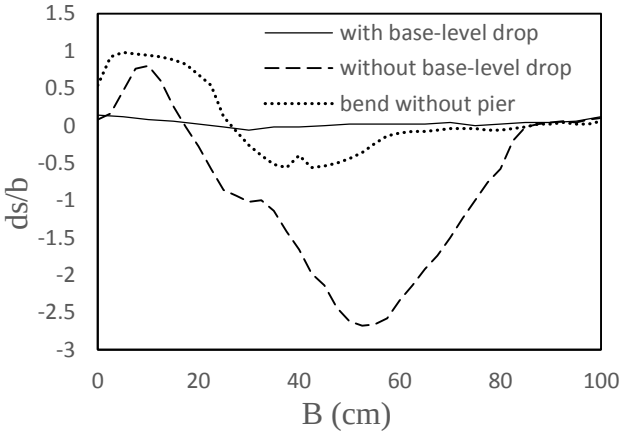
is formed from the 75 to 110 degree sections of the bend. The maximum depth of this scour is 3.32 times the pier width in the 87 degree section of the bend (the pier nose). The sediments washed at the pier nose are piled up from the 115 to 145 degree sections of the bend. The maximum height of sedimentation is equal to 1.24 times the pier width in the 125 degree section of the bend. However, in the case of base-level drop, the scour hole is formed from the 85 to 95 degree sections of the bend. Also, the maximum depth of this scour occurs in the 87 degree section of the bend (the pier nose), as large as 0.9 times the pier width. In the case of empty bend, the maximum scour depth of 0.66 times the pier width occurred in the 75 degree section of the bend. As is evident in Figure 10-e, in the case of no base-level drop, after the main scour hole, a secondary scour hole is formed at the distance between the 110 and 145 degree angles due to water falling from sediment piles.



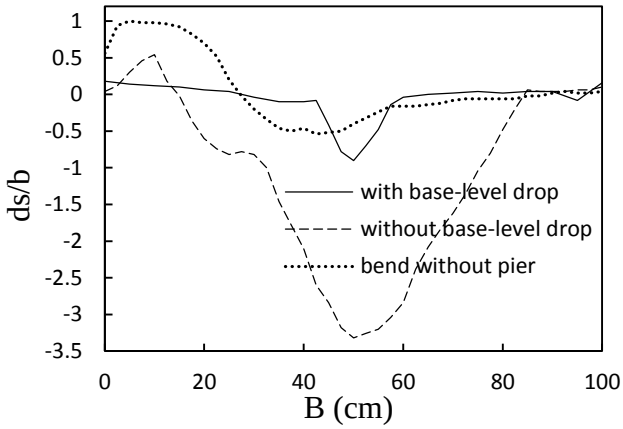
(a)



(b)



(c)



(d)

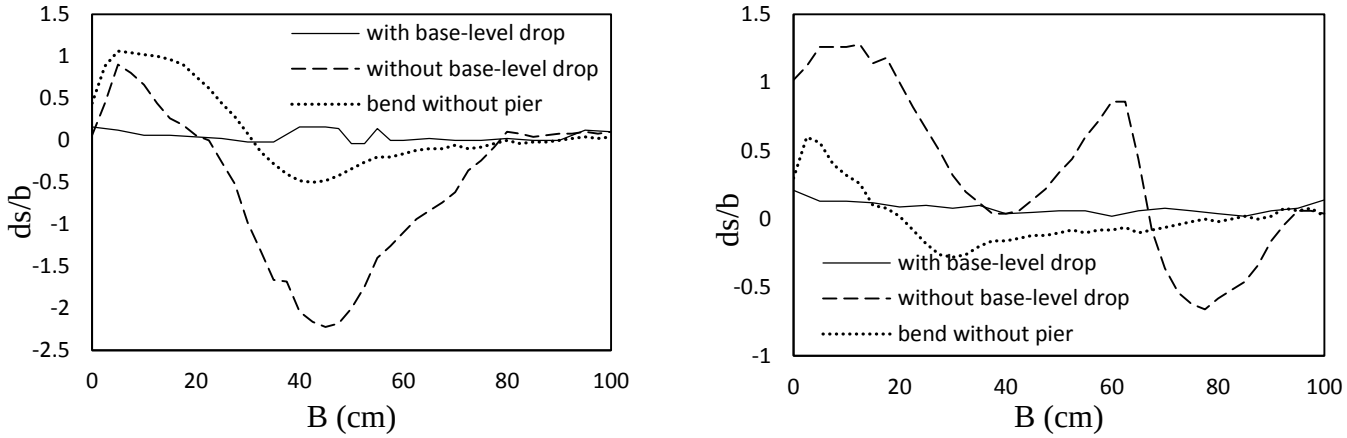
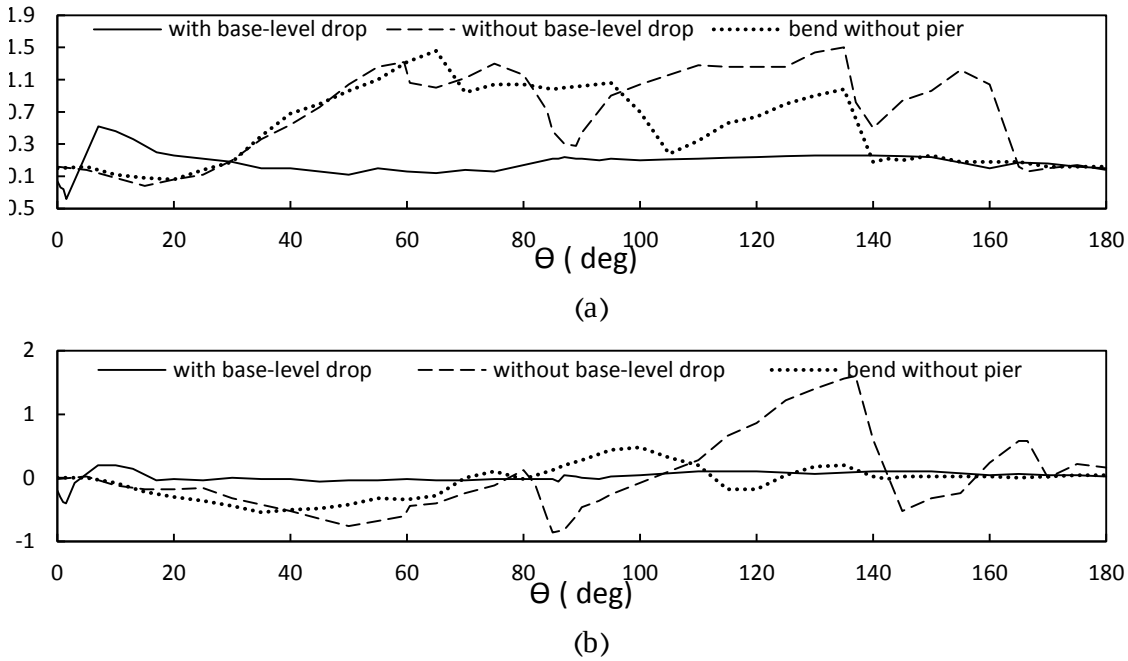
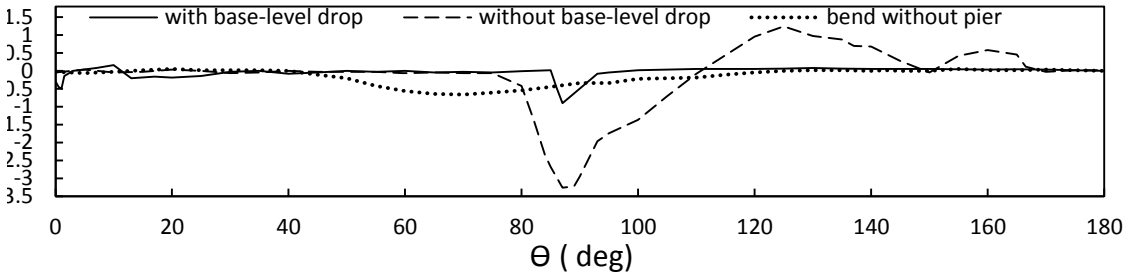
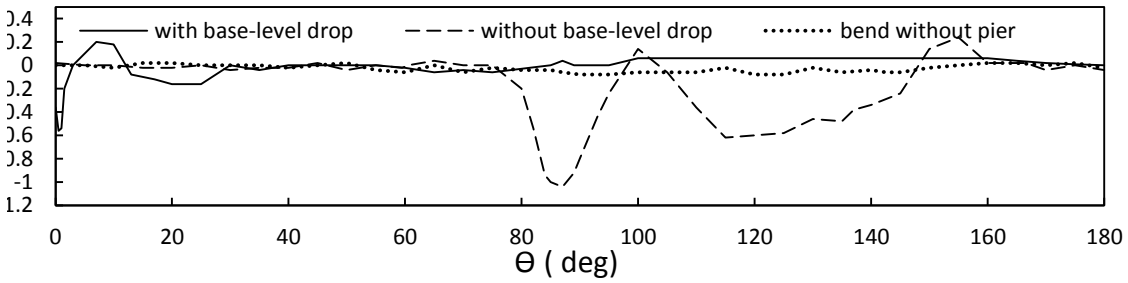


Figure 9. cross sections of a) the beginning of the bend, b) 17 times the pier width at the upstream side of the pier (65 degrees), c) 3 times the pier width at the upstream side of the pier (85 degrees), d) the pier nose, e) 3 times the pier width at the downstream side of the pier (95 degrees), and f) 17 times the pier width at the downstream side of the pier (115 degrees)

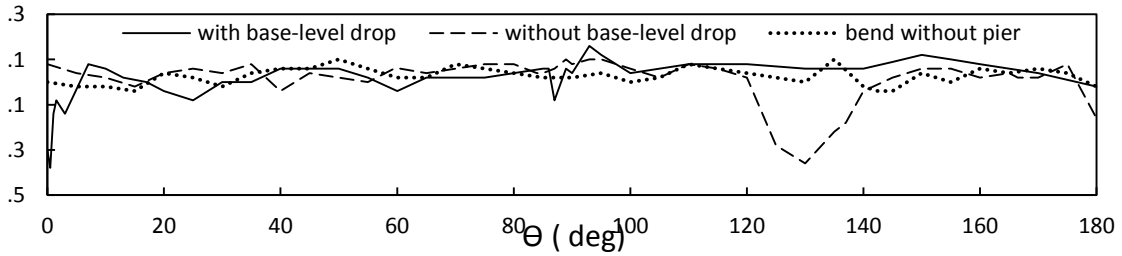




(c)



(d)



(**e**)

Figure 10. longitudinal sections at distances of a) 5, b) 25, c) 50, d) 75, and e) 95% of the channel width from the inner bank

The maximum depth of the secondary scour hole, equal to 0.6 times the pier width, occurred in the 115 degree section. In the case of base-level drop at the beginning of the bend, a scour hole is created with the maximum depth of 0.56 times the pier width. In addition, the sediment pile with a height of 0.2 times the pier width is formed in the 7 degree section of the bend. In the case of empty bend, the bed variations along the bend are insignificant. According to Figure 10-d, in the case of no base-level drop, a scour hole with the maximum depth of 0.36 times the pier width is created in the 130 degree section of the bend, in the vicinity of the outer bank, under the influence of the secondary flows, and their interaction with the longitudinal flow and formation of a helical flow. In the case of base-level drop at the beginning of the bend, a scour hole has occurred with a depth of 0.38 times the pier width, and bed variations after this scour hole are insignificant to the end of the bend. Also, there have been few changes in the case of empty bend.

4. Conclusion

This paper addressed the effect of base-level fall on scour around a rectangular bridge pier located in the 90 degree angle of a 180 degree sharp bend. The most important findings are as follows:

The maximum scour occurred for 16.6 cm, equal to 3.32 times the pier width at the pier nose after installation of the pier in the intended position. However, with the position of the pier, after applying base-level fall, the maximum scour depth occurred for 4.5 cm, equal to 0.9 times the pier width, the fact which indicates a 73% reduction in the scour hole around the pier. In both cases, the maximum scour depth occurred at the nose of the pier. After creating a base-level drop, the volume of scour hole around the pier reduced by 97%, and a wide scour hole with a size of 28 times the third power of the pier width, and the maximum depth of 0.6 times the pier width formed at the downstream side of the slope.

5. Reference

1. Begin, Z. E. B., Schumm, S. A. and Meyer, D. F. (1980). "Knickpoint migration due to base level lowering." Journal of the Waterway, Port, Coastal and Ocean Division, 106(3), 369-388.
2. Brush, L.M. and Wolman, M.G. (1960). "Knickpoint behavior in non-cohesive material: A laboratory study." Geological Society of America Bulletin, 71: 59-74.
3. Cantelli, A. and Muto T. (2014). "Multiple knickpoints in an alluvial river generated by a single instantaneous drop in base level: experimental investigation." Earth Surf. Dynam, 2: 271–278.
4. Chiew, Y.M. and Melville, B.W. (1987). "Local scour around bridge piers." Journal of Hydraulic Research, 25 (1), 15–26.
5. Garcia, M. H. and G. Parker. (1993)."Experimental on the entailment of sediment into suspention by a dense bottom current." J. Geophys.Res. (Oceans) 98:4793-4807.
6. Grimaud, J.L., Paola1, C. and Voller, V. (2016). "Experimental migration of knickpoints: influence of style of base-level fall and bed lithology." Earth Surf. Dynam, 4: 11–23.
7. Holland, W.N. and Pickup, G. (1976). "Flume study of knickpoint development in stratified sediment." Geological Society of America Bulletin, 87: 76-82.
8. Julien, P. Y. (2002). "River mechanics." Cambridge University Press.
9. Leschziner, M. A. and Rodi, W. (1979). "Calculation of strongly curved open channel flow." Journal of the Hydraulics Division, 105 (10), 1297–1314.
10. May, J.H. (1989). "Report 4: Geologic and hydrodynamic controls on the mechanics of knickpoint migration." U.S. Army Engineer Waterways Experiment Station, Vicksburg, MS.
11. Melville, B.W. and Chiew, Y.M., (1999), *"Time Scale for Local Scour Depth at Bridge Piers."* Journal of Hydraulic Engineering, ASCE, Vol.125, No.1, 59-65.
12. Melville B. W. and Sutherland A. J. (1988). "Design method for local scour at bridge piers." American Society of Civil Engineering. Journal of the Hydraulics Division, Vol. 114, No. 10, pp. 1210–1225.
13. Migeon, S., T. Mulder., B. Savoye. and F. Sage. (2011). "Hydrodynamic processes, velocity structure and stratification in natural turbidity currents: results inferred from field data in the turbidite system." J. Sedimen Geo. 245:48-62.
14. Oliveto, G. and Hager, W.H., (2002). "Temporal evolution of clear-water pier and abutment scour." Journal of Hydraulic Engineering, 128 (9), 811–820.
15. Raudkivi, A.J. and Ettema, R., (1983). "Clear-water scour at cylindrical piers." Journal of Hydraulic Engineering, 109 (3), 338–350.

16. Turmel, D., Locat, J. and Parker, G. (2012). "Upstream migration of knickpoints: geotechnical considerations." In Submarine Mass Movements and Their Consequences (pp. 123-132).
17. Vaghefi, M., Akbari, M. and Fiouz, A. R. (2016). "An experimental study of mean and turbulent flow in a 180 degree sharp open channel bend: Secondary flow and bed shear stress." KSCE Journal of Civil Engineering, 20(4), 1582-1593.

Journal of Hydraulic Structures
***J. Hydraul. Struct.*, 2017; 3(2):47-61**
DOI: 10.22055/jhs.2017.13490



OPEN ACCESS

Developing Optimal Operating Reservoir Rule-curves in Drought Periods

Soroosh Alahdin[1]
Hamid Reza Ghafouri[2]

Abstract

In this study, a simulation-optimization model is developed for deriving operational rule-curves in drought periods. To each reservoir, two rule-curves with adjustable monthly levels are introduced dividing the reservoir capacity into three zones between the normal water level and minimum operation level. To each zone of the reservoir and for each month of the year a hedging coefficient is introduced that determines the release from the reservoir. Accordingly, an optimization problem is developed in which the objective is the minimization of water demands deficits in drought and the decision variables are the rule-curves levels and hedging coefficients. For optimization, a genetic algorithm equipped with a self-adaptive constraint handling strategy is used. To evaluate the objective function and constraints violations, the flexible and widely-used WEAP (Water Evaluation and Planning) simulation model is exploited and coupled with the optimization solver. The model is then applied to the Zohreh three-reservoir system in the southwest of Iran and compared to the Standard Operation Policy (SOP). According to the sustainability indices for the system operated in drought, the obtained operating rule-curves are found significantly superior to the SOP. As a result of applying the rule-curves, the modified shortage index (MSI) and vulnerability (extent) of the system are respectively improved by 22% and 28% compared to the SOP. Consequently, the developed policy application resulted in longer periods of deficit (but less severe) as shown by decrease in reliability (5%) and resilience (40%) indices.

Keywords: Operating policy, Rule-Curve, Sustainability Indices, Optimization Model, Hedging.

Received: 09 August 2017; Accepted: 20 November 2017

[1] Ph.D. Candidate, Department of Civil Engineering, Engineering Faculty, Shahid Chamran University of Ahvaz, Ahvaz, Iran, s-alahdin@phdstu.scu.ac.ir (**Corresponding author**)
[2] Professor, Department of Civil Engineering, Engineering Faculty, Shahid Chamran University of Ahvaz, Ahvaz, Iran.

CC BY

1. Introduction

Handling the operational challenges has been always a serious concern for reservoirs operators, but when a water resources system is suffering from water scarcity, demands are more strongly competing for water and the system operation becomes even more complicated and challenging.

Application of simulation and optimization models has shown great advances in planning and management of water resources problems. Currently, there are several softwares like HEC3, HEC5, HEC-ResSim, MIKEBASIN, RIBASIM, WATHNET, OASIS, ARSP, CalSim, RiverWare, MODSIM, WRAP, SWD SUPER and WEAP that can simulate operation of a reservoir system with its all components in details. A simulation model can evaluate the system performance for any decision on the reservoirs releases and operations over a certain time period and return the values of objective functions and constraint violations introduced to the system.

A reservoir system is operated following prescriptions on the system releases as a function of time and available water. These prescriptions or more precisely rule-curves are traditionally derived through intensive simulation techniques [1], but to derive optimum operating ones for a multi-reservoir system, it is required to develop and solve optimization models. The optimization systematically changes the operational parameters and the simulation model evaluates the effects of each change on the system operation over a long period. This process continues until the best feasible performance of the reservoir system is achieved. This is the main skeleton of every simulation-optimization model that has recently become very popular and well-developed for solving a variety of water resources problems. In this context, many researchers have tried to cope with the challenges associated with the operation of reservoir systems in arid and semi-arid areas as well as during drought periods. The existing approaches are different in concept ranging from simplified rules of thumb to sophisticated model-based operating rules.

To minimize the impacts of a drought event, water is stored in the system for future even if enough water exists to satisfy the current demands. The purpose of a hedging decision in a reservoir operation is to lessen the burden of water scarcity in the future by distributing the demands' deficits over an extended period of operation. In general, hedging rules can be categorized into two main groups of continuous and discrete methods. Through the continuous approach, the decisions on the amount of water to be rationed are mathematically represented by a linear, nonlinear or fuzzy function [2-13]. Whereas, in the discrete methods the decisions are made based on the discrete representation of the reservoir and water resources conditions [1, 14-17]. Many investigations with the aid of simulation and optimization models were published to extend and modify these approaches. These studies put forth and answered two key questions of, "when to start rationing" and "how much rationing". However, this issue is highly case-dependent and needs a thoughtful insight into the system’s objectives, limitations, hydrology and other specifications.

An important concern in deriving hedging rules is the employment of proper solvers. The applied methods are the mixed integer programming [1-2, 14-15], dynamic programming [10], Markov Model [6, 7] and recently, heuristic nature-inspired algorithms [8-9, 11-12, 16-18]. For the sake of dimensionality problems associated with the large-scale multi-reservoir systems, some investigations were inevitably restricted to single-reservoir case studies or short-term time-series [2-10, 14-15, 19].

Some studies were carried out based on surrogate simulation models rather than simulating the system with all details. For example, to make the process of simulation-optimization more efficient Dariane et al., [5], trained and substituted an artificial neural network for the system simulation and Guo et al., [16], used an equivalent reservoir for a multi-reservoir system and

assumed constant weighting factors for different types of water supplies. However, issues like the interaction between the reservoirs and other components of the system as well as the role of long-term data encompassing different hydrological conditions are very significant in deriving the system operating rules. Paying attention to these concerns, Taghian et al., [17], developed a comprehensive long-term simulation model based on the ARSP for a three-reservoir system facing with severe droughts. All water demands were also simulated in the model using the network flow scheme. They proposed a discrete hedging rule by hybridizing a genetic algorithm for hedging optimization and a linear programming model for allocation water to downstream demands. In this context, the present study aims at developing a complete simulation-optimization model for multi-reservoir systems in drought periods with some modifications. The powerful, comprehensive and easy-to-use simulation software, WEAP is used to serve as objective function and constraint values provider. Then, the problem is formulated as a constrained nonlinear optimization problem and is solved using a self-adaptive Genetic Algorithm (GA). The model is applied to a three-reservoir case study in Iran, and the results are discussed and compared with those obtained by the SOP.

2. Case study and problem statement

As a case study, drought-stricken Zohreh river system located in the south-western of Iran with an area of 15460 squared kilometer is studied. The schematic of the system is shown in Figure 1. The system comprises of three reservoirs, eight input stream flows, thirteen irrigation networks, three public demands and two minimum flows. The conservation storage volumes for Kosar, Chamshir, and Kheirabad reservoirs are respectively, 418, 1862, and 105 million cubic meters (mcm) as presented in Table 1 in details.

Table 1. Properties of hydropower plants

Properties of dam	Chamshir	Kosar	Kheirabad
Normal level (meter above sea level)	598	625	259.6
Minimum level of operation (meter above sea level)	543.7	580	238
Volume storage in min. level (mcm)	454.5	74.2	0.93
Volume storage in normal level (mcm)	2316.7	492.8	106.3
Installed capacity (Mega Watt)	165	-	2.5
Plant factor (%)	25	-	-
Plant efficiency (%)	91	-	85
Maximum turbine flow (cms)	144.4	-	7.26

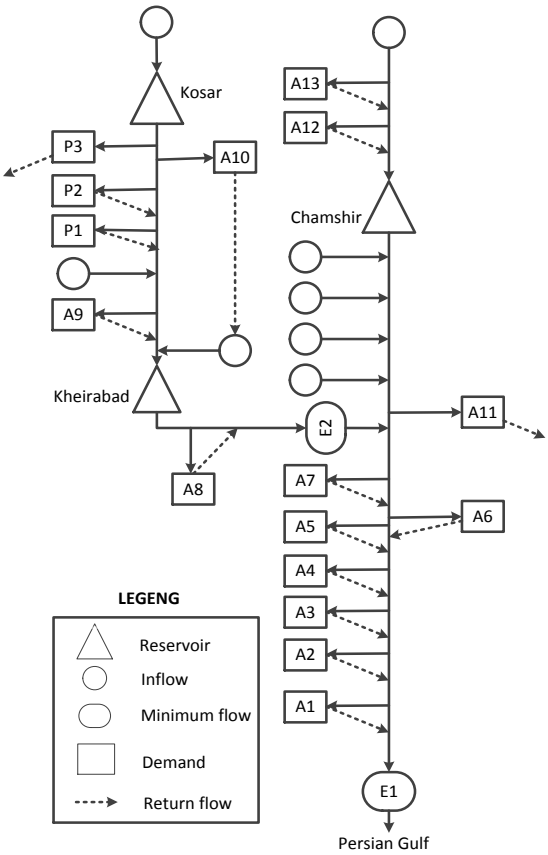


Figure 1. Schematic configuration of the water supply system

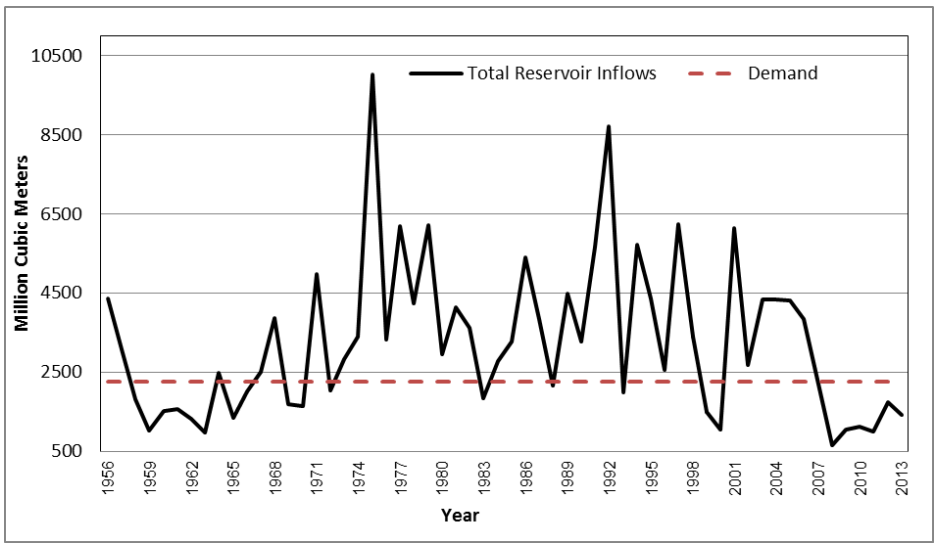


Figure 2. Total annual inflow and demand of the system

The total annual inflow to the system (sum of all reservoirs' inflows) and the total demand are depicted in Figure 2. The average value of total annual inflow is about 3247 mcm and the average value of the last seven years (2007-2013) is 1330 mcm. Comparison of these two average parameters reveals two long periods of drought in the initial and the last stages of the time-series. Target values for demands are given based on the planned water demand for the future horizon (2259 mcm), distributed as 73% for agriculture, 16% for the minimum flow, and 11% for public demands (Table 2).

Table 2. Characteristics of demands

Demand title	Type	Annual demand (mcm)
A1	Agriculture	20
A2	Agriculture	480
A3	Agriculture	60
A4	Agriculture	77
A5	Agriculture	49
A6	Agriculture	138
A7	Agriculture	114
A8	Agriculture	28
A9	Agriculture	38
A10	Agriculture	48
A11	Agriculture	365
A12	Agriculture	101
A13	Agriculture	132
P1	Public	32
P2	Public	10
P3	Public	210
E1	Minimum flow	315
E2	Minimum flow	41
SUM		2259

3. The simulation-optimization model

After construction of large-scale water storage projects, attention must be on improving the operational effectiveness and efficiency. To achieve this goal, a simulation-optimization model is developed in this study as a general framework for drought management (Figure 3). To this end, WEAP is embedded into a genetic algorithm and the hedging rule is included.

In addition to optimizing water allocation, this work aims at mitigating the drought consequences in the reservoir system. The objective is to alleviate the effects of water shortage by rationally distributing water in a longer horizon. In operation of this system, there are 74 decision variables including, two monthly rule-curves coordinates for each dam (Chamshir, Kheirabad and Kosar dams) and two hedging factors for the whole system. The objective function is to minimize the modified shortage index as Eq. 4. The performance constraints e.g. rationing rule-curve attributes are added in the constraint handling procedure of optimization algorithm. The physical constraints, mass balance, performance constraints and hedging rules are the main components that are included. To solve the problem, a constrained optimization algorithm is coupled with a standard simulation model as illustrated in Figure 3. All the physical constraints like the maximum dam release, reservoir storage, and channel capacity are handled in the general simulation model. To evaluate the long-term performance of reservoir system operation, 58-year (from 1955 to 2013) time-series of monthly inflows are used, resulting in a total of 696 months. In what follows, the simulation and optimization models are introduced in details and the results of case study optimization are presented and discussed.

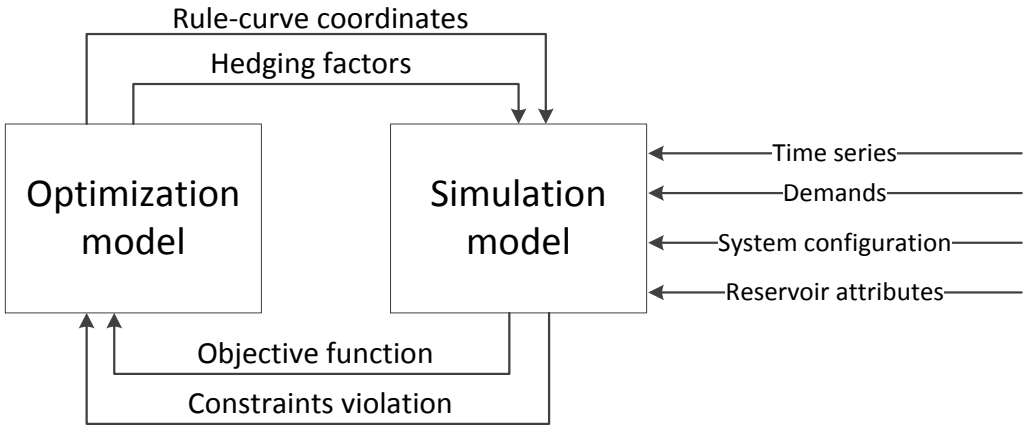


Figure 3. Conceptual model

3.1. Simulation Model (WEAP)

Reservoir simulation models are based on the mass balance in the system of reservoirs and demands. WEAP calculates water mass balance for every node and link in the system on a monthly time step. Implementing hedging rules in the simulation model adds three constraints (Equations 1, 2 and 3) to it. In drought periods, the inflow may not be adequate to keep the water storage level (S_t) on or above the first rule-curve if the target demand is satisfied. Releasing current available water from the reservoir to completely supply the target delivery may threat safe supply in future. Therefore, rationing is introduced to diminish the current reservoir release, and retain an adequate amount of water in storage for future consumption. When the initial reservoir storage level is between the two rule-curves (in the first hedging zone, $Zone_1$), the reservoir releases water to meet the first phase of hedging ($\alpha_1 Demand$, α_1 is the first hedging coefficient). For more severe droughts, when the beginning reservoir storage is below the second rule-curve (in the second hedging zone, $Zone_2$), less water is released from the reservoir to meet the second phase of hedging ($\alpha_2 Demand$, α_2 is the second hedging coefficient). The coordinates of the two rule-curves and hedging coefficients are decision variables which will be optimized in the simulation-optimization procedure.

$$if\ S_t \notin (Zone_1\ And\ Zone_2)\ Then\ Demand = Demand \times 100\% \quad \textbf{(1)}$$

$$if\ S_t \in Zone_1\ Then\ Demand = Demand \times \alpha_1 \quad \textbf{(2)}$$

$$if\ S_t \in Zone_2\ Then\ Demand = Demand \times \alpha_2 \quad \textbf{(3)}$$

3.2. Optimization model

The Genetic Algorithm starts with a randomly generated group of chromosomes known as the population. In each chromosome, there are as many genes as the number of decision variables. In this study the number of individuals in each generation was set to 104. In the first step, the costs and associated chromosomes are ranked from lowest to highest for the population. Survival of the fittest, is translated into discarding the chromosomes with higher costs. Therefore, the better chromosomes are selected to continue, while the rest are deleted. The selection rate (here 50%) is the fraction of the population that survives for the next step of reproduction.

Mating is reproduction of one or more youngsters from the parents selected in the pairing

procedure. The most common form of mating involves two parents producing two children. The uniform mating which is adopted here randomly assigns the gene from one parent to one offspring and the gene from the other parent to the other offspring.

In the next step, random mutations alter a certain percentage of the genes in the list of chromosomes. Mutation is the second way of a GA exploring a cost surface. It can introduce traits, not in the original population and keeps the GA from converging too fast before sampling the entire feasible space. The mutation rate was used for 2% of the genes of all the population.

After the occurrence of mutations, the costs associated with the offspring and mutated chromosomes are calculated. The process described above is iterated. The number of generations depends on whether an acceptable solution is reached or a number of *iterations* is exceeded. After a while all the chromosomes and associated costs would become the same if it were not for mutations. The flowchart in Figure 4 provides an overview of a constrained continuous GA. The primary difference with the usual algorithm is the constraint handling procedure which is discussed in the constraints section.

3.2.1. Objective Function

In the past for drought management, many objective functions were suggested and used, but the most used indices are SI and MSI. The shortage index (SI) was presented by the U.S. Army Hydrologic Engineering Center [20-21]. Because the SI index is the average of the "annual" deficit rate squared, to characterize the "monthly" fluctuations of the hydrologic time series, a modified shortage index (MSI) is defined as the following,

$$MSI = \frac{100}{n}\sum_{t=1}^{n}\left(\frac{TS_t}{TD_t}\right)^2 \quad \textbf{(4)}$$

Where TS_t is shortage in tth period; TD_t demand in tth period; and n number of periods [22]. For the energy production, the success or failure in each time step is evaluated based on the installed capacity of the hydropower plant. When the generated energy or the equivalent minimum volume of water discharge considering plant factor and minimum operation head, in that period is less than the installed capacity, a failure is counted. Then the deficit will be the difference between the turbine flow and the flow requirement to generate energy as much as installed capacity [23].

3.2.2. Constraints

To make the derived rule-curves meet the operational and real situation standards, two points must be noticed. First of all, the maximum difference between two consecutive operating reservoir storage targets (rule-curve coordinates) must not be more than a defined value [24]. This is because refilling and emptying a reservoir and generally fluctuations in reservoirs in the real world will follow a supply-demand pattern and its configuration could not be scattered. In mathematical expression, this could be written as,

$$|S_t - S_{t-1}| \leq S_{allowed} \quad \textbf{(5)}$$

Where S_t and S_{t-1} are corresponding to two consecutive operation rule-curve components (storage or trigger value here), and $S_{allowed}$ is the maximum allowable difference. Second, because at the end of the water year and the start of the new one, no significant hydrologic and demand changes are expected to take place in the basin, it is not logical that the difference between the first (S_1) and the last (S_{12}) components of a rule-curve be noticeable. Therefore, the second constraint would be written as follows,

$$(1-\varepsilon)\times S_1 \le S_{12} \le (1+\varepsilon)\times S_1 \quad \textbf{(6)}$$

Where, ε is a small number. To implement these constraints in the algorithm, a method based on the preference of feasible solutions over infeasible ones called self-adaptive is used. This method is implemented in the selection and ranking process in GA (Figure 4) and has the following characteristics: 1) as long as no feasible solution is found, the constraint violation is the rank determinant of the individuals; 2) once there is a combination of feasible and infeasible solutions in the population, feasible solutions will be ranked higher; and 3) the feasible solutions will be ranked based on their objective function values.

In addition, there are two other points that are considered in the algorithm. First, since no project can survive with less than 20% of its demand supplied and on the other side, there is no point in rationing with supply more than 80% of the demand, practical and operational view suggests that the hedging coefficient cannot be less than 20 or greater than 80 percent. Although in theory the allocation outside this range is possible. Second, lots of trial and errors with the simulation-optimization model have shown that two rule-curves for each dam reservoir may cross each other. Therefore, a mechanism must be devised to go around this issue. To do this in the optimization routine after mutation process, the values of the second hedging rule-curve are checked and forced to be less than the first phase (Figure 4).

4. Results

In order to show the efficiency and clarify algorithm's performance in multi-reservoir system mangement, in addition to the objective function value (MSI), other statistical measures like reliability, resilience, and vulnerability are also calculated. These criteria are defined as,

$$Reliability = \frac{number\ of\ satisfactory\ values}{total\ number\ of\ values} \quad \textbf{(7)}$$

$$Resilience = \frac{number\ of\ times\ a\ satisfactory\ value\ follows\ an\ unsatisfactory\ value}{total\ number\ of\ unsatisfactory\ values} \quad \textbf{(8)}$$

$$Vulnerability\ (extent) = expected\ extent\ given\ unsatisfactory\ values \quad \textbf{(9)}$$

The system operation performances for the SOP and the developed rule are compared in the next tables and figures; they display the long-term system performance and the annual system performance during recent failure years.

Table 3. Long-Term System Performance during the Period 1955–2013

Index	SOP	Optimum rule-curve
α_1	-	70.9
α_2	-	35.2
MSI	5.35	4.13
Average reliability	69.3	65.5
Average resilience	26.5	15.8
Average vulnerability extent	8.7	6.2

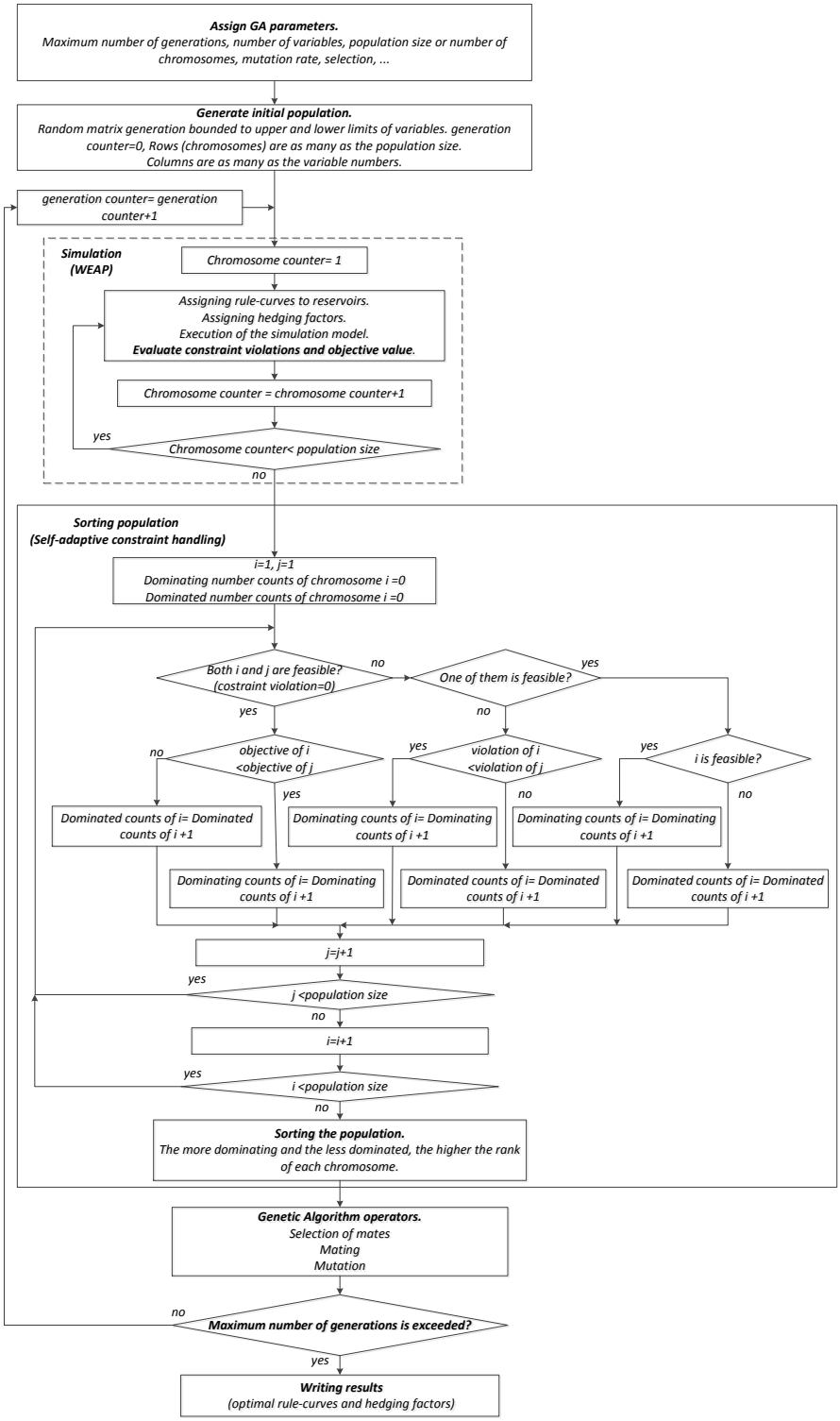


Figure 4. Flowchart of the proposed simulation-optimization model

The long-term performance criteria are given in Table 3. Comparing the two scenarios, it is indicated that total MSI value is improved by 22% in the proposed method. The distribution of severe droughts cause neighboring deficit periods join together, nevertheless resilience (which is defined as the number of recoveries) decreased from 26.5 to 15.8. Since the idea is to spread deficits to smoothen them in a longer horizon that could be more tolerable for the demands, the decrease in reliability (5%) is reasoned.

These points are rechecked and confirmed in Table 4 as well. The developed policy appears to be superior to the SOP, which is attributed to the inclusion of hedging rules. The hedging rule inherently tends to adjust the demand by rationing before and during the occurrence of severe shortages. Therefore, the SOP resulted in a better reliability than the value introduced by the model (Tables 3 and 4). The direct result of this kind of management is that the failures are less severe but more frequent and therefore, the resilience (the number of system restoration regarding to supplied water) is less for the planned policy compared to the SOP.

Table 4 gives long-term performance criteria for various demand groups. Almost the same pattern which was discussed in table 3 is dominating here. The agricultural demand's behavior which is accountable for 73% of the total system demand reveals the total demands' behavior. The difference in the performance criteria for the two management methods in public, environment and hydropower demands are negligible, since they all together are only 27% of the whole system demands and therefore model is biased towards fulfilling the agriculture demands.

Table 4. Long-term performance criteria for various demand groups

Demand type	Reliability (optimum)	Reliability (SOP)	resilience (optimum)	resilience (SOP)	vulnerability extent (optimum)	vulnerability extent (SOP)
Agriculture	68.1	75.1	7.5	23.7	4.8	7.4
Public	43.1	41.4	24.0	25.0	2.1	2.2
Environment	93.1	86.2	60.0	47.0	6.9	6.4

The annual objective function values for the recent drought (Table 5) show that the maximum value of MSI is reduced in three different groups of users. This point means that the proposed drought management is working well. The biggest difference in MSI values is in hydropower demand which is reduced more than 50 units in the 7-year drought. In this table, the hydropower objective function values show very informative changes during 2008 to 2012 for the two policies, that confirms the idea behind the optimization. In 2008, the optimum model used hedging and as a result the MSI value is higher (8.04> 7.06) but by saving water in this year, the system benefited in the next four years (21.05-29.17 for optimum and 81.72 to 82.25 for SOP).

Table 5. Objective function values for various users in recent drought

	Objective function value					
Year	Agriculture (optimum)	Agriculture (SOP)	Minimum flow (optimum)	Minimum flow (SOP)	Public (optimum)	Public (SOP)
2007	0.47	0.47	0.00	0.00	3.45	3.45
2008	6.72	1.48	0.05	0.27	15.32	16.45
2009	28.62	23.24	0.39	0.60	9.89	11.04
2010	23.92	20.11	0.00	0.17	1.49	2.56
2011	24.71	31.34	0.07	0.32	7.35	8.83
2012	17.98	5.03	0.22	0.35	5.34	6.17
2013	12.44	11.25	0.00	0.03	0.07	0.28
Max	28.62	31.34	0.39	0.60	15.32	16.45

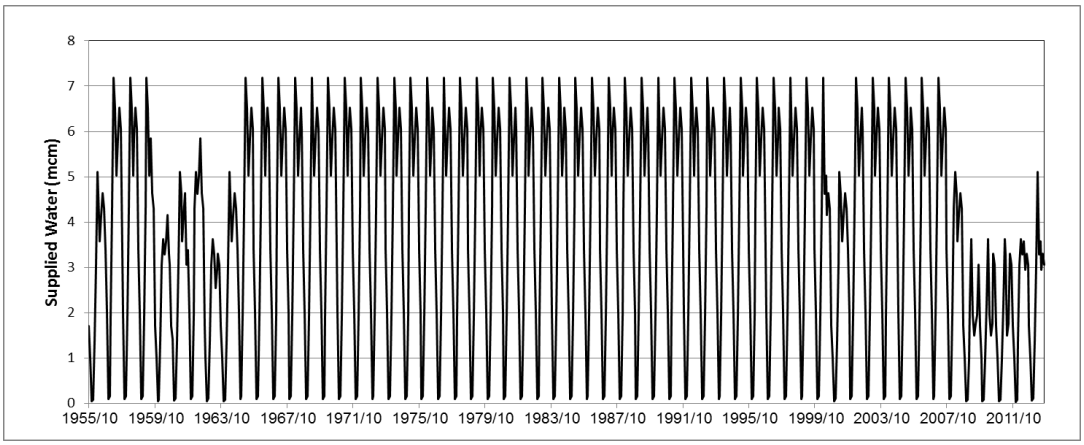


Figure 5. Optimal policy supplied water for the A5 project

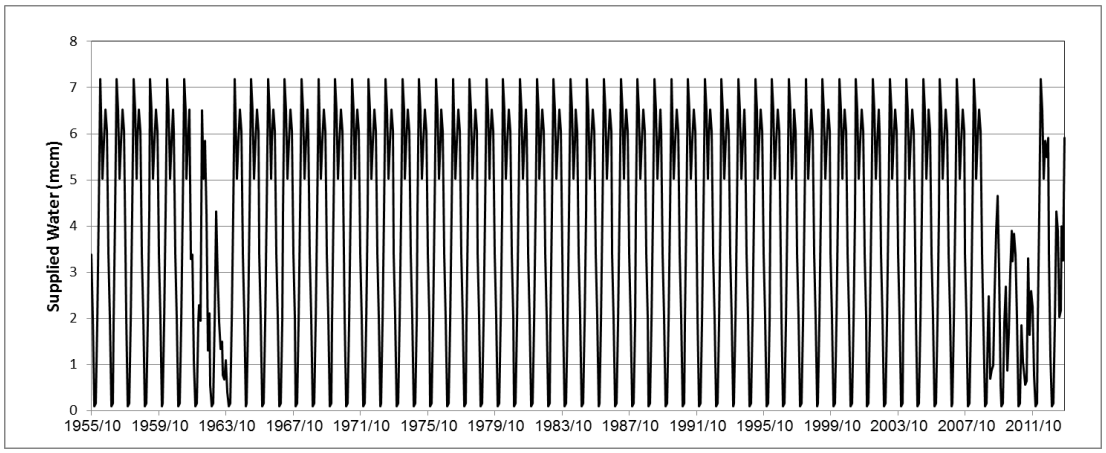


Figure 6. SOP supplied water for the A5 project

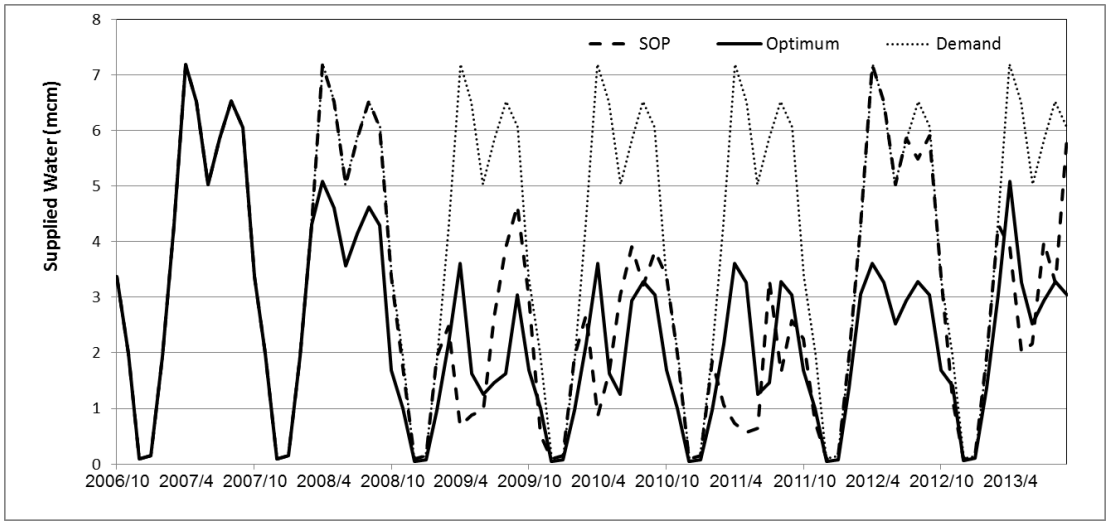


Figure 7. A5 project demand, SOP, and optimal policy supplied water in recent drought

For A5 project which is located in Zohreh system downstream (see Figure 1), the details of operation (water supplied) are presented by SOP and optimal rule-curves in Figures 5 and 6. Visual comparison of two policies' performances (SOP and optimal rule-curve with hedging) are illustrated in Figure 7. This figure graphically shows the superiority of the new routine through the smooth behavior, good correlation with demand and less severe deficits.

Since this optimal operation policy is prescribed based on the whole 58-year historical records, trigger water levels are general and synchronized for all hydrological conditions experienced including successive droughts, particularly 9-year in the initial and 7-year recent drought in the last stages of the record. But if in a particular event another policy performs better (SOP in 1999-2000, Figures 5 and 6), it corresponds to the peculiar hydrologic attributes of that event. However, it is known that in the SOP, if insufficient water is available to satisfy the demands, the reservoir releases all the water available and becomes empty; if inflow is high, the reservoir will fill and spill its excess water. Becuse this policy does not provide a mechanism for decreasing release in the early stages or during indications of impending drought.

Optimal rule-curves coupling to hedging rules for Kheirabad, Kosar, and Chamshir reservoirs are shown in Figs. 8–10. These monthly trigger levels of reservoir are optimized for management during droughts.

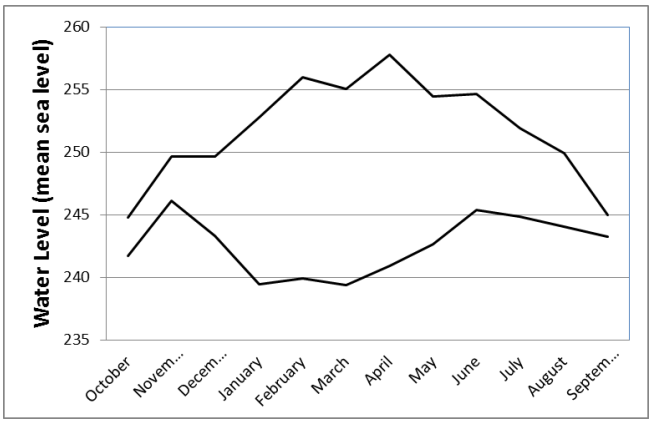


Figure 8. Optimal rule-curves for Kheirabad

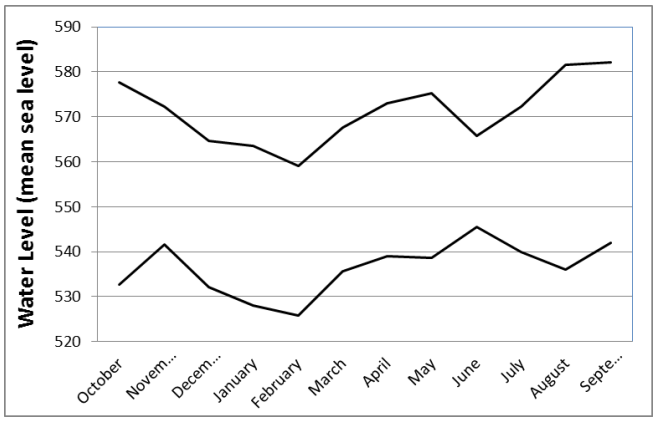


Figure 9. Optimal rule-curves for Kosar

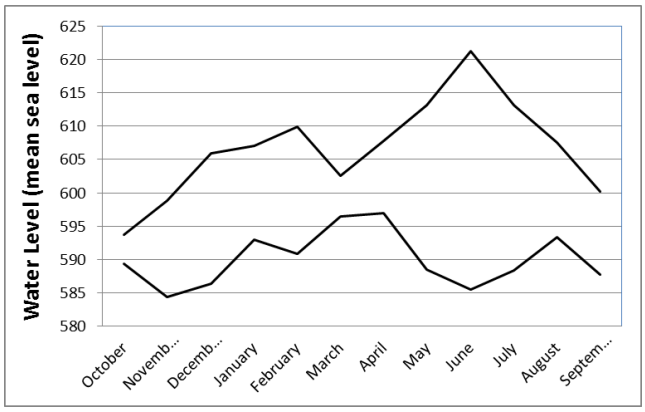


Figure 10. Optimal rule-curves for Chamshir

The rule-curves structures illustrated in Figures 8-10 indicate that the implementation of Formulas 5 and 6 in the developed model algorithm as constraints is logical. As a result, the difference between two susequent coordinate points and the difference between the first and the last month of water year is kept bounded based on the considerations and operational views of the water resource managers.

5. Conclusion

In this paper, a drought management simulation-optimization model was introduced to derive the rule-curves and rationing factors for multi-purpose multi-reservoir systems. The system of reservoirs and demands is mathematically simulated using a flexible and general WEAP model. In the simulation model, all physical constraints of the case-study are systematically satisfied. In a higher level, a self-adaptive GA is used to optimize the reservoirs rule-curves and hedging factors with the objective function of modified shortage index (MSI). The model was applied to a real three-reservoir drought-stricken system. After the optimization, the system performance was compared to the results of the SOP. The rule-curves derived from the historical 58-year period data systematically consider different climate conditions experienced by the system and would be able to manage similar conditions in the future. The proposed operating rules can mitigate the water shortage consequences by rationing current demands and saving water for future uses in drought periods. In terms of agriculture, public and hydropower supply of demands, with regard to the performance criteria, the model outperforms the SOP.

6. References

1. Tu M. Y., Hsu N. S., Yeh W. W. G., (2003). Optimization of reservoir management and operation with hedging rules. Journal of Water Resources Planning and Management, DOI: 10.1061/(ASCE)0733-9496(2003)129:2(86), 86–97.
2. Shih J. S., ReVelle C., (1994). Water-supply operations during drought: Continuous hedging rule. Journal of Water Resources Planning and Management, DOI: 10.1061/(ASCE)0733-9496(1994)120:5(613), 613–629.
3. Srinivasan K., Philipose M. C., (1996). Evaluation and selection of hedging policies using stochastic reservoir simulation. Water Resources Management, 10(3), 163–188.
4. Srinivasan K., Philipose M. C., (1998). Effect of hedging on over year reservoir performance. Water Resources Management, 12(2), 95–120.

5. Draper A. J., Lund J. R., (2004). Optimal hedging and carryover storage value. Journal of Water Resources Planning and Management, 130(1), 83– 87.
6. You J. Y., Cai X. M., (2008a). Hedging rule for reservoir operations. 1. A theoretical analysis. Water Resources Research, 44(1), W01415.
7. You J. Y., Cai X. M., (2008b). Hedging rule for reservoir operations. 2. A numerical model. Water Resources Research, 44(1), W01416.
8. Shiau J. T. (2009). Optimization of reservoir hedging rules using multi-objective genetic algorithm. Journal of Water Resources Planning and Management, DOI: 10.1061/(ASCE)0733-9496(2009)135:5(355), 355–363.
9. Shiau J. T., (2011). Analytical optimal hedging with explicit incorporation of reservoir release and carryover storage targets. Water Resources Research, VOL. 47, W01515, DOI: 10.1029/2010WR009166.
10. Eum H., Kim Y., Palmer R.N., (2011). Optimal drought management using sampling stochastic dynamic programming with a hedging rule. Journal of Water Resources Planning and Management 137(1):113–122. DOI: 10.1061/(ASCE)WR.1943-5452.0000095.
11. Dariane A., B., Karami F., (2014). Deriving Hedging Rules of Multi-Reservoir System by Online Evolving Neural Networks. Water Resources Management. DOI: 10.1007/s11269-014-0693-0.
12. Ahmadianfar I., Adib A., Taghian M., (2016). Optimization of Fuzzified Hedging Rules for Multipurpose and Multi-reservoir Systems. DOI: 10.1061/(ASCE)HE.1943-5584.0001329.
13. Huang C., Zhao J., Wang Z., Shang W., (2016). Optimal Hedging Rules for Two-Objective Reservoir Operation: Balancing Water Supply and Environmental Flow. Journal of Water Resources Planning and Management, 04016053, DOI: 10.1061/(ASCE)WR.1943-5452.0000699.
14. Shih J. S., ReVelle C., (1995). Water supply operations during drought: A discrete hedging rule. European Journal of Operational Research, 82(1), 163–175.
15. Tu M. Y., Hsu N. S., Tsai F. T. C., Yeh W. W. G., (2008). Optimization of hedging rules for reservoir operations. Journal of Water Resources Planning and Management, DOI: 10.1061/(ASCE)0733-496(2008)134:1(3), 3–13.
16. Guo X., Hu T., Zeng X., Li X., (2013). Extension of parametric rule with the hedging rule for managing multi-reservoir system during droughts. Journal of Water Resources Planning Management, 10.1061/(ASCE) WR.1943-5452.0000241, 139–148.
17. Taghian M., Rosbjerg D, Haghighi A., Madsen H., (2013). Optimization of Conventional Rule-curves Coupled with Hedging Rules for Reservoir Operation. Journal of Water Resources Planning and Management, DOI: 10.1061/(ASCE)WR.1943-5452.0000355.
18. Ashrafi S.M., Ashrafi S.F., Moazami S., (2017). Developing Self-adaptive Melody Search Algorithm for Optimal Operation of Multi-reservoir Systems. Journal of Hydraulic Structures, 3(1):35-48, DOI: 10.22055/jhs.2017.13282.
19. Zhao J., Cai X., Wang Z., (2011). Optimality conditions for a two-stage reservoir operation problem. Water Resources Research, 47, W08503, DOI: 10.1029/2010WR009971.
20. Hydrologic Engineering Center, Reservoir yield; generalized computer program, 23-J2-L245. U.S. Army Corps of Engineers, Davis, Calif, 1966.

21. Hydrologic Engineering Center, Hydrologic engineering methods for water resources development; Vol. 8, reservoir yield, U.S. Army Corps of Engineers, Davis, Calif, 1975.
22. Hsu S. K., (1995). Shortage indices for water-resources planning in Taiwan. Journal of Water Resources Planning and Management, 121(2), 119–131.
23. Ahmadi Najl A., Haghighi A., Samani H.M.V., (2016). Deriving Optimum Trade-Off between the Benefits and Costs of Inter-basin Water Transfer Projects. International Journal of Optimization in Civil Engineering, 6(2):173-185.
24. Suen J. P., Wayland E. J., (2006). Reservoir management to balance ecosystem and human needs; Incorporating the paradigm of the ecological flow regime. Water Resources Research, VOL. 42, W03417, DOI: 10.1029/2005WR004314.

Journal of Hydraulic Structures
***J. Hydraul. Struct.*, 2017; 3(2):62-77**
DOI: 10.22055/jhs.2018.24762.1064



OPEN ACCESS

Finding the Causes and Evaluating Their Impacts on Urmia Lake Crisis Using a Comprehensive Water Resources Simulation Model

Alireza B. Dariane[1]
Leila Eamen[2]

Abstract

Urmia Lake in northwestern Iran has been facing critical water level shrinkage in recent years with serious environmental consequences. It is expected that with the current trend, the lake will be completely dried out in a few years from now. This study attempts to assess the impacts of human activities on water level fluctuations of Urmia Lake by developing a comprehensive hydrologic simulation model. Model development and calibration was carefully accomplished by utilizing effective water resources management components in the basin. An important contribution was accomplished by properly estimating the agricultural water demand and consumption in the absence of measured data. Result of long-term simulation reveals that excessive water consumption by inefficient and expanding irrigated agriculture is the main reason for Urmia Lake shrinkage. It was found that main reservoirs are only responsible for 23% of current situation. Whereas, 77% of the current crisis has been caused by miscellaneous agricultural water withdrawals in the basin.

Keywords: Agricultural Development Projects, Comprehensive Water Resources Simulation, Lake Level Fluctuations, Urmia Lake Basin.

Received: 12 August 2017; Accepted: 24 November 2017

1. Introduction

Lakes are fundamental constituent of any ecosystem around the world. The lives of many species and habitats depend on proper functioning of these water bodies. Recent changes in the trend of climatic variables along with over exhausting of limited water resources through intensified irrigated agriculture has resulted in serious escalations in lake ecosystems around the

[1] Department of Civil Engineering, K.N. Toosi University of Technology, Valiasr St., Tehran, Iran, Associate Professor, borhani@kntu.ac.ir (**Corresponding author**)
[2] Department of Civil Engineering, K.N. Toosi University of Technology, Valiasr St., Tehran, Iran, Graduate student, leilaimen@gmail.com

CC BY

globe. Nevertheless, in some cases like the Aral Sea the consequence has been devastating leaving a permanent damage without any hope of reconstructing the original system. Obviously, the first step in solving any problem is to get a proper and sufficient knowledge of the problem itself.

On the other hand, natural systems are very complicated and usually require extensive time, expertise, and nationwide willingness to tackle the problem. This requires having a multi-objective prospective of the problem so that a tradeoff could be made between the expansions of, for example, water utilization projects and the wellbeing of the basin ecosystem. This is another way of setting a balance between the short term benefits from water utilization projects and the long term damages caused by altering the ecosystem of the basin. Through this process the optimum level of developments could be established. Moreover, the consequences of overexploitation of water resources of the basin on key components of the system can be determined through these investigations. Therefore, a comprehensive study should consist of modeling all factors that are important in shaping the future of the basin.

Human activities have a substantial impact on the quantity and quality of water resources of a basin, mainly through extended irrigated agricultural practices. An ongoing population growth, water pollution and lack of efficient water supply system along with competitions among different water use sectors for maximizing their share of water consumption are main factors, besides the climate change, that threaten the sustainability of water resources systems around the world. As a result, the number of basins with water scarcity crisis and irreparable damages, like the Aral Sea basin, is continuously increasing. Under these circumstances, proper management and planning of water resources for allocating the scarce available water becomes very crucial. On the other hand, basin planning that considers only one aspect of water use, such as the agriculture, would eventually intensify the problem by neglecting the role of other sectors of the system. Hence, the right solution would be through adopting an integrated water resources management (IWRM) approach for the basin. Successful IWRM requires strong political supports and is essential for sustainable use of water resources through environmental considerations. One of the first steps in integrated water resources management is to evaluate the amount of water resources and the demands of the basin and go through a long term simulation to find out how the system behaves. This is accomplished by developing comprehensive simulation models.

There are several basin wide simulation models that have been used in IWRM studies. Sulis and Sechi (2013) made a comparison of five generic basin-wide simulating models including AQUATOOL (Valencia Polytechnic University), MODSIM (Colorado State University), RIBASIM (DELTARES), WARGI-SIM (University of Cagliari) and WEAP (Stockholm Environmental Institute) [1]. There is wide range of researchers find the Water Evaluating and Planning system (WEAP) a powerful tool to simulate water resources and demands of river basins and investigate results of different development, water policy and other scenarios on water balance of the basin including Raskin et al. (1992), Levite et al. (2003), Bharati et al. (2009) and Mourad and Alshihabi (2016) [2,3,4,5]. Hashemi et al. (2010) proposed an integrated methodological framework to implement IWRM in Urmia Lake basin [6].

Urmia Lake is a terminal lake without any outflow. Thus, evaporation is the only means for the water loss through the Lake. Therefore, considering the large water surface area of the Lake, any change in the evaporation rate would directly influence the Lake Water Level (LWL). The only other means by which the LWL changes, is through the Lake inflow. Any change in precipitation and temperature not only affects the evaporation rate from the Lake surface, but also changes the demands for water throughout the basin and hence the inflows to the Lake. The

continuous development of irrigated agricultural projects throughout the basin in the past decades along with changes in the trend of precipitation and temperature have worked together to dry up nearly 90% of the Lake surface today [7]. It is also interesting to note that the long term mean LWL of the Lake Urmia, which was about 1276 metre (m) during 1976-1998 period, dropped as much as 4.9 m during 1999-2009 decade [8].

Other studies also point out that the climate change and irrigated agriculture are the main factors affecting Urmia Lake water level [e.g. 9,10,11]. A main problem with the past studies in this basin is the lack of water demand and consumption, mainly agricultural, that made them to use rough estimations. It is evident that without any reliable measured data, rough assumptions could lead us to erroneous results. Therefore, this paper attempts to solve this problem through developing a comprehensive basin-wide simulation model, which once calibrated could be used for the evaluation of different planning scenarios. Also, it would be used to evaluate the impacts of agricultural water use on the LWL by implementing different scenarios. Through this the role of each water use sector (especially agriculture) in causing the current critical situation of the Lake is determined. This information could be used for finding solutions to revive the Lake and also for laying out the future plan of the basin.

1.1. Study Area

Urmia Lake basin with an area of about 52 thousand square kilometres is located in northwestern Iran. Three provinces sharing the basin are west Azerbaijan, east Azerbaijan and Kurdistan. Main rivers discharging into the Lake are Zarrineroud, Simineroud, Ajichay, Shahrchay, Sufichay, Mahabadroud, Godarroud, Ghalechay, Barandouzchay, Nazloochay, Rozechay and Zoolachay. During recent decades various development projects were proposed in the basin. Some of these projects are now in operation while some others are under construction or feasibility study phases. In this study six main operational reservoirs are considered in the simulation model, including Boukan, Mahabad, Shahrchay, Alavian, Hassanlou and Nahand reservoirs. Figure (1) shows the location of Urmia Lake basin, main rivers and main operational reservoirs.

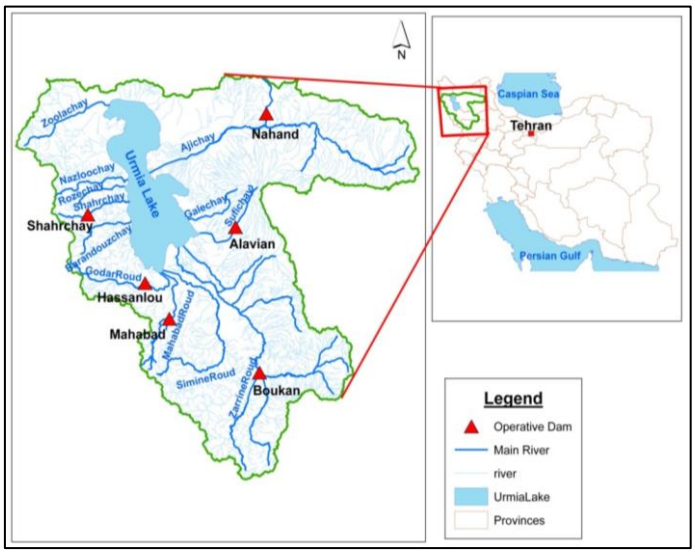


Fig. 1 The location of Urmia Lake basin, main rivers and six operational reservoirs

Average annual mean temperature and precipitation of the basin shows the climatic condition

during 1966-2012 period (Figure 2). As it can be seen from Figure 2, during critical decade of 1995-2004, precipitation mostly remained below the long-term average (≈360 mm), while at the same time above average temperatures (≈11°C) were observed, indicating a critical condition on water resources of the basin. High temperatures result in increased agricultural water demand, whereas low precipitations limit the amount of water production in the basin. Together, they can cause severe drought and stressful condition as it was also observed during those years in the region. Year 1995 is also the period where the shrinkage in the Lake Urmia began (see Figure 5) and the lake level continued to fall up to now. It is also interesting to note that although after 2004 the precipitation began to rise above the long-term average (Figure 2), the lake level decline did not stop and continued to fall to more sever lower levels (Figure 5), probably due to persistent more higher than normal temperatures resulting in higher water demands throughout the basin.

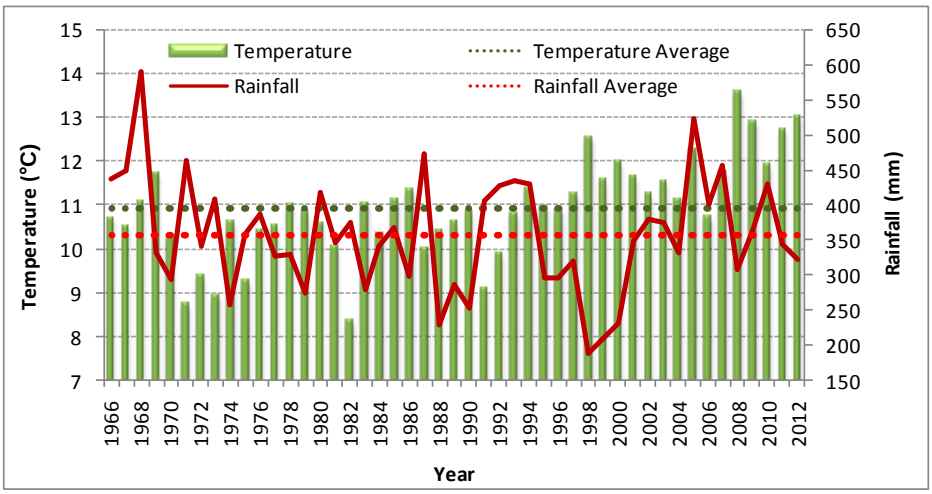


Fig. 2 Mean annual temperature and precipitation of the basin

Figure (3) shows total inflow to the Lake during the study period. As it can be seen from this Figure, during critical period of 1995-2012 the inflow to the Lake is mostly below the long-term average (solid line). We can divide the critical period beginning from 1995 into two distinct period of 1995-2004 and 2004-2012. During the first decade-long critical period, precipitation is considerably below average, temperature is slightly above average (Figure 2), and annual lake inflow has sharply dropped below average (i.e., 2904 million cubic metre (mcm)) with an exception in 2002 (Figure 3), probably as a result of consistent precipitation rise which began in 1998 and relatively near normal annual temperature during this year. During the second critical period, temperature is even higher and well above the long-term average, but precipitation has also increased to above normal levels (Figure 2). However, total inflow has continued to stay in below average condition (Figure 3) regardless of higher precipitations, which could be attributed to exceptionally higher temperatures during these years. Regardless of the aforementioned trends and variations in the precipitation trend, the lake level has continued to drop sharply since 1995 throughout the last year in the study period (i.e., 2012).

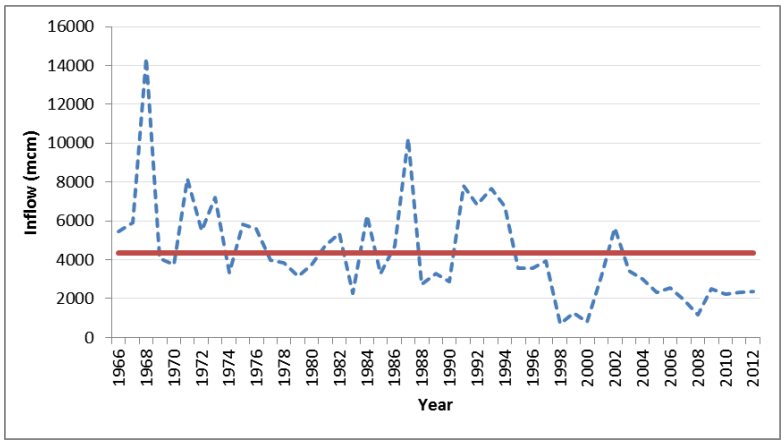


Fig. 3 Total inflow to the Lake and its long term average (solid line)

2. Methods

2.1. Simulating Model

Integrated approach in studying water resources systems requires the development of a proper model which is capable of handling different components of the system with the needed precision. In this study, WEAP software was used for developing a model to simulate the interactions among water resources and demands on the one hand and the Urmia Lake level fluctuations on the other. WEAP, developed at the Stockholm Environment Institute, is a policy oriented simulating model which can be used for comprehensive water resources studies. It has an integrated approach in simulating water resources systems [12]. The model, using a linear programming algorithm, is capable of allocating available water among different demand sites with user-defined priorities. In fact, the priorities could be set for both sources (i.e., reservoirs, surface and groundwater) and sinks (i.e., water demand sites).

In this research, observed data during the historical period of 1966-2012 were used for the development and evaluation of Urmia Lake basin model. Spatial information such as the basin boundary, rivers and location of operational reservoirs were first generated in a Geographic Information System (GIS) and then used in the WEAP model. Schematic of WEAP model for Urmia Lake basin is shown in Figure (4).

Initial data required for modeling consists of surface and groundwater data, amounts of agricultural, municipal and industrial water demands, and information on operational reservoirs in the basin. The amount of agricultural water consumption, as the main water user in the basin, was initially assumed and then estimated through calibration process for each sub-basin. The initial assumption was made using the data obtained from the most recent Iranian agricultural census [13], which is highly imprecise and does not represent the whole irrigated agriculture in the basin. Moreover, the census data is available only for few specific years. Therefore, due to uncertainties, monthly agricultural water demand for the whole historical period was estimated during calibration process using a nonlinear development trend as explained in the following section.

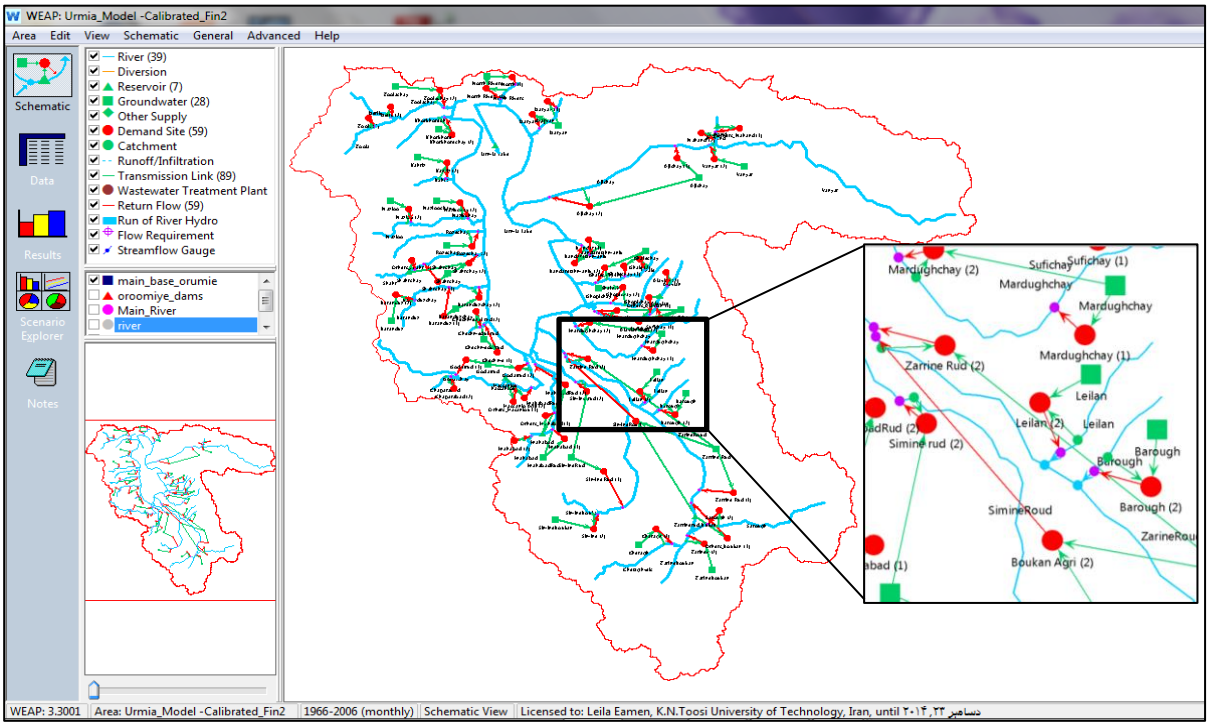


Fig. 4 Schematic of Urmia Lake basin water resources system model in WEAP

It should be mentioned that in most developing countries, like Iran, surveys and censuses are not processed regularly each year but rather they are gathered every few years. Therefore, valid information about the amounts and characteristics of water resources and demands, mostly for agricultural use, are unavailable in a regular basis and estimating methods should be applied to fill the gaps. Meanwhile, the surveys are very rough and mainly concentrate on large areas. Noting that the size of agricultural fields in Iran is mainly small and unlike many countries farmers own scattered small size fields, an accurate estimation of irrigated area is very challenging.

2.2. Calibration Method

Model calibration in a basin with many uncertainties that mainly arise from poor data, both quantitatively and qualitatively, is a tedious task and becomes even more complicated by realizing that there is not even a single reliable comprehensive set of data measurement during the whole period. Agricultural water consumption data throughout the Urmia Lake basin is only measured in certain limited locations with an amount which is only a fraction of the total irrigation water use throughout the basin. In fact, there are many unregistered wells, diversion canals, and even Qanats with unknown water yield in the basin which are not counted in censuses data gathering. Therefore, it is not possible to determine a certain figure that accounts for the amount of water demand and/or consumption in the area per each time period. Based on our knowledge from the region, we used a nonlinear trend for the agricultural water consumption during the study period (1966-2012) to overcome the problem. The trend was linearized by realizing four distinct periods in the historical data (Figure 5) as explained in the following:

Period 1: 1966-1976 (mean LW L: 1275.81 m)
Period 2: 1977-1990 (mean LWL: 1275.80 m)
Period 3: 1991-1997 (mean LWL: 1277.12 m)
Period 4: 1998-2012 (mean LWL: 1273.14 m)

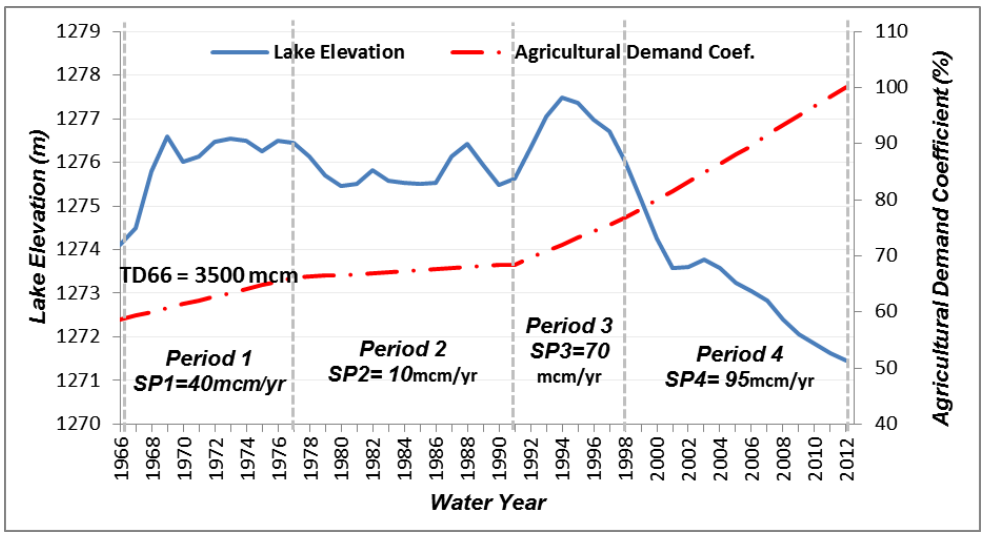


Fig. 5 Linearized agricultural demand coefficients during four periods

The first period indicates the initial stage with the least development in the basin until 1977 when the Boukan (see Figure 1) as the first major reservoir began to operate. Period 2 includes the beginning of Boukan reservoir operation until 1991 when the Lake water level started to rise (Figure 5) due to increased precipitation (Figure 2) and increased lake inflow (Figure 3). 1977 to 1991 was also the period of imposed Iraq war on Iran where the trend of various project developments including the agriculture was very slow due to the nations' budgetary limitations. The third period is the era of so called "reconstruction" after the war. It also represents a duration of high water level in the Urmia Lake due to above normal precipitations (Figure 2), below normal temperatures (Figure 2), and mostly above normal inflows (Figure 3). In 1998 the Lake began to fall below its mean LWL of 1276.1 m by that time, a trend which has consistently continued up to now. Thus, the fourth period resembles the period of Lake Urmia shrinkage and desiccation. The calibration process determines both the level of initial agricultural water consumption in year 1966 and the slopes of developments during the above mentioned four periods as shown in Figure 5 through a trial and error process.

Other parameters used in calibrating the model include evaporation rate from the Lake surface, groundwater recharge after continued drought periods, and adjustments on agricultural water supply by the main reservoirs. As it was explained earlier, there are uncertainties on some measurements because they are not available either for the period or at the location of interest. Lake evaporation rate from freshwater can be estimated using either evaporation pan measurements or through certain relationships. However, for saltwater it is not possible to directly use these procedures. And although we were able to establish a relationship between evaporation rate from fresh and salt water using limited available data, it would be only a rough estimate since the density of salt is also a factor in determining the actual evaporation from saltwater surface. On the other hand, since the area of Urmia Lake is considerable (between 4000 to 6000 km^2) a small change in the evaporation rate would have a substantial impact on the

volume of the water losses through evaporation. Therefore, the mass balance equation of the Lake is highly sensitive to the rate of evaporation, and in the absence of precise measurements and concerning the uncertainties inherent in the process, must be determined through calibration using the initially estimated values.

Groundwater recharge is another important parameter in the basin water balance model which must be also determined through calibration process in the absence of any data. The effect of recharging groundwater through precipitation and surface water was included through applying reductions on the river flow as a function of continued droughts. Therefore, the amount of surface water used for recharging groundwater is assumed to be a function of both drought intensity and its persistence. A coefficient was defined and found by calibration to adjust the amount of total water used for recharging the groundwater in each sub-basin under a defined drought condition. Therefore, three main categories are used for accomplishing the model calibration where each may involve several decision variables. These include adjustments on agricultural water demand during each of the above mentioned periods, adjustments on evaporation from lake's surface (saltwater), and finally adjustments on groundwater recharge rate as function of continued drought period.

The objective of the calibration process is to minimize the sum of errors between the observed and simulated LWLs during the historical period (1966-2012). A trial and error method is used for calibrating the model. Statistical criteria used for evaluating the performance of the model during the calibration and test periods are coefficient of determination (Equation 1), Nash-Sutcliffe efficiency (Equation 2) and Root Mean Square Error (Equation 3).

$$R^2 = \left(\frac{\sum_{i=1}^{n} \left((OL_i - \overline{OL})(SL_i - \overline{SL}) \right)}{\sqrt{\sum_{i=1}^{n} (OL_i - \overline{OL})^2 \sum_{i=1}^{n} (SL_i - \overline{SL})^2}} \right)^2 \quad \textbf{(1)}$$

$$NSE = 1 - \frac{\sum_{i=1}^{n} (OL_i - SL_i)^2}{\sum_{i=1}^{n} (OL_i - \overline{OL})^2} \quad \textbf{(2)}$$

$$RMSE = \sqrt{\frac{\sum_{i=1}^{n} (SL_i - OL_i)^2}{n}} \quad \textbf{(3)}$$

Where, OL_i and SL_i are the observed and simulated LWLs at the beginning of month i, and $\overline{OL}$ and $\overline{SL}$ are the average of observed and simulated LWL data, respectively. Figure 6 shows the flowchart of the model and its calibration process.

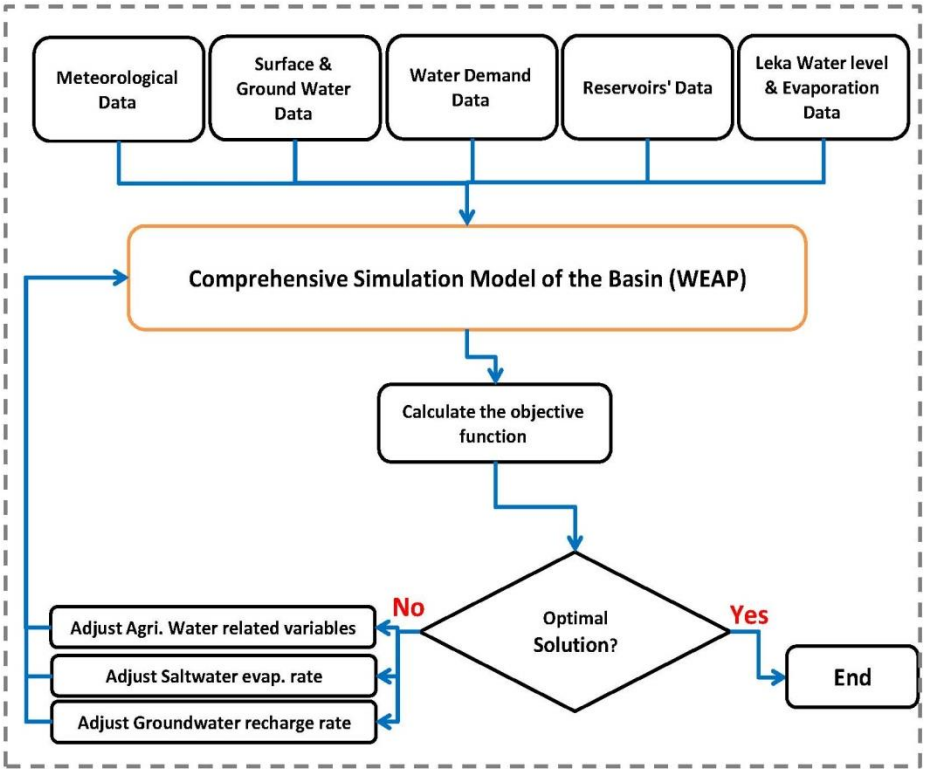


Fig. 6 Flowchart showing the simulation model structure and its calibration

Figure (7) shows the calibrated and observed LWL of Urmia Lake during the study period (1966-2012). A visual comparison of modeled and observed LWL indicates a good fit. Moreover, the performance of the calibrated model was evaluated by coefficient of determination (R^2), Nash-Sutcliffe Index (NSE) and root mean square error (RMSE), where their corresponding values were found as 0.98, 0.97 and 0.005 respectively.

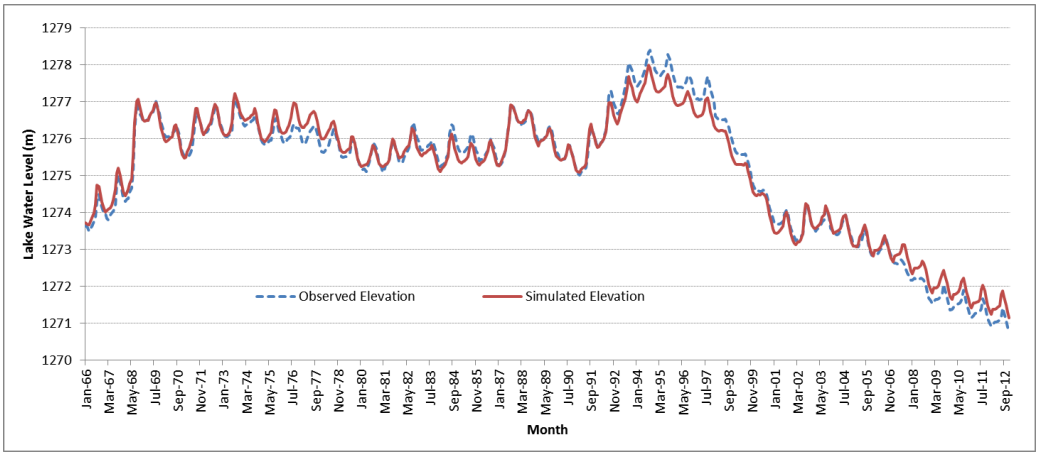


Fig. 7 Simulated and observed LWL of Urmia Lake (1966-2012)

Scatter plot of monthly observed and simulated water level of the Lake for the study period is

also shown in Figure (8) where the solid line indicates the perfect match.

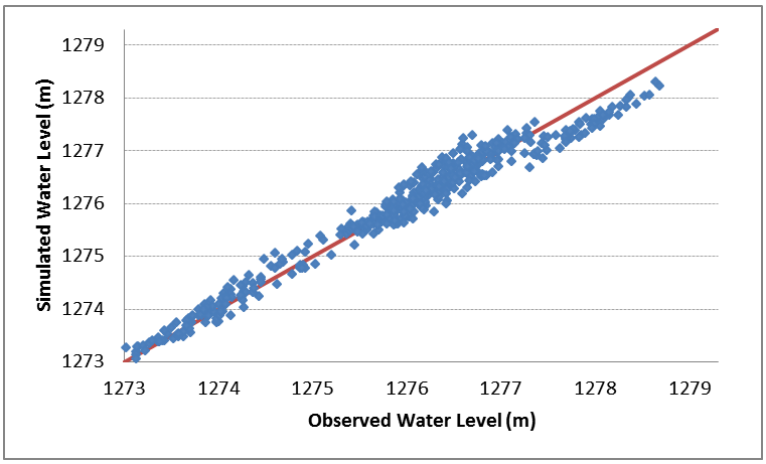


Fig. 8 Observed and simulated LWL of the Lake

As it can be seen from Figure (8), performance of the model is very good especially for LWLs under 1277 m. However, for water surface elevations above this level the model shows an underestimation trend. It is possible that the bias for high LWLs is due to measurement errors in hydrometric stations during wet years where large floods occur. Another source of error during wet years could be due to less water consumption by crops where part of their demand is met by precipitation. Also, in wet years greater part of irrigation demand could be supplied through groundwater sources that have been replenished by plentiful precipitation. All these may contribute to actually more water flows into the Lake during wet years. The simulation model however is not able to capture such a process due to the lack of precise information. Meanwhile, the overall error and fitness of the model is very good and in accordance with the objectives of this research. The model has been able to closely catch the variations of LWL indicating that the proposed algorithm has been successful.

Furthermore, a comparison of total water demand estimated by the model with few available census data indicates a good agreement in terms of their trend. For example, the ratio of total water demand estimated by the model to the census data during 1996, 2001, and 2006 is respectively 1.3, 1.2, and 1.4, which indicates the precision of the model. Nevertheless, as mentioned earlier the recorded data are expected to underestimate the true water demand of the basin by focusing on major water use projects. On the other hand, the model shows that the true water demand of the basin is about 30% more than that indicated by the recorded data.

2.3. Scenarios

The Lake level study in this paper was initially carried out for revealing the main causes of the current critical situation. These findings can then be used to determine short-term and long-term solutions for restoring the Lake Urmia.

After finalizing the comprehensive hydrologic model, the role of different water use sectors on the LWL changes is investigated. This is done by grouping different main water use activities including: (a) water allocations through main reservoirs, and (b) all other types of water withdrawals in the basin (other than that allocated by reservoirs). The existing Lake level is a result of all existing water use projects besides hydro-climatic conditions. Therefore, by eliminating each main component of the system we can assess the role of that component on

LWL changes through long term model simulation.

Water use scenarios are defined as follows:

1. **No Operational Reservoirs (NoRes):** Impact of operational reservoirs and their water demands (mainly agricultural) is evaluated in this scenario by eliminating them from the system according to their starting operation date.
2. **No Other Withdrawals (NoWdr):** All other water withdrawals (mainly agricultural) are eliminated to assess their role on Lake level fluctuations.
3. **No Reservoirs and No Other Withdrawals (NoRes & Wdr):** This scenario is implemented to show the impact of combined actions. In fact, it shows a situation where human related water use activities in the basin are removed and thus indicates the natural and intact basin condition.

It is worthwhile to mention that in Urmia basin nearly 92% of water consumption is used by agriculture, 6% by municipal, and the remaining 2% by industrial sectors. Therefore, agriculture is the main water use sector in the area either through regulated reservoir releases or other types of water withdrawals from surface and groundwater sources.

According to a study the minimum acceptable water level required for the Lake to survive ecologically is found to be 1274 m [14]. The Lake is home to a unique brine shrimp species, artemia urmiana, and supports many species of reptiles, amphibians and mammals [15]. Water levels less than this elevation may cause serious hazards on ecology of the Lake including the artemia population and the basin as well.

3. Results and Discussions

The normal values are usually calculated using the whole study period, i.e., 1966-2012 in this case. However, noting that the lake has entered a completely drying and abnormal situation more than a decade ago, such a calculation would not represent the lake hydrology and the conclusions derived from these figures could be erroneous. For example, long-term mean LWL would be 1275 meters using 1966-2012 period which indicates that years 1968 through 2000 (about consecutive 32 years) are all above normal or otherwise wet periods. The mean LWL, surface area and storage volume calculated using the whole period is 1275.15 m, 5076 km^2, and 30335 mcm, respectively. This divides the lake into two distinct period of above normal 1966-2000 and below normal 2001-2012. However, if only the healthy period of the lake is considered, using the years 1966 through 2000 mean LWL, surface area and storage would be 1276.03 m, 5405 km^2, and 34944 mcm, respectively. In this case, alternating above and below normal situations are observed. Obviously in both cases the period after year 2000 is considered as abnormally dry.

The calibrated model was used to evaluate the impacts of different human activities on water level fluctuations of the Lake. As explained in the previous section, the role of different activities including reservoir constructions and other miscellaneous water withdrawals on current Lake crisis is investigated.

Water levels of Urmia Lake under different water resources development scenarios are found by removing the corresponding activity and then simulating the system using the calibrated WEAP model. As it can be seen from Figure (9), the impact of NoWdr scenario is considerably greater than that of NoRes on Urmia Lake water level fluctuations. This is in contradiction to what many environmental activists in Iran had been calling for, at least during the last decade where the reservoir construction was blamed as the main source of Lake water shrinkage.

However, our investigation shows (not included in this paper) that also unlike what official authorities have been claiming the climate change is not to be blamed for the extent of current situation. The current situation is rather a direct consequence of ignoring the principles of sustainable development in the region. At least in the last three decades the development of agriculture industry with a goal of self-sufficiency has been the main objective in the country. Therefore, it is not surprising to see the rapidly growing demand for water and the rushing emergence of various water resources projects in the basin during the "reconstruction" era after the early 1990s when Iran-Iraq war ended. A closer look at the slope of agricultural water demand after 1992 (periods 3 and 4) in Figure 5 makes it clear that water consumption gained a rapid slope after this date.

According to our results, by removing water consumption through "Other Withdrawals" (i.e., NoWdr scenario) the LWL would have risen by 5.2 meters (equivalent to 22,325 mcm in volumetric measures) in 2012. Whereas, for removing water consumptions through operational reservoirs (i.e., NoRes scenario) the rise in LWL would be only 1.9 meters (6,676 mcm of lake water), which indicates much less impact than the aforementioned scenario. As it can be seen from Figure (9), combined removal of "No Other Withdrawals" and "No Operational Reservoirs" scenarios would increase the LWL by about 6.4 meters (29001 mcm of water) in year 2012. Therefore, main reservoirs are only responsible for 23% of current situation. Whereas, miscellaneous agricultural water withdrawals are responsible for 77% of the current Lake Urmia crisis.

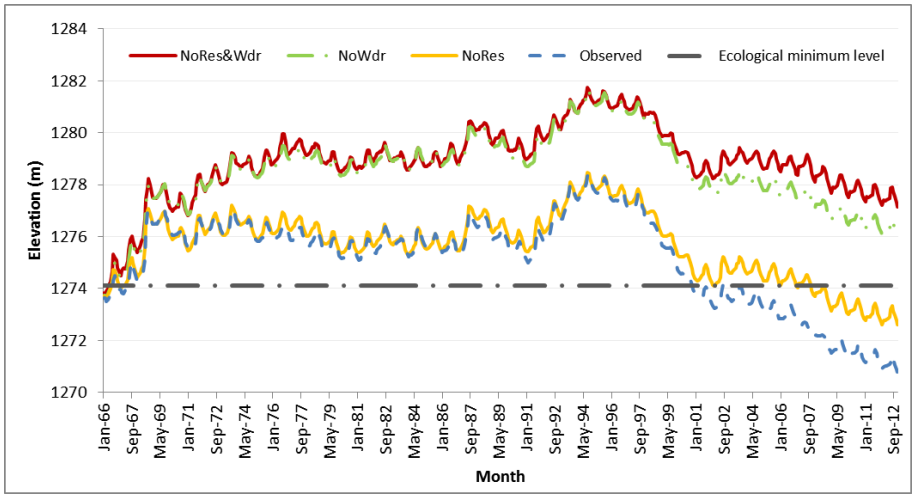


Fig. 9 Comparison of LWL under different water resources development scenarios

Observed and simulated LWL under different scenarios at the ending year of the four time stages are shown in Figure 10. As it can be seen from this Figure, in all four years the water withdrawal by means other than the operational reservoirs (i.e., NoWdr scenario) has the most considerable impact on LWL. In addition, the impact of operational reservoirs (NoRes) becomes more considerable as we proceed through the time as a consequence of new reservoir construction. For example, removing reservoirs during periods 1 and 2 has insignificant impact on LWL which is evident by comparing the observed and NoRes LWLs. However, the gap becomes wider as we move to periods 3 and 4. It should be mentioned that in the first time stage (1966-1976) no reservoir was yet built in the basin. Therefore, as it can be seen from Figure 10 the LWL for NoRes option is the same as the observed level. Moreover, the impact of water use

by “other withdrawals” also increases with time as a result of increased water demand. While removing other withdrawals (i.e., NoWdr) in the first stage raises the LWL by less than 3 meters, in the second (1977-1990), third (1991-1997) and final stage (1998-2012) it raises the LWL by about 3.6, 3.5, and 5.2 meters, respectively. A review of the gap between the observed LWL and NoWdr scenario reveals the growing extent of miscellaneous water use projects in the basin during these years.

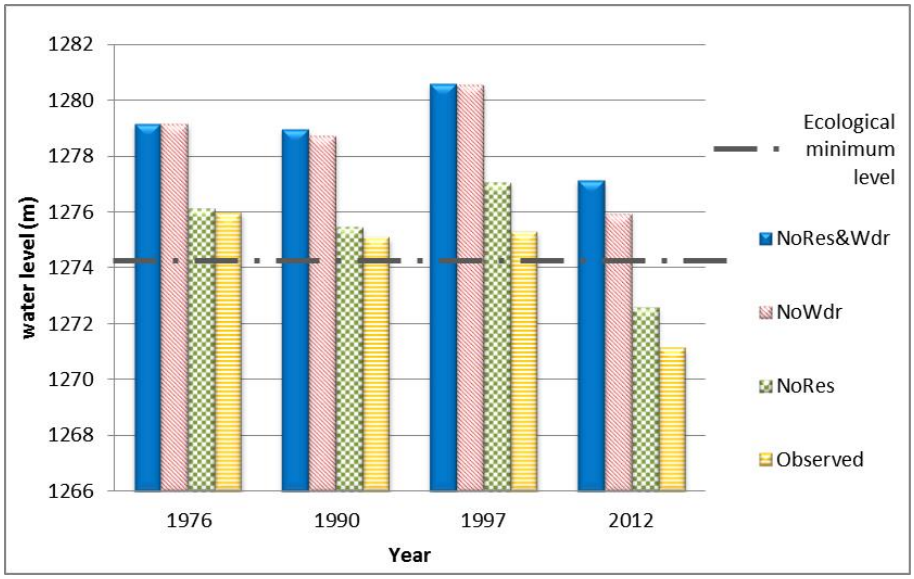


Fig. 10 Comparison of LWL under water resources development scenarios at the ending year of four time periods

Since Urmia is a shallow lake, small changes on the Lake level considerably affects its surface area. Figure 11 compares the surface area of Urmia Lake under different water resources development scenarios during the four periods. The observed surface area of the Lake was about 3.4 thousand square kilometers in 2012, while it would have reached to about 6 thousand square kilometers if both operational reservoirs and all other withdrawals were removed from the system. It is noteworthy to mention that in the same year only by eliminating other withdrawals the Lake surface area would have reached to 5.4 thousand square kilometers, an increase of about 1.9 thousand square kilometers. Thus, we would have seen a normal situation in Urmia Lake even by having all the existing operational reservoirs but removing all other withdrawals. On the other hand, under the situation of NoRes, as it is shown in Figure 11, the area of the Lake would have increased only by 0.7 thousand square kilometers in 2012.

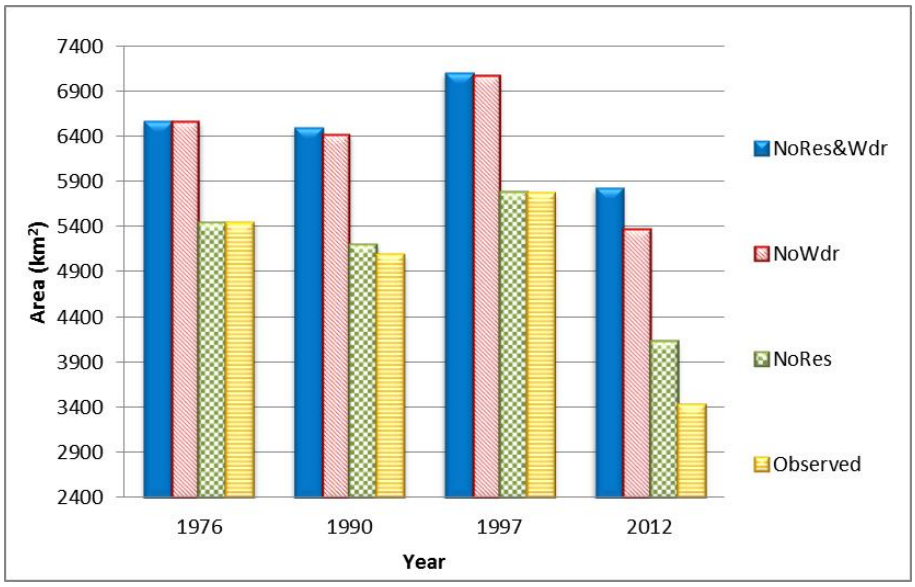


Fig. 11 Comparison of Urmia Lake surface area under different scenarios at the ending year of four time periods

The results of this study reveal that the number one factor in causing the current Urmia Lake crisis is the miscellaneous water withdrawals throughout the basin by means other than reservoirs. These water withdrawals consist of legal and illegal surface and in specific groundwater. In the surface water, there are also small reservoirs mostly without any documentations and records that were constructed by local authorities mainly during the last three decades. Since these reservoirs are very small and numerous, and mostly without any documentation, we do not include them in "operational reservoirs" category which consists only of large reservoirs in the basin. There are also many illegally constructed wells which are scattered around the basin and in specific near the Lake shores. Nevertheless, the total water utilized through these small projects has much considerable impact on the LWL than the main reservoirs. These projects were made gradually through the time by local people without any concern on their long-term impact. People in the region highly rely on these projects which are twisted with their daily life. Therefore, there seems to be no short-term and quick solution to the problem. However, noting that the current irrigation efficiency in the area is less than 35% and that 92% of the total water utilization is by the agriculture, a long-term solution should aim at modernizing the irrigation system and freeing more water into the Lake.

Unfortunately, the fact is that the current critical situation of the Urmia Lake is a direct consequence of neglecting the Lake itself in various water resources projects and agricultural developments in the basin during last half a century. In developing countries where private sector has the least role in regional and national decision makings, local and national water and agricultural authorities are mainly responsible for the crises created. Nevertheless, this study shows that unless a comprehensive and integrated approach is followed and implemented, the current critical condition of Urmia Lake will be even more escalated in the future considering the climate change. The projected LWL reveals that the existence of this water body which is very crucial for the whole northwestern Iran needs prompt and quick attention. The solution should consist of short-term and long-term comprehensive action plans and should consider all effective components in the region.

4. Conclusion

A simulation model was developed using WEAP software to study the water resources system of Urmia Lake basin. A calibration procedure was proposed and carried out using the historical data for 1966-2012 period with NSE equal to 0.97. Further analysis showed that the miscellaneous water withdrawals (mainly through wells, Qanats, and river diversions) play an important role on the hydrology of the Lake Urmia. The operational reservoirs and their corresponding demand sites are the next important factor in causing the current critical situation of the Lake. It was found that by removing other withdrawals (i.e., NoWdr scenario) the LWL would have risen by 5.2 meters (equivalent to 22,325 mcm of lake storage) in 2012. Whereas, for removing water consumptions through operational reservoirs (i.e., NoRes scenario) the rise in LWL would be only 1.9 meters (equivalent to 6,676 mcm of lake storage), which indicates much less impact than the aforementioned scenario. Therefore, main reservoirs are only responsible for 23% of current situation. Whereas, miscellaneous agricultural water withdrawals are responsible for 77% of the current Lake Urmia crisis.

It is suggested that the solution should consist of short-term and long-term comprehensive action plans and should consider all the effective components in the basin.

5. References

[1] Sulis A, Sechi GM (2013) Comparison of generic simulation models for water resources systems. Environmental Modeling & Software, 40, 214-225.

[2] Raksin P, Hansen E, Zhu Z, Stavisky D (1992) Simulation of water supply and demand in the Aral Sea region. Water International, 17(2), 55-67.

[3] Levite H, Sally H, Cour J (2003) Testing water demand management scenarios in a water-stressed basin in South Africa: application of the WEAP model. Physics and Chemistry of the Earth,28, 779-786.

[4] Bharati L, Smakhtin VU, Anand BK (2009) Modeling water supply and demand scenarios: the Godavari-Krishna inter-basin transfer, India. Water Policy, Supplement 1, 140-153.

[5] Mourad KA, Alshihabi O (2016) Assessment of future Syrian water resources supply and demand by the WEAP model, Hydrological Science Journal, 61:2, 393-401.

[6] Hashemi M, O'Connell PE, Amezaga JM, Parkin G (2010) A socio-technical framework for implementing Integrated Water Resources (IWRM) plan in Lake Urmia basin, Iran. In: Managing Consequences of a Changing Global Environment, BHS Third International Symposium, British Hydrological Society, 19-23 July 2010, Newcastle University.

[7] MEHRNEWS (2014) http://www.mehrnews.com/detail/News/2343495, [Accessed 5 August 2014, In Farsi].

[8] Raveshty MA, Maruyama Y (2010) Study of Urmia Lake level fluctuations and predict probable changes using multi-temporal satellite images and ground truth data period (1976-2010). In: Map Asia 2010 & ISG 2010, 26-28 July 2010, Kuala Lumpur, Malaysia.

[9] Eimanifar A, Mohebbi F (2007) Urmia Lake (Northwest Iran): a brief review. Saline Systems, 3:5. 1-8.

[10] Hassanzadeh E, Zarghami M, Hassanzadeh Y (2012) Determining the main factors in declining the Urmia Lake level by using System Dynamics Modeling. Water Resources Management,26, 129-145.

[11] Azizi G, Abbasi F (2013) The climate change technology and management in the drying Lake Urmia. In: EIC Climate Change Technology Conference, 27-29 May 2013, Concordia University, Montreal, Quebec.

[12] Sieber J, Purkey D (2011) WEAP User guide. Stockholm Environmental Institute, U.S. Center.

[13] Mahab-Ghodss Consulting Engineering (2012) Integrated Water Resources Management Study of Urmia Lake basin. (InFarsi).

[14] Regional Council of Lake Urmia Basin Management (2012) Drought risk management plan for Lake Urmia basin. Working group on sustainable management of water resources and agriculture. (In Farsi).

[15] United Nations Environment Programme (UNEP) (2012) The drying of Iran's Lake Urmia and its environmental consequences, Technical report,Global Environmental Alert Service (GEAS).

نشریه تخصصی

سازه های هیدرولیکی

صاحب امتیاز: دانشگاه شهید چمران اهواز

مدیر مسئول: دکتر حمیدرضا غفوری
سردبیر: دکتر علی حقیقی
مدیر داخلی: دکتر سید محمد اشرفی
گروه مهندسی عمران، دانشکده مهندسی، دانشگاه شهید چمران اهواز، اهواز، ایران

دارای اعتبار **علمی پژوهشی** از وزارت علوم تحقیقات و فناوری

Print ISSN: 2345-413x
Online ISSN: 2345-5156

اعضای هیأت تحریریه

دکتر حسین محمدولی سامانی
گروه مهندسی عمران، دانشکده مهندسی، دانشگاه شهید چمران اهواز
(تخصص: سازه های هیدرولیکی)

دکتر محمود شفاعی بجستان
گروه سازه های آبی، دانشکده مهندسی علوم آب، دانشگاه شهید چمران اهواز
(تخصص: سازه های هیدرولیکی)

دکتر علی حقیقی
گروه مهندسی عمران، دانشکده مهندسی، دانشگاه شهید چمران اهواز
(تخصص: آب و فاضلاب و هیدرولیک)

دکتر محمدسیروس پاکباز
گروه مهندسی عمران، دانشکده مهندسی، دانشگاه شهید چمران اهواز
(تخصص: ژئوتکنیک)

دکتر سعیدرضا صباغ یزدی
دانشکده مهندسی عمران، دانشگاه صنعتی خواجه نصیرالدین طوسی (تخصص: سازه های هیدرولیکی و مدلسازی عددی)

دکتر مجتبی لبیب زاده
گروه مهندسی عمران، دانشکده مهندسی، دانشگاه شهید چمران اهواز (تخصص: سازه و سازه های هیدرولیکی)

دکتر هلنا راموس
گروه مهندسی عمران، دانشگاه لیسبون پرتغال (تخصص: هیدرولیک سیستم های تحت فشار و هیدروانفورماتیک)

دکتر عبدالرسول تلوری
گروه مهندسی عمران، دانشگاه آزاد اسلامی، واحد تهران شمال
(تخصص: هیدرولوژی و منابع آب)

دکتر آرش ادیب
گروه مهندسی عمران، دانشکده مهندسی، دانشگاه شهید چمران اهواز
(تخصص: هیدرولوژی و منابع آب)

دکتر سید عباس حق شناس
گروه فیزیک فضا، موسسه ژئوفیزیک دانشگاه تهران (تخصص: سواحل و بنادر)

دکتر محمد واقفی
گروه مهندسی عمران، دانشکده فنی و مهندسی، دانشگاه خلیج فارس (تخصص: سازه های هیدرولیکی)

دکتر محمد ذونعمت کرمانی
بخش مهندسی آب، دانشگاه شهید باهنر کرمان (تخصص: هیدرولیک محاسباتی)

دکتر طاهر رجایی
گروه مهندسی عمران، دانشکده فنی و مهندسی، دانشگاه قم (تخصص: آب و محیط زیست)

Journal of
Hydraulic Structures
Scientific Professional Journal

Contents

Volume 3 - Issue 2 - 2017

Investigating the vulnerability downstream area of Taleghan dam due to dam failure (1-9)
H. Goharnejad; M. Azizkhani; M. Zakeri Niri; S. Moazami

An experimental study on hydraulic behavior of free-surface radial flow in coarse-grained porous media (10-21)
A. Rajabi; E. Hatamkhani; J. Sadeghian

Three-dimensional numerical modeling of score hole in rectangular side weir with finite volume method (22-31)
S. Ghotbi; A. Abdollahi; M. Azhdari Moghadam

Experimental Study of the Effect of Base-level fall at the Beginning of the Bend on Reduction of Scour around a Rectangular Bridge Pier Located in the 180 Degree Sharp Bend (32-46)
M. vaghefi; M. moghanloo; D. Dehghan; A. keshavarz

Developing optimal operating reservoir rule-curves in drought periods (47-61)
S. Alahdin; H.R. Ghafouri

Finding the Causes and Evaluating Their Impacts on Urmia Lake Crisis Using a Comprehensive Water Resources Simulation Model (62-77)
A. B. Dariane; L. Eamen

Address :
Engineering Faculty, Shahid Chamran University of Ahvaz
Phone: +986113330011 , +986113337010
Website: jhs.scu.ac.ir
Email: jhs@scu.ac.ir
Ahvaz, Khouzestan Province, Iran